8. Force and Moment Measurement

Measurement of steady and fluctuating forces acting on a body in a flow is one of the main tasks in wind tunnel experiments. In aerodynamic testing, strain gauge balances will usually be applied for this task as, particularly in the past, the main focus was directed on the measurement of steady forces. In many applications, however, balances based on piezoelectric multicomponent force transducers are a recommended alternative solution. Contrary to conventional strain gauge balances, a piezo balance features high rigidity and low interference between the individual force components. High rigidity leads to very high natural frequencies of the balance itself, which is a prerequisite for applications in unsteady aerodynamics, particularly in aeroelasticity. Moreover for measurement of extremely small fluctuations, the possibility exists to exploit the full resolution independently from the preload.

Concerning the measurement of small, steady forces, the application of piezo balances is restricted due to a drift of the signal at constant load. However, this problem is not as critical as generally believed since simple corrections are possible.

The aim of this chapter is to give an impression of the possibilities, advantages and limitations offered by the use of piezoelectric balances. Several types of external balances are discussed for wall-mounted models, which can be suspended one-sided or twin-sided. Additionally an internal sting balance is described, which is usually applied inside the model. Reports are given on selected measurements performed in very different wind tunnels, ranging from low-speed to transonic, from short- to continuous running time and encompassing cryogenic and high pressure principles. The latter indicates that special versions of our piezo balances were applied down to temperatures of −150 °C and at pressures of up to 100 bar.

The projects span from a wing/engine combination in a low-speed wind tunnel to flutter tests with a swept-wing performed in a transonic wind tunnel, and include bluff bodies in a high pressure and cryogenic wind tunnel, as well. These tests serve as examples for discussing the fundamental aspects that are essential in developing and applying piezo balances. The principle differences between strain gauge balances and piezo balances will also be discussed.

8.1 Steady and Quasi-Steady Measurement

The key measurement system in a wind tunnel is the multicomponent force and moment measurement instrumentation. More than 70% of the tests in a wind tunnel require some kind of force measurements. Historically the instruments were purely mechanical and their mechanism resembled balances for weighing; hence the use of the term *balance* today. Today these balances are often based on transducers or are constructed out of a single piece of metal, on which strain gauges are applied. All balances must have a minimum of one sensing element for every component to be measured. The strain sensor usually is a resistance foil strain gauge, but semiconductor gauges are also used. Illustrated in Fig. 8.1 is one of the first wind-tunnel balances built by Gustav Eiffel in 1907. The man on the upper gallery was responsible for balancing the lift generated by the airfoil in the tunnel below and simultaneously recording its associated lift.

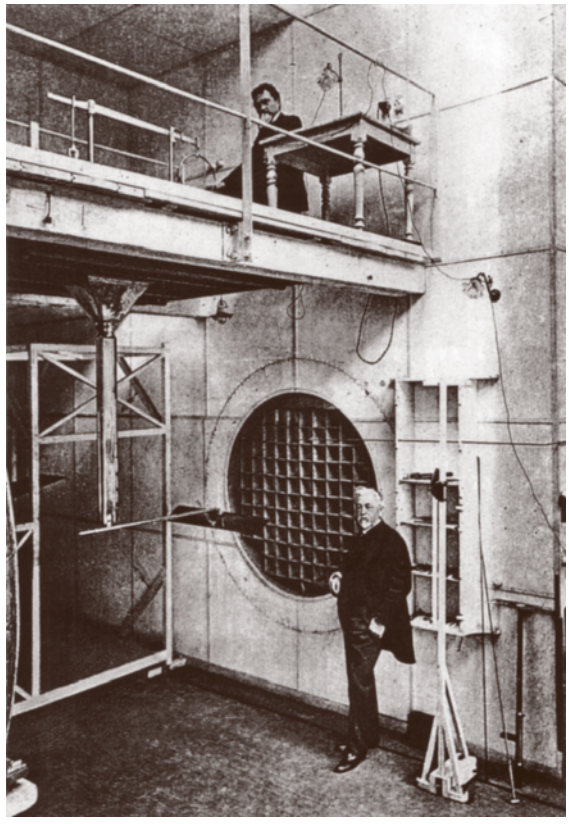

Fig. 8.1 Gustav Eiffel's wind tunnel with lift balance

8.1.1 Basics

Balance Types

Balance types are distinguished by the number of force/moment components that are measured simultaneously – one to six are possible – and the location at which they are placed. If they are placed inside the model they are referred to as *internal balances* and if they are located outside the model or the wind tunnel, they are referred to as *external balances*.

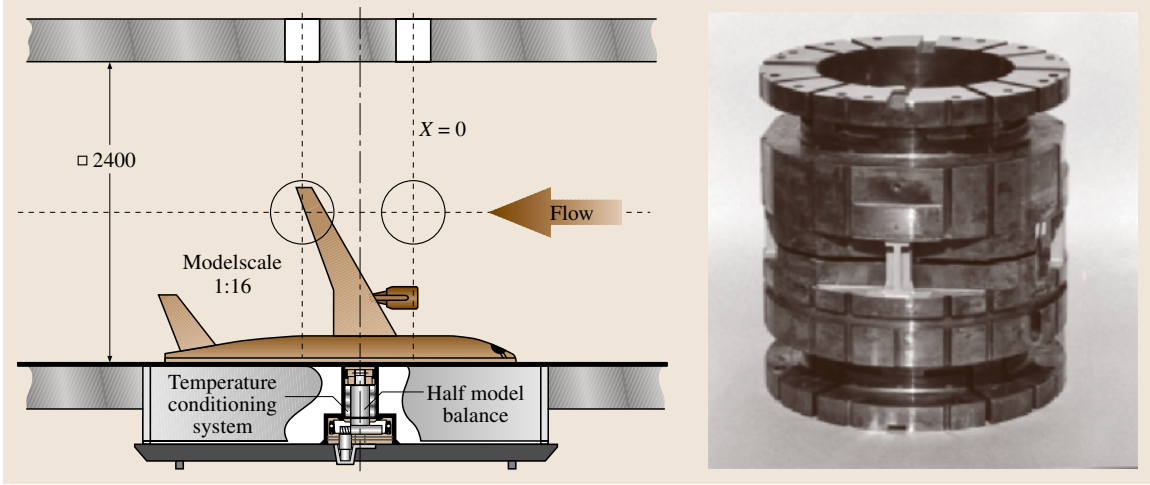

Fig. 8.2 Side-wall balance test configuration (*left*), and typical side-wall balance (*right*)

Fig. 8.3 External balance and support

External Balances

Two types of external balances exist. The first is the one-piece external balance (Fig. 8.3), which is constructed from one single piece of material and is equipped with strain gauges. Such balances are also referred to as *side-wall balances* (Fig. 8.2) as used in half-model tests.

The second type of external balance comprises single force transducers which are connected by a framework. Such a design can be built very stiff but needs more space compared to the one-piece design. However, there is usually plenty of space available around the wind tunnel for such a balance, and so the construction can be optimized with respect to measurement requirements, such as optimized sensitivity, stiffness and decoupling of load interactions.

Internal Balances

There is limited space inside the model itself, so internal balances have to be relatively small in comparison to external balances. There are two main types of internal balances. The monolithic type (Fig. 8.4), in which the balance body consists of a single piece of material, is

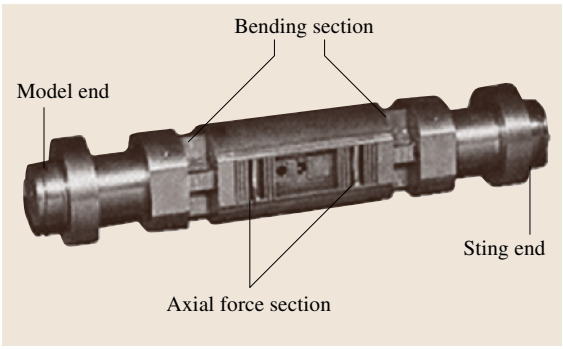

Fig. 8.4 Typical internal balance

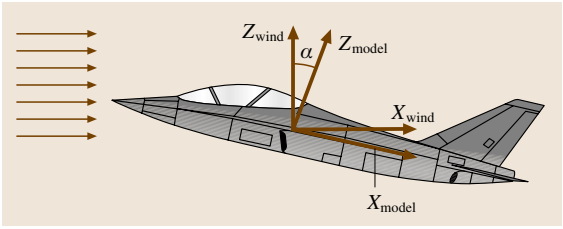

Fig. 8.5 Various possible coordinate systems for a wind tunnel and model

designed in such a way that certain areas are primarily stressed by the applied loads. The other internal balance type uses small transducers that are orientated with their sensing axes in the direction of the applied loads. Such a balance is combined into a solid structure. A balance measures the total model loads and therefore is placed at the center of gravity of the model and is generally constructed from one solid piece of material.

Loads

In this chapter the word *load* will be used to describe both the applied forces and moments. The task of a balance is to measure the aerodynamic loads, which act on the model or on components of the model itself. In total there are six different components of aerodynamic loads, three forces in the direction of the coordinate axes and the moments around these axes (Fig. 8.5). These components are measured in a certain coordinate system, which can be either fixed to the model or to the wind tunnel. For the measurement of loads on model parts such as rudders, flaps and missiles, normally fewer than six components are required.

Definition of Coordinate Systems

One possible coordinate system is fixed to the wind tunnel – the wind axis system – and is aligned to the

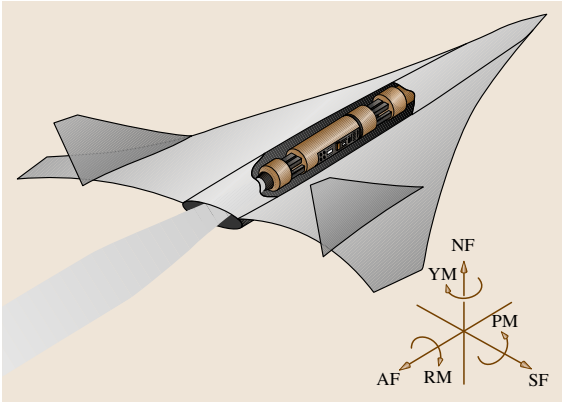

Fig. 8.6 Definition of wind axis system in the USA

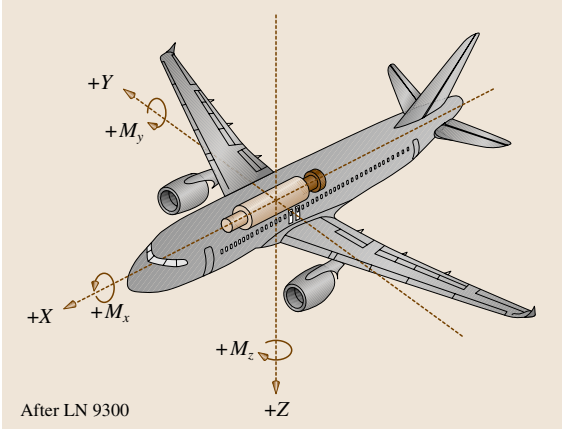

Fig. 8.7 Definition of model-fixed axis system in Europe

main flow direction. The lift force is generally defined as the force on the model acting vertically to the main flow direction whereas the drag is defined as the force acting in the main flow direction. This definition is common all over the world. However, the definition of the positive direction of the forces is not universal. Whereas lift (normal force) and drag (axial force) are defined positive in the USA (Fig. 8.6), in Europe (Fig. 8.7) weight and thrust are defined as positive in the wind axis system.

To form a right-hand axis system, the side force in the USA has to be positive in the starboard direction. The definitions of the positive moments do not follow the sign rules of the right-hand system. The pitching moment is defined as positive turning right around the y-axis, but yawing and rolling moments are defined positive turning left around their corresponding axes. This makes this system inconsistent in a mathematical sense.

Table 8.1 Definition of positive axis direction

Balance axis system	Name of component	European	USA
		Positive direction	Positive direction
X	Axial force	In flight	In wind
Y	Side force	To starboard	To starboard
Z	Normal force	Down	Up
M_x	Rolling moment	Roll to starboard	Roll to starboard
M_y	Pitching moment	Turn up	Turn up
M_z	Yawing moment	Turn to starboard	Turn to starboard

The European axis system is consistent with the right-hand system and the definition is based on a standard given by DIN-EN 9300 or ISO 1151. A balance which always stays fixed in the tunnel, and relative to the wind axis system, always gives the pure aerodynamic loads on the model.

In the case of the model-fixed axis system, the balance does not measure the aerodynamic loads directly. The loads acting on the model are given by the balance and the pure aerodynamic loads must then be calculated from these components by using the correct yaw and pitch angles. The difference between the American and European definitions of the positive direction remains the same in this case.

Specification of Balance Load Ranges

Before a balance can be designed, the specifications of the load ranges and the available space for the balance are required. This is a challenging step prior to the design of a balance since cost and accuracy considerations must be made long before the first tests are performed.

The maximum combined loads specify the load ranges for the balance design. The maximum design loads of a balance are defined in various manners. For example, if several loads act simultaneously, then the load range must be specified as the *maximum combined load*. If the maximum load acts alone, then the load range is defined as the *maximum single load*. Usually such single loads do not exist in wind-tunnel tests and combined loads must be expected. Such combined loads stress the balance in a much more complicated manner and therefore deserve very careful attention. The stress analysis of the balance has to take into account this situation. Furthermore, the combination of two loads usually re-

Table 8.2 Determination of maximum combined loads for an external balance

			Wind axis system							Model axis system					
Test type	q	A	C_x	C_y	$C\ldots$	Drag	Side force	$F\ldots$, $M\ldots$	max α, β, γ	F_x	F_y	F_z	M_x	M_y	M_z
	(Pa)	(m^2)				(N)	(N)	(N), (N m)	(deg)	(N)	(N)	(N)	(N m)	(N m)	(N m)
Full model															
Half model															
etc.															

quires that the balance carries higher loads. To determine which balance can be used for a given setup, the balance manufacturer provides the test engineer with loading diagrams that define the maximum load combinations for various available models.

In the case of external balances the available space is usually not a limiting factor. External balances have been used for several decades in wind tunnels and therefore specifications of the design load ranges are orientated more to the capabilities of the wind tunnel itself and the associated model setups such as half-model and full-model tests, or the possibility of aircraft, car and building testing. For the design of an external balance, load ranges of the principle balance configuration must first be defined. Two different options are possible.

The first option is to mount the turntable inside the weighbridge. In this case the balance stays in the wind axis system and therefore the balance always measures the wind loads. The disadvantage of this option is that the whole turntable mechanism has to be mounted on the metric side of the balance such that the balance is preloaded by the weight of this mechanism.

The second option is to mount the whole balance on a turntable. In this case some components stay in the wind axis system and some stay in the model axis system, so a calculation of the aerodynamic loads from the balance loads is necessary. For example, in the case of a full model setup, as shown in Fig. 8.9, the balance will always measure the aerodynamic loads when the angle of attack changes. In a half-model setup, as shown in Fig. 8.11, the balance will move with the model when the angle of attack changes and will measure the loads in the model axis system.

This makes the determination of the balance load ranges rather difficult. Therefore it is useful to fill out a table where the maximum loads for the different test setups are first calculated in the wind axis system. In order to do this some assumptions of the aerodynamic coefficients and the model size must be made. By assuming values for the maximum angle of attack or yaw angle, the maximum loads in the model axis system can be calculated.

From such a table the maximum of each component can be taken as the maximum load for the balance. Naturally this leads to a balance with rather high load ranges and for some cases the load range could be too high to measure with high resolution. However, if a certain test requires a high resolution and this test is mostly performed in the tunnel, it is generally better to accept the lower load range to obtain higher resolution and higher accuracy. These considerations must be made for all components to ensure a balance with the best

Table 8.3 Determination of maximum combined load for an internal balance

			Wind axis system							Model axis system					
Test type	q	A	C_x	C_y	$C\ldots$	Drag	Side force	$F\ldots$, $M\ldots$	max α, β, γ	F_x	F_y	F_z	M_x	M_y	M_z
	(Pa)	(m^2)				(N)	(N)	(N), (N m)	(deg)	(N)	(N)	(N)	(N m)	(N m)	(N m)
Transporter															
Landing															
Cruise															
Combat															
Other															

fit of the load range for the normal operation of the tunnel.

For an internal balance the available space is a major concern. The available space for balances is restricted by the diameter of the fuselage. As transport aircraft become larger, the scale for models also become larger, complicating matters since the cross sections of wind tunnels have not grown at the same rate as the aircraft. As a result the available diameter for internal balances has become smaller.

For combat aircraft the loads in relation to the available space inside the model are very high. This is the case since wind-tunnel tests for this type of aircraft are mostly performed in pressurized wind tunnels to obtain the correct Mach number. The high static pressure leads to relatively high loads on the model in comparison to tests at atmospheric pressure.

These two effects lead to higher specific loads on the balance, making it much more complicated to develop a balance with high accuracy. Therefore the definition of the load ranges and the definition of the available space must be performed very carefully to ensure a high-quality balance design.

The specification for an internal balance should therefore be made related to the model and the loads on this model during the tests, and not on the tunnel capabilities themselves. If these specifications are not carefully performed, the internal balances will provide insufficient sensitivity and accuracy for the tests.

Unlike an external balance, where some of the components are always fixed to the wind axis system, the internal balance always measures the loads in the model axis system and therefore the lift and drag are always a combination of the axial and normal forces. Because of this, the angle of attack at which maximum loading occurs must be taken into account. For combat aircraft maximum loads can act at an angle of attack as high as 40°, whereas the maximum forces for a clean transport aircraft occur in and around an angle of attack of 15°.

Because an internal balance is mounted inside the model and does not change in orientation relative to the model itself, no maximum single load occurs. For different test setups (transporter, combat, high lift, cruise condition, etc.) different maximum combined loads occur, so it is also useful to prepare a table to determine the maximum combined loads on the balance.

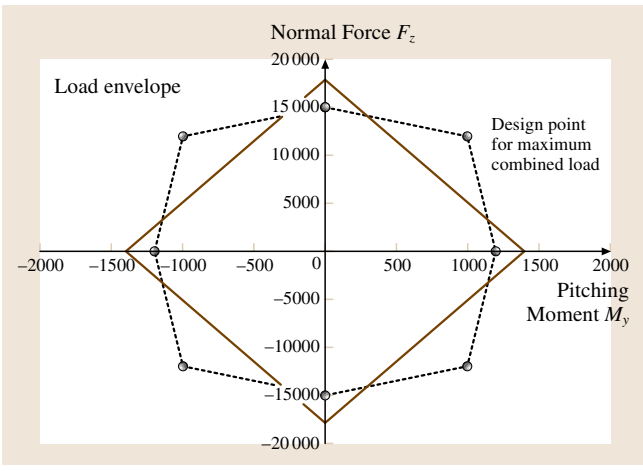

Fig. 8.8 Load rhombus and load trapeze

Maximum Combined Load: Maximum Single Load

The definition of the maximum load can differ between a combined load acting simultaneously, termed the maximum combined load, and a maximum load acting alone, defined as the maximum single load. The maximum single load forms a load trapeze, which does not automatically cover the test requirements (Fig. 8.8). The maximum combined load specifies the load range for the balance design. Usually single loads do not occur in wind-tunnel testing. Combined loads stress the balance in a much more complicated way, so the stress analysis of the balance has to take this situation into account. With the combination of only two loads the balance usually can carry higher loads than defined by the maximum combined loading. To estimate which load can be carried for a given situation the balance manufacturer provides a loading diagram (load rhombus) which allows the test engineer to judge whether the load combination of the planned test is within the limits of the balance.

Which one of the aforementioned loads is used as the *full-scale load* depends on the balance manufacturer's philosophy. The user should specify the definition of the full-scale load, because by definition the relative uncertainty of the balance can vary by a factor of two without any difference in the absolute uncertainty. This is discussed in detail in the following section.

8.1.2 Basic Terms of Balance Metrology

In this section brief definitions are given of the terms used. Most of these terms are defined in some international standard such as the *Guide of uncertainties in measurement (GUM)* [8.1] or in the case of the United States, the American Institute of Aeronautics and Astronautics (AIAA) standards documented in *Assessment of Experimental Uncertainty with Application to Wind*

Tunnel Testing [8.2] and the *Calibration and Use of Internal Strain Gauge Balances with Application to Wind Tunnel Testing* [8.3].

Full-Scale Load or Output. Full-scale load or output can be interpreted in several ways. The most obvious definition is the maximum combined load or the signal corresponding to this load. It is also possible to define the full-scale load or output as the maximum of the single loads. The maximum single loads are usually much higher than the maximum combined loads, so uncertainties related to these values are much smaller than those related to the maximum combined loads. This has to be taken into account if balances from different manufactures are compared. However, for a particular wind-tunnel test the maximum of the single loads seldom occur and the use of maximum combined loads or signals as the full-scale reference yields much more realistic information about the accuracy of the balance.

Systematic Errors or Bias of an Instrument. Systematic errors are repeatable errors that occur at every measurement. If the cause of a systematic error can be detected, it can be eliminated by calibration or compensation. If the source of a systematic error cannot be detected under repeatable conditions it is then simply accepted as the difference between the measured value and the true value.

Random Errors. Random errors are defined as the difference between the mean value of an infinite number of measurements under repeatable conditions and a single measurement. The value of the random error is equal to the difference between the total error minus the systematic error.

Resolution. Resolution is the smallest value that can be detected by a balance. Similarly it can be defined as the smallest detectable difference between two loads. The maximum resolution should be in the range of 0.005% of the full-scale load. For a normal wire strain gauge, resolution in this range is not a problem and the limits of the resolution are given by the measuring equipment. Good equipment today offers a resolution of less than 0.0003% of the full-scale load. Effectively the more money one spends on the equipment, the better the obtainable resolution.

Repeatability. If a certain balance loading is repeated after a certain amount of time, the repeatability is measured as the difference in the two signals. This is a very important characteristic for a balance, since many tests in a wind tunnel compare different model configurations. Most often wind-tunnel tests cannot exactly reproduce conditions found in reality. This means that, if the test itself does not represent reality yet the engineers attempt to compare the difference between two designs under wind-tunnel test conditions, the extrapolation of results to reality can be very challenging. Repeatability can be as good as the resolution but is usually worse. The repeatability of a good balance is in the range of 0.005% of the full-scale load. Repeatability also depends on time, so it is distinguished between short-term repeatability, for example between two wind-tunnel runs, and long-term repeatability, which is for example the difference between two complete wind-tunnel installations. Both short- and long-term repeatability are of equal importance since the loads on a new aircraft as well as the loads on an older aircraft design must be measured with the same accuracy as the differences between the new model configurations. The main challenge is often the discrepancy in the flow parameters between the model and reality, especially the Reynolds number. Most of the uncertainty in the force prediction on real aircraft is then caused by this Reynolds-number gap; therefore relative measurements to the model of an older aircraft design are used to reduce this level of uncertainty.

Interactions and Interference. One of the major systematic errors of a wind-tunnel balance is caused by the interactions or interference of the model with surrounding components. For example, the sensor measuring the axial force might also pick up the loads from other components. This additional signal can be several percent of the measured axial force signal. As mentioned above, such a systematic error can be corrected through proper calibration.

Accuracy. The term accuracy is very broad and generally describes the agreement between the measured data, in this case the wind-tunnel test data, and the true value that will be measured in the flight test after wind-tunnel testing is completed. There are many influencing factors, such as the measurement of static and dynamic pressure, wall and sting interactions, the precision of the model geometry, flow quality, angle of attack and balance uncertainty. Since there are so many potential errors, it becomes difficult to specify the accuracy for a wind-tunnel test. Balance uncertainty alone must be taken into account through balance calibration.

Absolute Error and Uncertainty. The absolute error is defined as the difference between the real load acting on the model (the true value) and the load detected by the balance. Normally the true value is unknown; therefore in practice a *conventional true value* is used. Besides all the error sources in the instrumentation and the balance, the error of the load measurement is strongly influenced by the balance calibration, since in this process the relation between the signals of the balance and the true loads are determined. According to the *Guide to the Expression of Uncertainties in Measurement* [8.1], often abbreviated as GUM, the absolute error is defined as the uncertainty of the measurement and can be given as the experimental standard deviation of the whole process. For a given wind tunnel test the uncertainty of the measured data is not only dependent on the measurement of the loads, but also influenced by the measurement of the angle of attack, the dynamic pressure, the model geometry, the flow quality and all the instrumentation which are used to determine the aerodynamic performance and associated derivatives. Regarding the desired precision of the test result, minimum requirements for the load measurement can be estimated from flight test data of an existing aircraft.

Accuracy Requirements. The requirement placed on accuracy is a function of the price of the balance. If a balance is specifically designed and built for one particular set of wind-tunnel tests, it should be only as accurate as those tests require. This is however not usually the case. The high cost of balance construction usually restricts a given tunnel to a small number of balances, which should ideally cover the range of test capabilities for that particular tunnel. An estimate of the maximum required accuracy for the development of transport aircraft [8.4, 5] can be made by defining which differences between a developed aircraft and the new aircraft are to be investigated. The usual outcome of such an accuracy requirement study is that the balance must be able to measure a difference of 1–2 drag counts, which is equal to an accuracy requirement of the balance of better than 0.07% to 0.1% of the full-scale load. This value is a global one yet should be specified for every new test setup.

8.1.3 Mounting Variations

When using external balances, there are many different possibilities for mounting the models. For example, a full model aircraft can be supported by a three-sting arrangement (Fig. 8.9) or a central sting (Fig. 8.10). For cars and buildings more than three supports are sometimes necessary. The external balance support system should provide for as many arrangements as possible.

The struts on the wing support the model at the quarter-chord positions and carry most of the load, except for the pitching moment, which is balanced by the strut at the tail of the model. All links to the model are jointed around the y-axis, so that a vertical movement of the tail strut allows for easy variation of the angle of attack. Yaw angles are set by moving the whole setup on the turntable.

Using the central-sting mounting the model is fixed inside the fuselage in all directions. The adjustment of the angle of attack is done through y-axis mechanism inside the fuselage. All loads must be carried by this

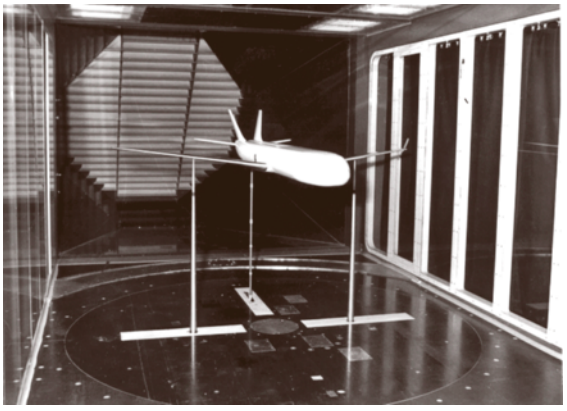

Fig. 8.9 Three-sting mounting on external balance

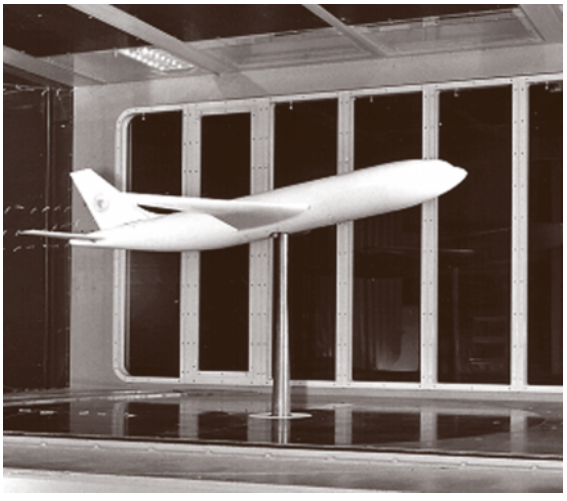

Fig. 8.10 Centre-sting mounting on external balance

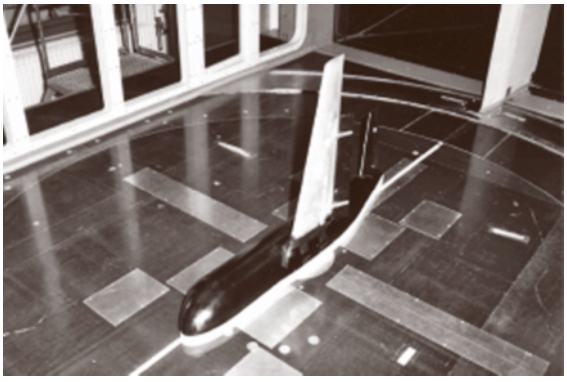

Fig. 8.11 Semi-span models on external balance

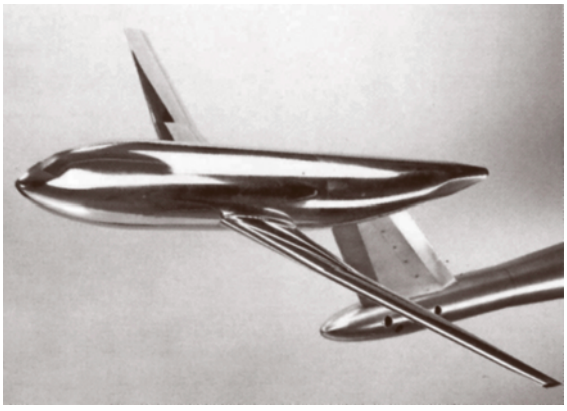

Fig. 8.12 Tail sting with fin attachment on lower side

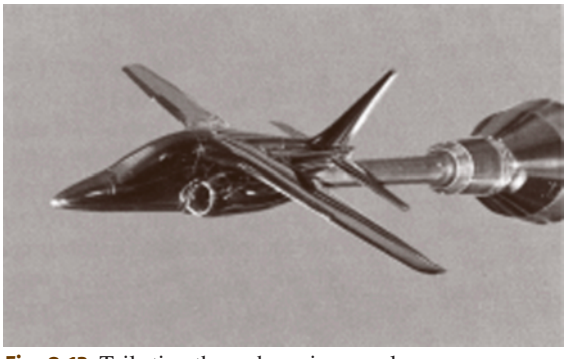

Fig. 8.13 Tail sting through engine nozzle

support and therefore it must be very rigid to minimize dynamic movements of the model during testing.

Semi-span models (Fig. 8.11) are used to increase the effective Reynolds number of the tests by increasing the geometry of the model. Besides the higher Reynolds number, the lager model size makes models with variable flaps and slats much easier to construct, thus semi-span models are often used for testing of take-off and landing configurations.

Fig. 8.14 Twin-sting rig with dummy tail sting

The most common setup using an internal balance is the back-sting arrangement (Fig. 8.13), in which the sting is attached through the after body of the fuselage. In some cases the vertical fin (Fig. 8.12) is also used to support the model.

For tests that require free flow around the after body two-sting setups (Fig. 8.14) can be used. In such cases one balance is needed inside each sting. To determine the influence of the tail sting two measurements are performed, one with a dummy tail sting and one without the dummy tail sting in place.

Today the support of the model by wires is seldom used anymore (Fig. 8.15). In such cases the balance must be an overhead external balance and the model hangs from the balance through wires. To keep the model stabile in the tunnel, the system must be preloaded by weights (Sp), which are usually dampened in a water basin under the test section. The advantage of such a model support is the very low interference on the flow around the model.

In Fig. 8.15 the model hangs upside down in the tunnel, minimizing the preload. This is beneficial since the balance cannot measure loads smaller than the preload. Sometimes modern wind tunnels test the model in an upside-down position in order to preload the balance in the lift direction. This way the lift generated by the model contributes to the preload such that the balance signal does not pass through zero as in a normal setup. In such a way the additional nonlinearities associated with the zero-load regime can be avoided.

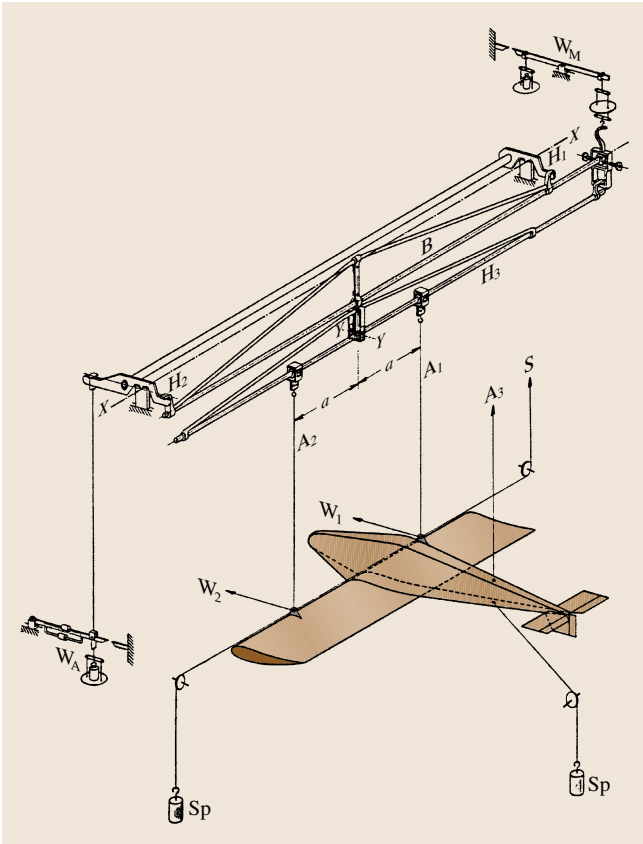

Fig. 8.15 Wire-supported model on overhead external balance

Mounting Interference

The aerodynamic loads on the model itself are always affected by the presence of the model mounts. The mounting loads themselves are subtracted from the model loads by performing tests without the model in place. The second effect to be considered is the influence of the mounts on the flow field around the model and the influence of the model on the flow field around the mounts. A complete separation of the effects is not possible. Therefore it is not possible to eliminate the influence of the model–mount interference completely. Several methods for the compensation of model–mount inference are described in [8.6].

8.1.4 Strain Gauges

Strain Gauge Fundamentals

The basic technique to measure forces with any kind of wind-tunnel balance is the measurement of the strain on an elastic spring that is deformed by the aerodynamic loads acting on the wind-tunnel model. In this chapter the fundamentals of strain measurement and strain sensors are described. For wind-tunnel balances two major types of strain sensors are used. The most commonly used is the wire strain gauge sensor. Also of importance is the semiconductor strain gauge.

The wire strain gauge is based on an electromechanical effect developed by *W. Thomson (Lord Kelvin)* in 1856. Thomson measured the electrical resistance of a metal wire and found that it could be correlated to the strain in the wire while stressed.

This effect was subsequently used by *E. Simmons* (Caltech) and *A.C. Ruge* (MIT) in 1938 in the development of the wire strain gauge. Simmons was the first to build a force transducer based on the wire strain gauge technique while Ruge used his wire strain gauges to perform experimental stress analyses. Ruge's strain gauge was very successful since it was cheap and easy to handle. Industry needed many of them such that in 1952 a technique was patented to produce the foil strain gauge in great numbers. No longer was a wire glued onto a carrier foil. Rather a thin metal foil was glued onto the carrier and the contour of the wire was etched out of the metal foil by a photochemical process. This technique is still used today to produce the foil strain gauge sensors, as it produces very precise sensors with high resolution at a low price [8.7, 8].

The physical principle of a wire strain gauge is that a change in electrical resistance is produced when a strain is applied to the gauge. The electrical resistance of a wire can be written as:

$$R = \frac{\rho l}{A} , \tag{8.1}$$

where R is the resistance of wire, l the length of the gauge grid, A the cross section of the wire and ρ the specific electric resistance.

The specific electric resistance is given as:

$$\rho = \frac{2 m v_0 A l}{N_0 e^2 \lambda} , \tag{8.2}$$

where m is the mass of an electron, v_0 the velocity of the electrons, N_0 the number of free electrons, e the charge of an electron and λ the free wavelength of the electrons. With the above equation for the specific electric resistance, the resistance of a wire can be formulated as:

$$R = \frac{2 m v_0 l^2}{N_0 e^2 \lambda} . \tag{8.3}$$

The relative change of the resistance of the wire is given by the following partial differential equation:

$$\frac{\mathrm{d}R}{R} = \underbrace{\frac{2\,\mathrm{d}l}{l}}_{\text{Influence of size}} + \underbrace{\frac{\mathrm{d}v_0}{v_0} + \frac{\mathrm{d}m}{m} - \frac{\mathrm{d}N_0}{N_0} - \frac{\mathrm{d}\lambda}{\lambda} - \frac{2\,\mathrm{d}e}{e}}_{\text{Piezoresistive effect}} . \tag{8.4}$$

The relative change of the length is related to the strain ($\varepsilon = \mathrm{d}l/l$). With subsequent substitution into (8.4):

$$\frac{\mathrm{d}R}{R} = 2\varepsilon + \frac{\mathrm{d}v_0}{v_0} + \frac{\mathrm{d}m}{m} - \frac{\mathrm{d}N_0}{N_0} - \frac{\mathrm{d}\lambda}{\lambda} - \frac{2\,\mathrm{d}e}{e} . \tag{8.5}$$

The relative changes in the mass ($\mathrm{d}m/m$) as well as the changes in the charge of the electrons ($\mathrm{d}e/e$) are equal to zero such that the sensitivity (k) of a strain gauge is defined as the relative change of the resistance divided by the strain. Then the sensitivity of a wire is given by the following equation:

$$k = \frac{\mathrm{d}R}{R\varepsilon} = 2 + \frac{1}{\varepsilon}\left(\frac{\mathrm{d}v_0}{v_0} - \frac{\mathrm{d}N_0}{N_0} - \frac{\mathrm{d}\lambda}{\lambda}\right) . \tag{8.6}$$

From the above equation it can be seen that the sensitivity of a wire is equal to two plus a term which itself is dependent on the strain. From real strain gauges it is known that the gauge factor is around two and constant. So for an ideal grid material the second term of (8.6) must be equal to zero such that the gauge factor remains at a value of two. For the application of strain gauge balances such gauges with a gauge factor of two are used:

$$\frac{\mathrm{d}R}{R} = k\varepsilon . \tag{8.7}$$

8.1.5 Wiring of Wheatstone Bridges

The relative changes of the electric resistance of a strain gauge are very small. For example a signal from a 1 mV/V strain gauge with a resistance of 350 Ω would be on the order of 0.0875 Ω. Such a signal must then be measured with an accuracy of 8.75 μΩ or better. For direct measurements this would require a resistance measurement instrument with a resolution of more than 40×10^6 parts. Such an instrument even today does not exist. In 1843, *Charles Wheatstone* developed a method to directly measure the small relative changes of an electrical resistance, the so-called *Wheatstone bridge*. Four resistors of the same nominal resistance value are arranged as shown in Fig. 8.16. The layout consists of two parallel pairs of resistors in series.

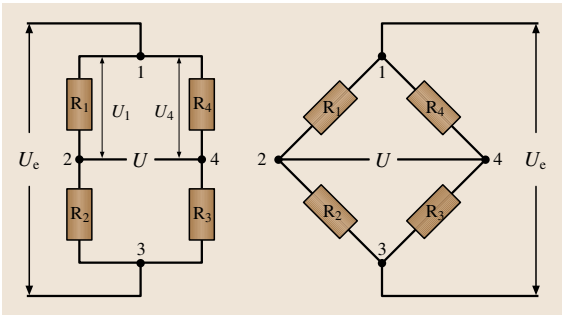

Fig. 8.16 Wheatstone bridge circuit

There is no common rule for the numbers of the resistors in Fig. 8.16. However, all equations that follow in this section are based on the numbering system found in the above figure and are valid if the following criteria are fulfilled.

1. The order of the numbers are arranged either in the clockwise or counterclockwise direction.
2. The excitation voltage is applied between points 1 and 3 and the output signal (U) is measured between points 2 and 4.

When excitation voltage is applied at points 1 and 3 the resistors R_1 and R_2 as well as resistors R_3 and R_4 each form a voltage divider. The voltages U_1 and U_4 can be described by the following equations:

$$U_1 = \frac{R_1}{R_1 + R_2} U_\mathrm{e} \quad \text{and} \quad U_4 = \frac{R_4}{R_3 + R_4} U_\mathrm{e} . \tag{8.8}$$

The difference between these two partial voltages is the voltage U, which is given by

$$U = U_1 - U_4 = \left(\frac{R_1}{R_1 + R_2} - \frac{R_4}{R_3 + R_4}\right) U_\mathrm{e} . \tag{8.9}$$

The relative change of the voltage U to the excitation voltage U_e is

$$\frac{U}{U_\mathrm{e}} = \left(\frac{R_1}{R_1 + R_2} - \frac{R_4}{R_3 + R_4}\right) , \tag{8.10}$$

$$\frac{U}{U_\mathrm{e}} = \frac{R_1 R_3 - R_2 R_4}{(R_1 + R_2)(R_3 + R_4)} . \tag{8.11}$$

It can be seen that the ratio of these two voltages, U/U_e, is proportional to the ratios of the resistances, but $U = 0$ if:

1. every resistor has the same value, i. e., $R_1 = R_2 = R_3 = R_4$,
2. the ratio $R_1/R_2 = R_4/R_3$.

If these criteria are satisfied then the bridge is termed *balanced*.

In the case of strain gauge measurements the resistors R_1 to R_4 are the strain gauges themselves, including the resistance changes of the gauges by the strain. For this case the resistors R_1 to R_4 in (8.11) are replaced by the initial resistance plus a resistance change ΔR_1 to ΔR_4 such that (8.11) can be written

$$\frac{U}{U_e} = \left(\frac{R_1 + \Delta R_1}{R_1 + \Delta R_1 + R_2 + \Delta R_2} - \frac{R_4 + \Delta R_4}{R_3 + \Delta R_3 + R_4 + \Delta R_4} \right) . \quad (8.12)$$

The relationship between the ratio of the voltages U/U_e and the ratio of the resistances $\Delta R_i/R_i$ is nonlinear. The nonlinearity can be around 0.1% if only one resistance changes. This is too large an error for a precision force transducer and therefore these nonlinearities cannot be neglected if only one strain gauge is used in the force transducer. This is the reason why most strain-gauge-based transducers use four active gauges instead.

For the case of a *full bridge*, as it is called when four gauges are active, the nominal values of the resistors R_1 to R_4 are the same and the changes in the resistances are very small, such that higher-order terms can be neglected and the (8.12) can be simplified to a linear equation:

$$\frac{U}{U_e} = \frac{1}{4} \left(\frac{\Delta R_1}{R_1} - \frac{\Delta R_2}{R_2} + \frac{\Delta R_3}{R_3} - \frac{\Delta R_4}{R_4} \right) . \quad (8.13)$$

The relation between the relative change of the resistance and the strain was found to be $\Delta R/R = k\varepsilon$ in (8.7). Now the linear relation between the relative change of the bridge output and the strain becomes:

$$\frac{U}{U_e} = \frac{1}{4} (\varepsilon_1 - \varepsilon_2 + \varepsilon_3 - \varepsilon_4) . \quad (8.14)$$

This equation is the basis for all strain-gauge-based measurement.

In this equation it can be seen that the relative resistance change or the strain in the bridge arms ε_2 and ε_4 is subtracted from the relative changes in the bridge arms ε_1 and ε_3. We now define tension to be a positive change of strain, e.g., a positive relative change of the resistance. If we form a full bridge with gauges that do have all the same tension ($\Delta R_1 = \Delta R_2 = \Delta R_3 = \Delta R_4$) no output will be measured at this bridge. As a consequence, for a force transducer we always need the strain situation to consist of two tension and two compression gauges. Such a configuration favors bending- or torsion-type transducers in force balances.

Influence of Bridge Wires

The influence of the bridge wiring can be explained by adding an imaginary wire resistance R_{wi} to every arm of the bridge (Fig. 8.17).

If it is assumed that the gauge resistance does not change ($\Delta R_i = 0$), then (8.13) can be rewritten as:

$$\frac{U}{U_e} = \frac{1}{4} \left(\frac{R_{w1}}{R_1} - \frac{R_{w2}}{R_2} + \frac{R_{w3}}{R_3} - \frac{R_{w4}}{R_4} \right) . \quad (8.15)$$

From this equation it can immediately be observed that the wires have no influence if their lengths are absolutely identical ($R_{w1} = R_{w2} = R_{w3} = R_{w4}$). This is difficult to achieve. Another possibility is to have two pairs of wires with equal lengths, i. e., $R_{w1} = R_{w2}$ and $R_{w3} = R_{w4}$. In this case the bridge is not unbalanced by the influence of the wiring such that the bridge zero output (no resistance changes in the gauges) is close to zero.

Compensation of Bridge Zero Output

An unloaded force transducer in its normal mounting position and without any load applied should have no output. Mostly this cannot be achieved even if the gauge and the wire resistances are the same, because some output is generated by the weight of the metric end of the transducer itself, causing deformation in the transducer. However, the primary reason for the bridge zero output is the difference in the nominal resistance of the strain gauges.

Looking at a data sheet of a normal foil strain gauge, the bandwidth of the initial resistance is as high as 0.4% of the nominal value. For example in the worst case the zero output of a bridge with a nominal resistance of 350 Ω is 4 mV/V, which is much higher than the signal achievable for a full-scale transducer (usually 2 mV/V).

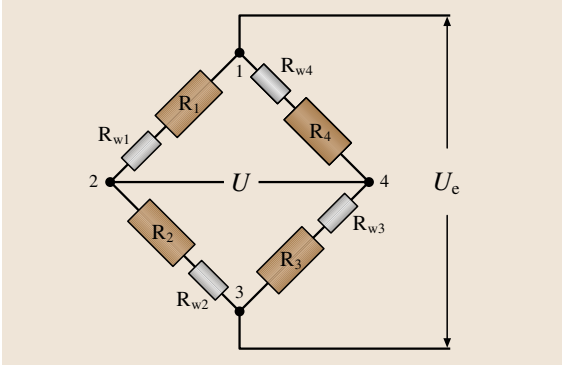

Fig. 8.17 Wheatstone bridge with imaginary wire resistances R_{wi}

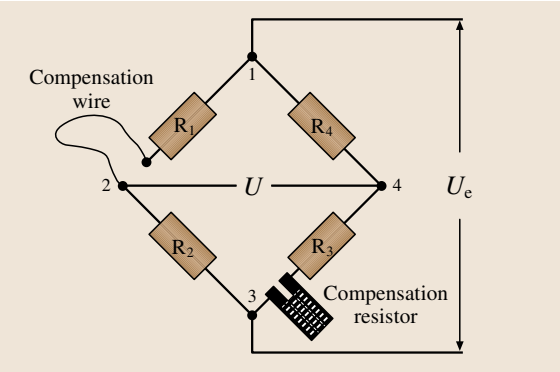

Fig. 8.18 Zero output compensation with constantan resistors

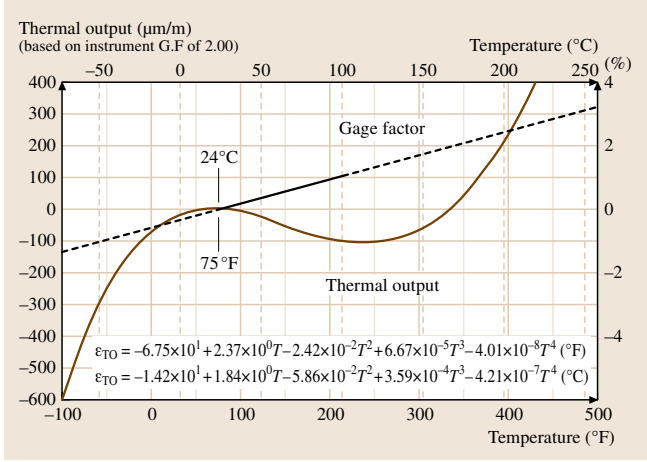

Fig. 8.19 A typical strain gauge apparent strain curve

If a strain gauge amplifier can be applied in the range up to 6 mV/V, or if the offset can be set to zero, then all problems would be resolved. However, with high-precision amplifiers this is not achievable and the zero output must be compensated to values lower than 5% of the nominal output. In order to do this the transducer or the balance must be set to its normal working position. In this position the output of the bridge must be measured and a compensation resistance must be calculated according to the following equation:

$$\Delta R_{\text{comp}} = \frac{U_0}{U_e} R_{\text{nominal}} , \qquad (8.16)$$

where R_{nominal} is the nominal resistance of the bridge and U_0/U_e is the zero output of the bridge. If a constantan wire for zero compensation is used, the length of the constantan wire must be calculated as follows:

$$L_{\text{const}} = \frac{U_0}{U_e} \frac{R_{\text{nominal}}}{R_{\text{wire}}} , \qquad (8.17)$$

where R_{wire} is the resistance per unit length of the constantan wire. Alternatively, commercially available adjustable resistors can be inserted into the bridge. In which bridge arm the compensation resistor must be installed depends on the sign of the zero output. If the zero output is negative the compensation resistor must be added into the arm which generates positive signals in the bridge and vice versa if the zero output is positive.

8.1.6 Compensation of Thermal Effects

Compensation of Zero Drift

Zero drift is defined as the change in the bridge zero output at different stable temperature conditions. It is important to have stable uniform temperature conditions, since temperature gradients inside the transducer can cause a much higher bridge output than the zero drift itself. Under stable conditions the zero drift is caused by the change in the resistance of the grid, the different heat expansion coefficients of the foil and the base material on which they are bonded. The cause of this temperature sensitivity is a combination of the direct resistance change as a function temperature as well as a real strain, which is applied to the gauge though no load is acting on the transducer. For a single gauge this output is called the *apparent strain*. Apparent strain curves are provided by the strain gauge manufacturer; a typical data sheet can be seen in Fig. 8.19.

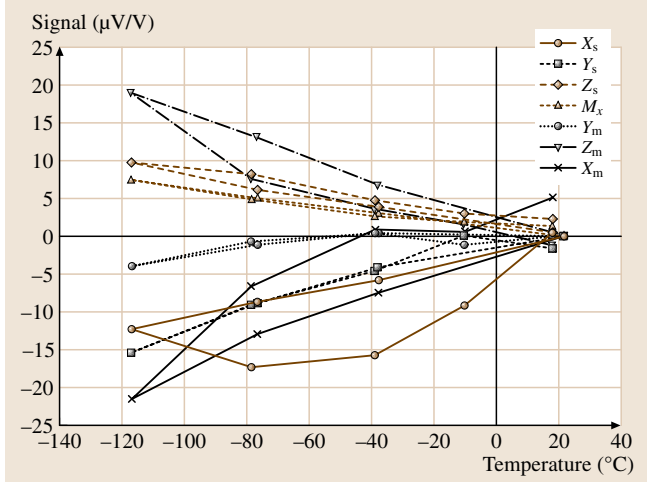

Fig. 8.20 Balance zero drift with matched gauges

For a single gauge this apparent strain is usually much higher than the zero drift of a full bridge, because at a stable uniform temperature level all four strain gauges have nearly the same apparent strain, thus canceling the effect out. This is another very important reason to use only full bridges for a general transducer or wind-tunnel balance. In Fig. 8.20 the zero drift of the balance bridges are shown where *matched gauges* are used for each bridge. This means that for every bridge four gauges were selected out of a large number to ensure that they have nearly the same apparent strain curve. This in turn minimizes the zero drift to $0.15\,\mu V/(V\,K)$. In this case selection was necessary, since the balance is operated over a large temperature range. Even for operating temperatures around ambient conditions such a selection process minimizes the zero drift to very low values.

Using matched gauges in a Wheatstone bridge is a complicated method to minimize zero drift. If the operating temperature is in the range of $-10\,°C$ to $60\,°C$, compensation with the addition of temperature-sensitive wires or prefabricated temperature-sensitive resistors is much easier. Copper wires or copper resistors are mostly used in this case.

The first step in such a compensation setup is to perform a temperature run with the unloaded balance in the normal setup position. Each temperature level has to be very stable and the temperature distribution must be uniform throughout the balance. This cannot always be easily accomplished, however every temperature gradient inside the balance causes internal mechanical stresses and their associated output signals do not belong to the zero drift of the bridge. Gradient effects are not repeatable if the model changes and a correction that includes such internal gradient effects will fail later when the setup is again changed.

After obtaining the zero drift for each bridge there are two methods to follow on with.

The first possibility is the determination of a compensation resistor using the following equations:

$$\left(\frac{\Delta R}{\Delta T}\right)_{\text{comp}} = \frac{U}{U_e}\frac{1}{\Delta T_{21}} R_{\text{nominal}}\,, \tag{8.18}$$

$$R_{\text{comp}} = \left(\frac{\Delta R}{\Delta T}\right)_{\text{comp}} \alpha_{\text{comp}}\,, \tag{8.19}$$

where ΔT_{21} is the difference in temperature between the lowest and the highest measured temperatures, $\Delta U/U$ is the change of the bridge signal due to the temperature change, R_{nominal} is the nominal bridge resistance, α_{comp} [1/K] is the coefficient of the resistance change of the material which is used for compensation and R_{comp} is the required resistance for the compensation. The compensation resistor must be included into the Wheatstone bridge wiring as shown in Fig. 8.18 and the resistor must be cut according to the instructions of the manufacturer.

The second possibility is to install a temperature-sensitive wire instead of a prefabricated resistor. If this method is selected then in a third step the length of the compensation wire must be calculated:

$$L_{\text{comp}} = \left(\frac{\Delta R}{\Delta T}\right)_{\text{comp}} \alpha_{\text{comp}} R_{\text{wire}}\,, \tag{8.20}$$

where L_{comp} is the length and R_{wire} [Ω/m] is the resistance per unit length of the compensation wire. Materials such as copper, nickel or Balco® are most often used. For optimal results the materials data should be used from the supplier and not from handbook data. The compensation wire must be installed into the bridge circuit as shown in Fig. 8.18. The compensation resistor must be added into the bridge arm which has a lower resistance when the temperature changes.

8.1.7 Compensation of Sensitivity Shift

Sensitivity shift is defined as the change in sensitivity of a transducer as a function of temperature. There are three causes for the change in sensitivity of a strain-gauge-based force transducer. The first is the change of the geometry of the transducer body caused by thermal expansion or contraction. The second cause is the change of the transducer stiffness due to Young's modulus as a function of the temperature. The third cause of the change in sensitivity is the change in the gauge factor as a function of temperature.

To demonstrate this point, the sensitivity shift is calculated for a cantilever beam with length l and rectangular cross section of $b \times h$, loaded by a force F as shown in Fig. 8.21.

The sensitivity of this transducer is defined as the ratio of the signal $(\Delta U/U)$ to the applied force (F)

$$\frac{\Delta U/U}{F} = \frac{k\varepsilon}{F}\,. \tag{8.21}$$

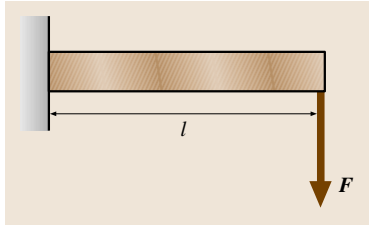

Fig. 8.21 Cantilever beam as a representative force transducer

The strain ε under the strain gauge is given by the equation: $\varepsilon = \sigma / E$, where σ is the mechanical stress under the strain gauge and E is the Young's modulus for the cantilever beam material. The stress σ can be calculated by using the following equations: $\sigma = M_\mathrm{b}/W_\mathrm{b}$, $M_\mathrm{b} = Fl_\mathrm{DMS}$ and $W_\mathrm{b} = bh^2/6$, where l_DMS is the distance from the tip of the beam to the location of the strain gauge.

Applying the above equations, (8.21) becomes

$$\frac{\Delta U/U}{F} = \frac{k}{E}\frac{6l_\mathrm{DMS}}{bh^2} \,. \tag{8.22}$$

On the right-hand side of (8.22) all parameters are a function of the temperature. It can be seen now that the sensitivity shift depends on the gauge factor, the Young's modulus and the geometry of the transducer. The change in the dimensions of the cantilever beam can be written $\Delta l_i = l_i \alpha_\mathrm{T} \Delta T$, such that the dimensions after the change in temperature are $l_i(T) = l_i + \Delta l_i$. Applying this to all geometric parameters in (8.22), the equation for the sensitivity temperature dependence becomes:

$$\frac{\Delta U/U}{F} = \frac{k(T)}{E(T)}\frac{1}{(1+\alpha_T \Delta T)^2}\frac{6l_\mathrm{DMS}}{bh^2} \,. \tag{8.23}$$

For the correction of the sensitivity shift there are two major results given by (8.23).

First, compensation is only possible if the gauge factor changes in the same direction as the Young's modulus of the cantilever material. This requirement can only be fulfilled by strain gauges using *Karma*® or an equivalent alloy, because the Young's modulus decreases as the temperature rises. Constantan behaves in the opposite way, so that it is impossible to compensate the sensitivity shift of a strain gauge transducer with constantan gauges.

Second, a perfect compensation can only be performed if the geometric effect is also compensated by the gauge factor variation. The consequence of this is that, for transducers with different geometries, different gauge factor drifts are necessary. The main difference appears if a bending-stress-type versus a shear-stress-type transducer is used. The influence of the geometry on a shear-stress-type transducer is bigger than that on a bending-stress-type transducer.

Typically the strain gauge manufacturers offer modulus-compensating (MC) strain gauges for the most common applications. This is done in order to compensate the main sensitivity shift caused by the Young's modulus change. The disadvantage of an MC gauge is that no self-temperature-compensation option can be chosen at the same time.

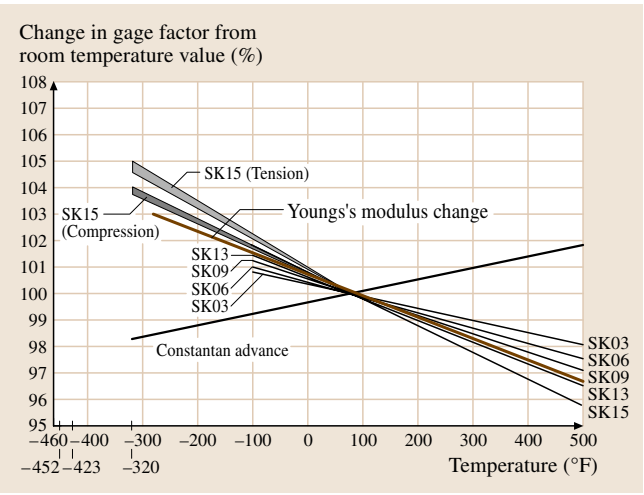

Fig. 8.22 Gauge factor shift of Karma and constantan

Another possibility is to change the excitation voltage in the same direction as the sensitivity shift change. In (8.21) it can be seen that the relative change of the signal stays constant. To achieve this, a temperature-sensitive resistor is integrated into the excitation voltage line of the bridge near the strain gauges, as shown in Fig. 8.23.

To determine the length of the compensation wire (l_wire) the following equation is used:

$$l_\mathrm{wire} = \left(\frac{S_0}{S_\mathrm{T}} - 1\right)\frac{RA}{\alpha_\mathrm{R}\Delta T \rho} \,, \tag{8.24}$$

where

S_0 [mV/V] = signal measured with force F acting at the reference temperature T_0 [K] and excitation voltage U_e [V],

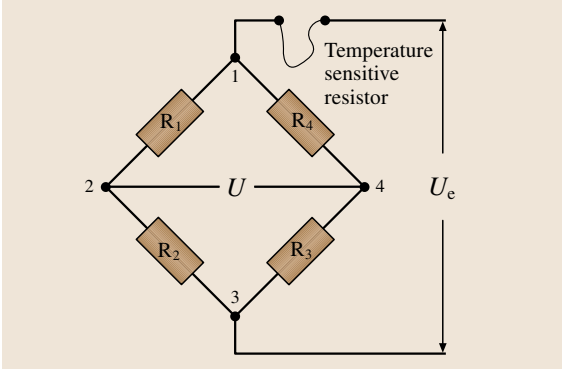

Fig. 8.23 Wheatstone bridge with sensitivity-shift compensation

S_T [mV/V] = signal measured with the same force F acting at the temperature T [K] and excitation voltage U_e [V],
R [Ω] = nominal resistance of the bridge,
A [m^2] = cross section of the wire,
α_R [1/K] = thermal expansion coefficient of the wire material,
ΔT [K] = temperature difference between the two tests,
ρ [Ω m] = specific electrical resistance of the wire material.

8.1.8 Strain Gauge Selection

The strain gauge selection process is very important in the design phase of a force transducer or balance. Many problems down the road can be avoided through the careful selection of strain gauges. The selection of the optimum strain gauge for a given transducer is an iterative process, moving between the requirements of the transducer and the characteristics of the available strain gauges.

As mentioned in Sect. 8.1.7, when using strain gauge balances gauges with a chrome–nickel alloy (*Karma*®, *Modco*®) should always be selected to achieve good sensitivity shift compensation. The gauges should be ordered from the same batch, which means they were manufactured with the same process and on the same sheet. Additionally they should be preselected to have a minimum difference of less than 0.05% in their nominal resistance.

The size and type of stress field to be measured by the gauge are the first determining factors for the gauge selection. To minimize the influence of stress concentrations, low-gradient strain fields are required. Usually the areas that fulfill this requirement are relative small, and so small gauges must be used. Sometimes on small balances even the smallest gauge does not fit on such an area without the need to cut the carrier foil.

On the other hand the excitation voltage should be as high as possible to get a high output signal. However, high excitation voltages will heat up the gauge and this will produce associated errors. Strain gauge manufacturers provide the diagrams that can be used to determine the maximum excitation voltage for a combination of the selected strain gauge area and spring material. In general, transducer materials with high heat conductivity and a gauge pattern with a large grid area allow higher excitation voltages.

It is always good practice to choose gauges with a high nominal resistance. The self-heating effect is relative small since at a constant excitation voltage the current through the bridge is lower and therefore the heating power of the gauge must be lower as well. Another advantage is the lower influence of the bridge wire thermal effects on the signal caused by the high ratio of bridge wire resistance to bridge resistance. Lastly, high-resistance gauges are small and fit into strain fields with small strain gradients. A disadvantage of high-resistance gauges is that the wires that are need to compensate zero, zero drift and sensitivity shifts must have relative high resistances too. This requires particularly thin wires that are not easy to handle.

With regard to gauge patterns, double gauges are preferred since their application is relatively simple and the two gauges sit perfectly parallel to each other. As the backing foil, fibre-reinforced epoxy laminate is the best choice for a wide temperature range and a high fatigue life. The solder dots on the gauge should be either pre-soldered or copper plated, since the chrome–nickel grid alloy needs an aggressive soldering flux in order to bind. This makes the attachment of the wires challenging and increases the risk of damage during wiring of the bridge. Welded lead wires out of copper–beryllium enables a higher fatigue life than those with copper.

8.1.9 Strain Gauge Application

The bonding of strain gauges onto the balance surface at first glance seems like a relatively simple process, however to achieve perfect adhesion requires a lot of experience. The strain gauge manufacturers themselves offer courses where all these bonding techniques can be learned. As well they provide precise instructions on how to use their adhesives and accessories. For the application of a balance or force transducer the use of adhesives supplied by the manufacturers is recommended, even if these are much more expensive than comparable ones on the market. Also important is not to apply such adhesives after their expiry date. Solvents and cleaning fluids must not be contaminated.

A study using experimental and numerical methods showed that most of the nonlinear interactions of an internal wind-tunnel balance are caused by the alignment errors of the strain gauges themselves. Consequently, near-perfect strain gauge positioning should be strived for. To minimize the errors associated with wire quality as well as to ensure durability, the wires should be as thick as possible. Stranded copper wire should be used in place of solid copper wire. As insulation *Teflon*® of *Kapton*® is preferable.

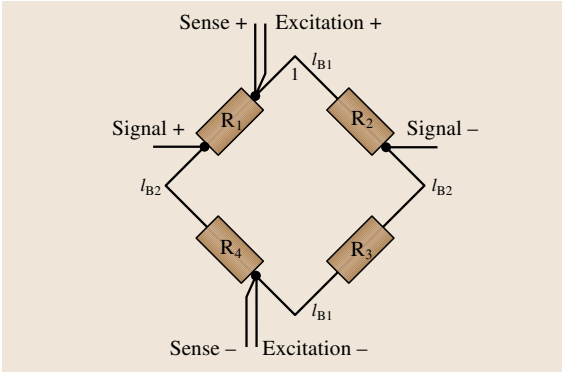

Fig. 8.24 Lead-wire connection locations

To minimize the resistance change associated with the wiring itself, either wires with equal lengths or two pairs of equal-length wire inside the bridge circuit must be used. The location of the lead wire connections can be seen in the following circuit diagram (Fig. 8.24).

8.1.10 Materials

Force transducers as well as balances are always constructed using metal. A list of often-used materials with their main physical and mechanical properties is given in Table 8.4. The selection of the material depends on the stress level and on the available space for the transducer. For high stress levels, high-strength tool steels, maraging steels, copper–beryllium or titanium are excellent materials. For low stress levels aluminum is a good choice. The material properties have a strong influence on the hysteresis, creep and repeatability characteristics of the force transducer. For the best results the yield strength of the material should be as far as possible away from the stress acting in the measurement section. Usually yield stress is three to five times higher than the stress felt by the strain gauge itself.

The mechanical properties that are of importance for the balance measurements, such as creep and hysteresis, are often not provided by the manufacturer. These properties depend on the heat treatment and the aging process. Sometimes to minimize hysteresis and creep it is advantageous to use a material with as low a tensile stress as possible. Again compromises must be made and often material tests must be made in-house. The machining process must be integrated into the heat treatment process to minimize internal stresses by forging and machining of the material. For maraging steel the integration of the manufacture into the aging process is shown in Fig. 8.25.

The time interval for each thermal step in the process depends on the material and the thickness of each part. For the best heat treatment results the instructions of the material supplier should be carefully followed. The steels that are used must be machined in an annealed condition. It is very important that electric discharge machining (EDM) is performed at this stage since EDM removes tensile stresses on and under the surface of the material. Such tensile stresses reduce the fatigue life of the balance under dynamic loads significantly. To further minimize this effect, the erosion period at the end of the EDM should be short.

The aging process will cause shrinking of the material. The dimensions of the joints, which have tight tolerances, must have an offset to allow final machining after the aging process. Grinding has nearly the same effect as EDM, so in areas with stress concen-

Table 8.4 Typical balance materials

Material	Short name	Material number	Yield stress	Tensile stress	Young's modulus	Shear modulus	Density	Coefficient of heat expansion
			(N/mm^2)	(N/mm^2)	(N/mm^2)	(N/mm^2)	(kg/m^3)	(µm/mK)
Maraging	X2 Ni Co Mo 18 8 5	1.6359	1760	1830	186000	71400	7920	11.6
Maraging	X2 Ni Co Mo 18 9 5	1.6354	1910	2010	191000	74600	8080	10.3
Maraging	X2 Ni Co MoTi 18 12 4	1.6356	2300	2400	190000	74600	8020	11.7
Maraging	X2 Ni Co Mo 18 8 3	1.6357	1430	1495	181300	68000	7920	9.0
Stainless	17-4-PH	1.4548	1170	1310	190000	75000	7780	10.0
Stainless	PH 13–8 Mo	1.4534	1150	1300	190000	75000	7760	10.0
Titanium	TI AL 6 V 4	3.7164	1000	1070	110000	43000	4430	8.6
Cu–Be	Cu Be 2	2.1247	1100	1500	123000	44000	8260	17.9
Aluminum	Al Cu Mg Mn	3.1354	300	430	72400	27600	2800	23.0
Aluminum	Al Zn Mg Cu Cr	3.4364	450	530	71000	27000	2800	23.0

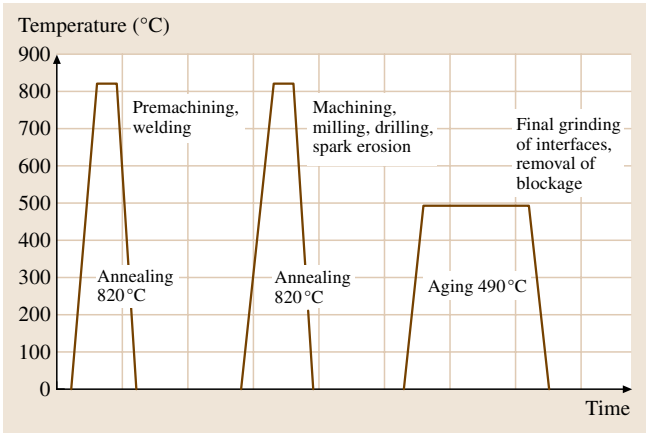

Fig. 8.25 Balance manufacture process for maraging steel

trations no grinding should be performed after the aging process.

Most steel used for balances can be machined in the annealed condition. Other materials, such as copper–beryllium, must be machined in their hardened state. The aging process of copper–beryllium causes high internal stresses, which is one reason why copper–beryllium has a high ultimate strength. The result of the aging process is the formation of large deformations, which must be corrected by machining. The advantages of copper–beryllium are the high heat conductivity, which minimizes temperature gradients inside the balance, and the low hysteresis and creep of the material.

The titanium alloy TiAl 6V4 is used in the aircraft industry for some highly loaded parts that cannot be built from aluminum. The heat conductivity is very low which forces careful cooling during machining. No heat treatment is necessary after the delivery of the material but it is very important to machine the material carefully to avoid internal stresses. Stress relief treatment can be done between 540 °C and 650 °C for about two hours, however resulting deformations may occur.

8.1.11 Single-Force Load Cells

In order to determine the forces on the model, the measurement of strain on a deforming body is needed. The strain on this body can be caused either by bending, shear or tensile stresses. In this section the different types of bending-, shear- and tensile-type single load cells are first discussed. Subsequently combinations of these types to a multicomponent force transducer will be discussed.

Bending-Type Load Cells

Load cells based on the measurement of the bending stress are the most frequently used. The main advantage of such load cells is that a bending moment always produces a positive and a negative stress of the same magnitude. This facilitates the application of a full Wheatstone bridge with a linear output and a reasonable signal magnitude. The simplest load cell is the cantilever beam, as shown in Fig. 8.26. Using this simple type of measuring beam as an example, the method to determine the dimensions of the transducer will be demonstrated.

The bending stress at the strain gauge location is defined as $\sigma_B = Fl/W_B$, whereas the measured strain is defined as $\varepsilon = \sigma_B/E$. The signal for the full bridge, with two gauges on the upper side and two gauges on the lower side, can be calculated as $\Delta U/U = k\varepsilon$. For steel ($E = 200\,000\,\mathrm{N/mm^2}$) with a gauge factor of about $k = 2$, a signal of about 2 mV/V should be strived for. In such a case the strain (ε) will be on the order of 1000 µD (microstrain = 1000×10^{-6} m/m) under the gauge or a stress of about $200\,\mathrm{N/mm^2}$. If these values are assumed, the dimensions of the gauged section can be derived from the equation $W_B = bh^2/6$. Commercially built transducers usually have a nominal signal of 2 mV/V. Some have a higher signal, but never more than 3 mV/V. All transducers designed for bending will be dimensioned using these aforementioned equations. The most challenging measurements are the bending moment (M_B) along with the section modulus (W_B). In most cases the equations for the bending moment and the section modulus are given by handbook formulas. The accuracy of these formulas is sufficient enough to determine the dimensions of a single force transducer.

These equations show that the force (F) is measured from the bending moment, such that the measured force also depends on the distance between the gauges and

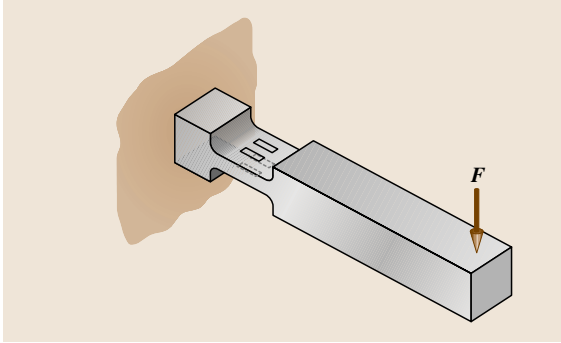

Fig. 8.26 Cantilever bending beam

the attachment point of the beam. If a force is not applied at the point where the calibration load is applied one will produce errors proportional to this misalignment. This problem can be overcome by using a different transducer design. Some possible designs are shown in Fig. 8.27. Their common design principle is that two bending beams should be coupled, forming a parallelogram. If the coupling element is stiff enough the load attachment point remains vertical, such that the transducer signal does not depend on the distance between this point and the gauge area.

Load cells that use the shear stress to determine either an applied force or a torque moment do have the same principle advantage that within the gauge area a positive and a negative shear stress is generated with the same magnitude. Therefore this type also has a linear output proportional to the applied load.

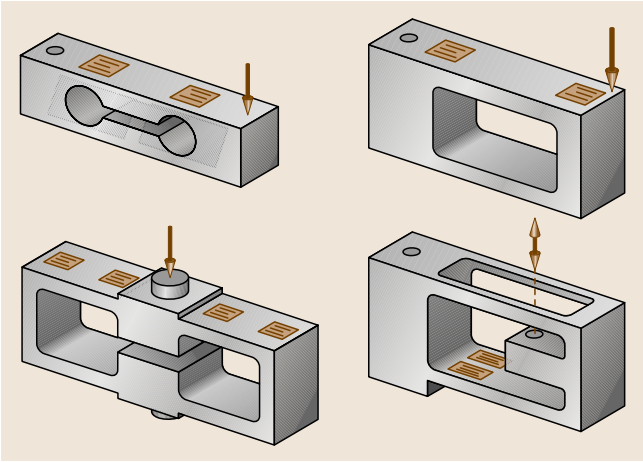

Fig. 8.27 Parallelogram-type load cells

Shear-Type Load Cells

The maximum shear stress on a cantilever beam (Fig. 8.28), produced by force F, appears at the center line of the beam at $\pm 45°$, where the tension of compression stresses are nearly zero. In such a case the maximum strain also appears at $\pm 45°$, therefore to get the maximum output the gauges must be bonded as shown in Fig. 8.28. The dimensions of the beam can be calculated by determining the stresses in $\tau_{max} = Fc/A$ [N/mm^2], where F is the applied force, $A = bh$ [mm^2] is the beam cross section, and c is a form factor that depends on the shape of the beam cross section. For a rectangular cross section $b \leq h/2$ and $c = 3/2$, whereas for a circular cross section $c = 4/3$. These formulas are approximations for the centerline. The strain gauge covers a certain area around the centerline such that the integrated value measured by the strain gauge will be smaller. The signal of the transducer can be determined using the equation $\Delta U/U = k\varepsilon_{45°}$ for the full bridge output as well as the equation $\varepsilon_{45°} = \tau_{max}/2G$ for the strain under the gauge.

For a torque transducer the shear stress must be calculated using $\tau_{max} = M_t/W_p$ [N/mm^2], where M_t [Nm] is the torque moment and W_p [mm^3] is the polar section modulus.

Tension and Compression Load Cells

The main difference between shear- and bending-stress transducers and load cells using tension and compression stress measurements is that in the latter there is no positive and negative stress of equal value. If the tension stress $\sigma_{tension} = F/A$ is defined as positive, the negative compression stress becomes $\sigma_{comp} = \nu F/A$, termed the Poisson stress. For metals $\nu = 0.3$ while the compression stress is only about 1/3 of the tension stress. Using a Wheatstone bridge with four gauges applied, as shown in Fig. 8.30, the output of such a transducer related to the force (F) will be nonlinear. This is not a big disadvantage as long as these nonlinearities are taken into account through calibration.

For standard load cells a nonlinear characteristic is not very common, however for applications in wind-tunnel testing they are sometimes advantageous since they do not require much space. Another advan-

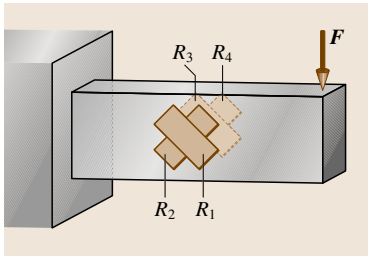

Fig. 8.28 Shear-type load cells

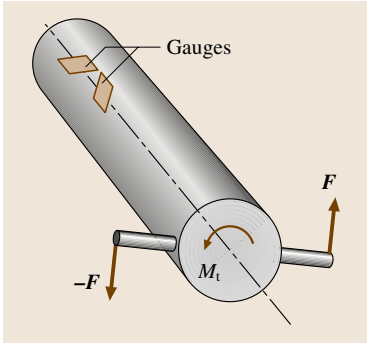

Fig. 8.29 Torque transducer

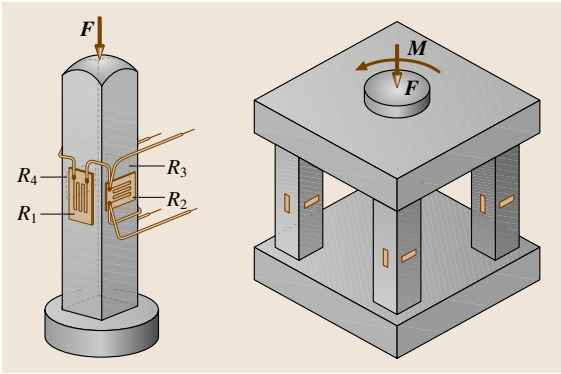

Fig. 8.30 Tension-type load cell (*left*) and cage of tension and compression columns (*right*)

tage of such a transducer is that the strain gauges are placed very close to each other, thus remaining at the same temperature. This minimizes the zero-drift and temperature-gradient sensitivity of the transducer. In some wind-tunnel balances such tension and compression columns can be arranged in a cage. In such a way it is possible to measure tension and compression as well as the moments acting on the metric side of the transducer [8.9].

8.1.12 Multicomponent Load Measurement

The fundamental criterion of all multicomponent load measurements is that all the loads acting on a model must be separated into single components as best as possible. In order to measure each single component at least one associated transducer per component must exist. This criterion can be best fulfilled in external wind-tunnel balances, where plenty of space is available to separate the load by decoupling rods with flexures. Sting balances are much smaller and so this criterion can be only partially fulfilled. Consequently, interactions or interferences in the measurement of the different components must exist.

The interactions inside a balance are systematic errors that can be determined through calibration. Therefore it is often necessary to measure more components in order to separate the errors during calibration. Another reason for having more measurement sections than components is to measure the errors caused by temperature gradients inside the balance. Temperature gradients cause deflections of the metric part against the nonmetric part, which in turn are measured by the strain gauges. This is also a systematic error which can be separated through calibration. In order to extract the loads from the balance signals, the following equation must be resolved:

$$\boldsymbol{F} = \bar{E}\boldsymbol{S}\,, \tag{8.25}$$

where $\boldsymbol{F}$ is the force vector, $\bar{E}$ is the evaluation matrix and $\boldsymbol{S}$ the signal vector.

Through calibration one obtains an evaluation matrix whose elements take all the interactions and systematic errors into consideration. For a balance with no interactions, the six sensitivities for each component are the diagonal of the evaluation matrix while all other elements become zero. For a balance where nonlinearities up to the third order are considered, the evaluation matrix consists of $6 \times 33 = 198$ elements [8.10].

8.1.13 Internal Balances

Two general groups of internal balances exist. The first group consists of the so-called box balances. These can be constructed from one solid piece of metal or can be assembled out of several parts. Their main characteristic is that their outer shape most often appears cubic, such that the loads are transferred from the top to the bottom of the balance. The second type of internal balance is termed a sting balance. These balances have a cylindrical shape such that the loads are transferred from one end of the cylinder to the other in the longitudinal direction. Both one-piece and multi-piece sting balances exist [8.11].

Sting Balances

Internal sting balances are divided into two different groups: the force-balance type and the moment-balance type. If the bridge output is directly proportional to one load component then these balances are termed *direct read balances*. Typically for all groups, the axial force and rolling moment are directly measured with one bridge. The measurements of lift force and pitching moment or for side force and yawing moment are done in different ways characterizing each group.

Moment-type balances and force-type balances have one main feature in common: the lack of a direct output

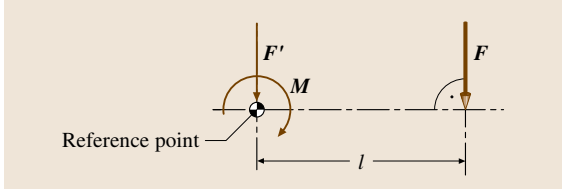

Fig. 8.31 Separation of force and moment

proportional to lift/pitch and side force/yaw. The signals that are proportional to each of these loads must then be calculated by summing or subtracting the signal from one another, before being fed into the data-reduction process. The advantage is that the associated concentrated wiring on each section is much less sensitive to temperature effects [8.12].

Force Balances. This type of balance uses two measurement sections placed in both the forward and the aft section of the balance. In these measurement sections a forward and aft force is measured most often through tension and compression transducers. These forward and aft force components are used to calculate the resulting force in the plane as well as a moment around the axis (perpendicular to the measurement plane). An example of a typical force balance is shown in Fig. 8.32.

Moment-Type Balances. Moment-type balances have a bending moment measuring section in the front as well as in the aft regions of the balance (S_1 and S_2 in Fig. 8.33).

The measurement of the two bending moments (S_1 and S_2) is used to obtain a signal that is proportional to the force in the measurement plane and a second one that is proportional to the moment around the axis (perpendicular to the measurement plane). The stress distribution shows that the moment M_y (M_z) is proportional to the sum of S_1 and S_2. However, the force F_y (F_z) is proportional to the difference in the signals S_1 and S_2.

To measure the rolling moment (M_x) one bending section must be applied with shear stress gauges to detect the shear stress τ. The most complicated part of the balance is the axial force section, which consists of flexures and a bending beam to detect axial force. These flexures enable axial movement whilst carrying the other loads.

Direct-Read Balances. A direct-read balance can be categorized as either a force-balance type or as a moment-balance type. Instead of measuring a force or a bending moment at each section separately, half bridges on every section are directly wired to a moment bridge while the other set of half bridges are directly wired to a force bridge. Thus the difference between direct-read balances and the other types is only in the wiring of the bridges. The disadvantage of such a wiring is the length of the wires from the front to the aft ends. Temperature changes inside these wires cause errors in the output signals.

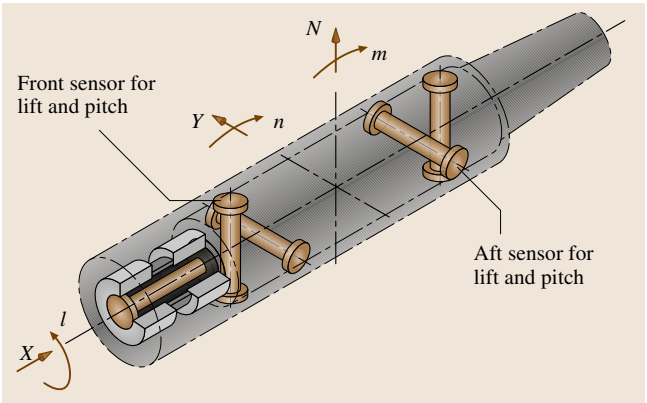

Fig. 8.32 Force balance with tension transducers in forward and aft sections (courtesy of Able Corp.)

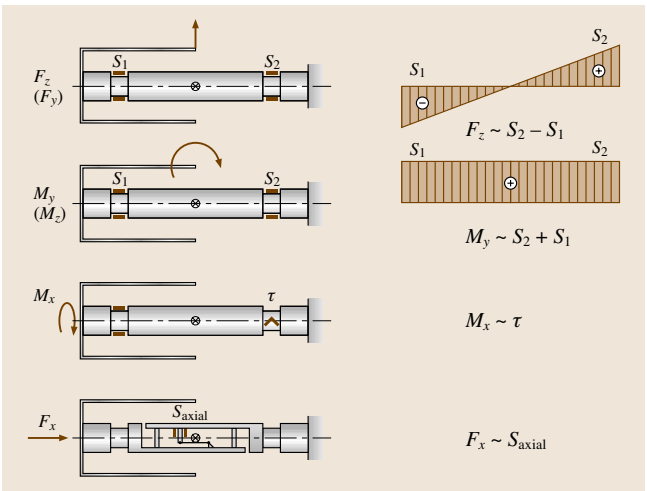

Fig. 8.33 Workings of a moment-type balance

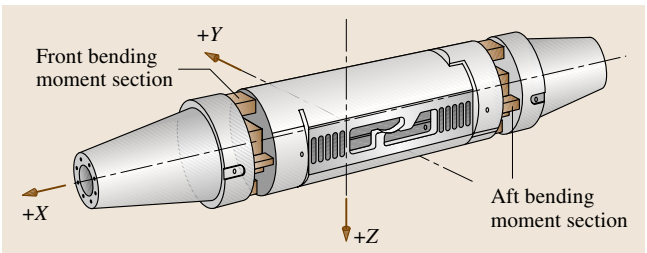

Fig. 8.34 Moment-type balance

Box Balances

The main difference between box balances and sting balances are the model and sting attachment area (Fig. 8.35). The load transfer in such balances is from

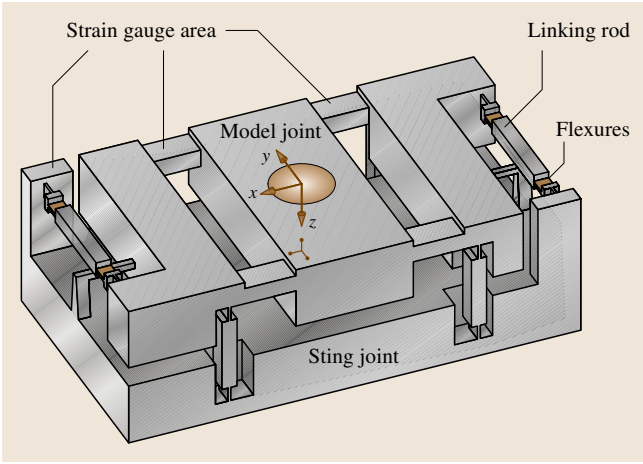

Fig. 8.35 Mono-piece box balance

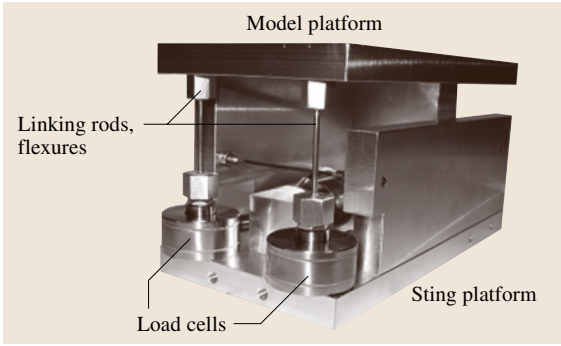

Fig. 8.36 Small box balance with load cells

top to bottom along the vertical z-axis. Therefore these balances use a central sting arrangement, as shown in Fig. 8.10 for the case of an airplane configuration. The mono-piece balance is constructed from one single piece of material. The advantage of this relatively expensive manufacturing process is the low hysteresis and good creep behavior, which are basic requirements for good balance repeatability. Multi-piece box balances are built from several parts, which can in turn be manufactured separately. The load transducers can either be integrated into the structure or separate load cells can be used instead. This enables a parallel manufacturing process with a final assembly at the end, in turn making the whole process quicker than that for a mono-piece balance. Box-type balances are considered to be internal balances, but have actually more in common with semi-span balances. In particular their temperature-sensitivity behavior is similar to that of semi-span balances.

Principle Design Equations

All internal balances measure the moment and the force in two different sections along the x-axis. The distance between the two sections defines the separation of the signal between force and moment. In the ideal case, half of the signal should be proportional to the force and the other half should be proportional to the moment.

To obtain the same output for the force and the moment, the distance $l = l_1 + l_2$ between the two sections has to be calculated. For a moment-type balance these relations can be described by the following equations

$$\sigma_1 = \frac{M_{B_1}}{W_1} = \frac{M + Nl_1}{W_1} ,$$

$$\sigma_2 = \frac{M_{B_2}}{W_2} = \frac{M - Nl_2}{W_2} , \quad W_1 = W_2 , \quad l_1 = l_2 , \tag{8.26}$$

where σ_1 and σ_2 are the stresses in sections 1 and 2, respectively. These stresses are caused by the moment M and the force N. W_1 and W_2 are the section moduli. The sum as well as the difference of these two stresses are

$$\sigma_1 + \sigma_2 = M\left(\frac{1}{W_1} + \frac{1}{W_2}\right) + N\left(\frac{l_1}{W_1} - \frac{l_2}{W_2}\right) = \frac{2M}{W} , \tag{8.27}$$

$$\sigma_1 - \sigma_2 = M\left(\frac{1}{W_1} - \frac{1}{W_2}\right) + N\left(\frac{l_1}{W_1} + \frac{l_2}{W_2}\right) = \frac{Nl}{W} . \tag{8.28}$$

In (8.27) it can be seen that the sum of the stresses is only proportional to the moment M, and in (8.28) it can be seen that the difference of the stresses is only proportional to the force N. Consequently the sum of the bridge signals S_1 and S_2 is proportional to the moment M while the difference of the bridge signal S_1 and S_2 is

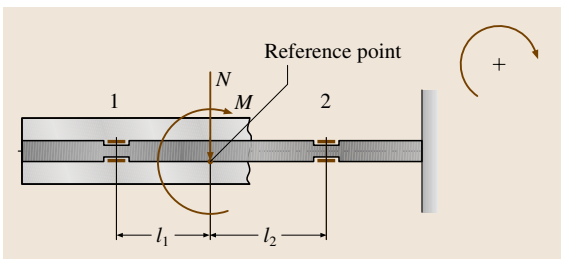

Fig. 8.37 Force and moment acting on a sleeve over the reference point

proportional to the force N

$$\sigma_1 + \sigma_2 \approx \Delta U_\mathrm{M} \,,$$
$$\sigma_1 - \sigma_2 \approx \Delta U_\mathrm{N} \,. \tag{8.29}$$

At this point the ratio of the sum and the difference of the signals can be calculated

$$\frac{\Delta U_\mathrm{M}}{\Delta U_\mathrm{N}} = \frac{2M}{Nl} \,. \tag{8.30}$$

For a given moment M and a given force N, the aim is to have the ratio of the signal equal to one. The distance l between the measuring sections can be calculated in the following manner:

$$l = \frac{2M}{N} \,. \tag{8.31}$$

This equation is also valid for force-type balances. Therefore for the same force and moment output, there exists an optimum distance between the measuring sections; thus the length of the balance can be determined in this way. If the required load combination results in a length that does not fit into the model, then the distance between the measuring sections must be compromised in such a way that the signals for the force or the moment are smaller than the other.

Another problem appears when the distance between lift and pitch in the x–z plane is different from the distance between the side force and yaw in the y–x plane. One solution is to use different measuring sections, but this will enlarge the total length of the balance and is usually avoided.

For a single-test setup normally the balance length can be easily optimized for the model. However, the balance load range definition is more often a compromise between requirements for different test setups, where the maximum loads for all tests form the envelope of the combined-load range specification. In such cases a good compromise for the balance dimensions can seldom be found.

Specific-Load Parameter. Before designing the bending section it is good to determine first whether the balance will have high loading or not. Loading in this case refers to the ratio between the loads and the available volume for the balance. This ratio expresses the magnitude of the stress level inside the balance before starting with the calculation. This ratio is also referred to as the *specific-load parameter*

$$S_\mathrm{round} = \frac{N + L/2 + M}{D^3} \,,$$

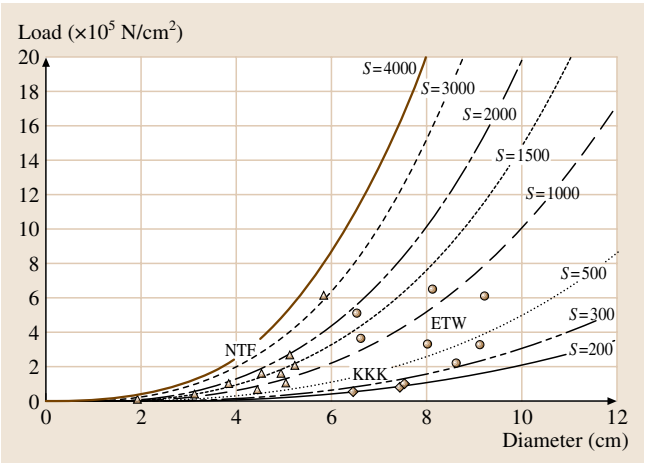

Fig. 8.38 Specific-load parameter of various balances

$$S_\mathrm{rectangular} = \frac{N + L/2 + M}{1,7BH} \,, \tag{8.32}$$

where L is the active length of the balance without interfaces, D is the diameter, and B and H are the maximum available width and height of the balance. The first equation is used when the main cross section of the balance is circular whereas the second is used when the main cross section is rectangular. Experience shows that highly loaded balances have a specific-load parameter greater than $1000\,\mathrm{N/cm^2}$. In this case the highly stressed areas occur not only in the area where strain gauges are applied, but also in the flexures of the axial force elements.

Bending Section Design. After the distance of the measuring section is fixed, the bending sections must be designed such that the output and full scale are on the order of 0.5–3 mV/V. The design output depends on the data-acquisition equipment to be used. Some systems have a maximum input and therefore it must be guaranteed that no overflow occurs. This is the case even for a single maximum load, which can be up to 100% higher than the maximum combined load. In most cases, for maximum output of the design loading, the sum of the full-scale output of the force and the full-scale output of the moment are the limiting factors. Usually the maximum full-scale output is around 1.5 mV/V.

In order to determine the geometry of the bending section it is sufficient to use handbook formulas. If a careful calculation is made the accuracy of the predicted full-scale output will be ±10%. Since the real gauge factor at this stage is not yet known, it is good to

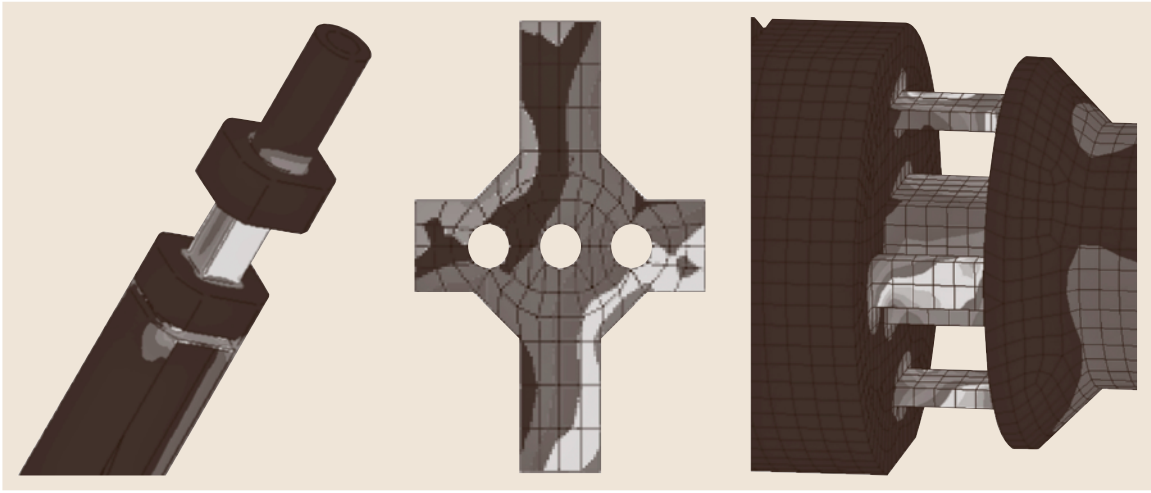

Fig. 8.39 Massive rectangular geometry (*left*), massive cross geometry (*center*) and cage with five beams (*right*)

use $k = 2$ by default. Normally the real gauge factor is somewhat higher and so the final output of the section is usually higher than calculated.

To design the optimum cross section many different designs are used. Some commonly used geometries are shown in Fig. 8.39.

Possible Geometries for Bending Section Design. On the surface of the massive cross sections (cross, rectangular or octagonal in shape) the surface stresses caused by the bending moment are measured. In a cage design the tension and compression stresses in the single beams are measured. This design is preferable when the specific-load parameter is lower than $300\,\mathrm{N/cm^2}$. During the bending section calculation the measurement sections for five components must be designed.

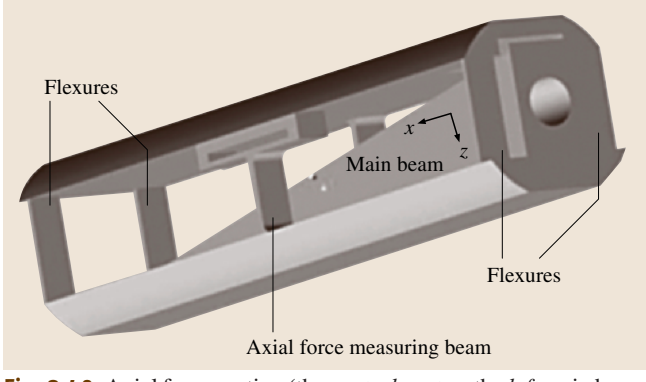

Fig. 8.40 Axial force section (the *central part* on the *left* main beam is cut out)

These components are: lift, pitch, side force, yaw and roll.

Axial Force Section Design. The axial force measurement requires much attention in the design and construction stages. Most of the cost for an internal balance is attributed to the axial force system. Usually the axial force is very small in comparison to the other forces and moments such that the sensitivity of this measurement must be extremely high. This in turn makes the axial force sensitive to interactions of the other components.

In Fig. 8.40 the components of a typical axial force section are shown. The left-hand and right-hand sides of the balance are connected by the flexures. These flexures carry the loads of all five components but are relatively flexible in the axial force direction. Most of the axial force (more than 60%) is supported by the cantilever beam in the middle of the balance.

The axial force measurements are best made in the middle of the axial force section, since the mechanical interactions are minimal in this position. For the compensation of thermal effects, in particular temperature gradients, it is better to have four rather than two axial force measuring beams placed near the flexures.

8.1.14 External Balances

Balances have been used since the beginning of aerodynamic testing. One of the first balances was built by *Otto Lilienthal*. In Fig. 8.42 Lilienthal's apparatus for the measurement of lift can be seen. The apparatus is a sim-

ple combination of a wind tunnel and a balance. Two airfoils of the same shape were fixed to a rotating arm at a certain angle of attack. Two cables were wrapped around a pulley in the center and at the other end of the cables two weights were connected. When the weights were released they fell to the ground and the arm began to rotate. During rotation the airfoils generated lift and this lift was then counterbalanced by the weights in the middle, thus measuring the aerodynamic lift.

The principle of counterbalancing weights for the measurement of aerodynamic forces on wind-tunnel models was used in many external wind-tunnel balances. Even today such external balances use weigh beams to measure the aerodynamic forces. With the advent of the strain gauge, load cells replaced these weigh beams. Subsequently the balances became stiffer, faster and more accurate. Modern external balances are the most accurate multicomponent force-measuring devices in use.

External balances can be separated into two groups, large external balances and semi-span (or half-model) balances. The latter are much more compact and are built either from one piece of material or are assembled from various. Large external balances are conversely built using a steel framework and separate load cells.

Sidewall Balances

The term sidewall balance is often used to refer to a compact external balance. Such a balance is often used for half-model testing. For semi-span model testing the balance has only five components since measuring the side force on a semi-span model is illogical. This very significant difference between a half-model balance and the external compact balance affords a completely different design.

The principle design of a semi-span balance is relatively simple. There are two massive parts, the earth end and the model end, both of which are connected by a flexure system and the measuring beams. The design of semi-span balances varies in the flexure system

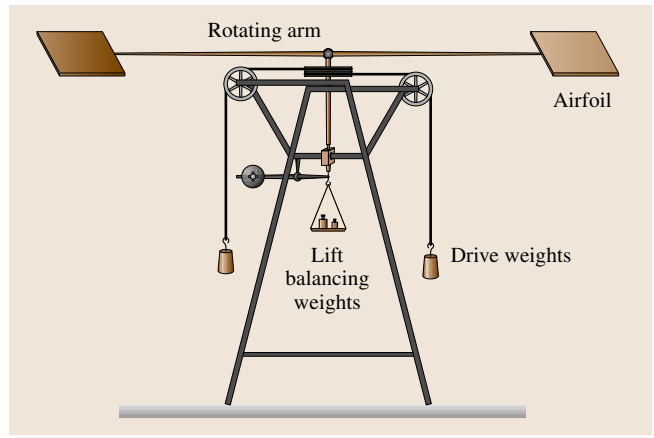

Fig. 8.41 Lilienthal's airfoil test rig with lift balance

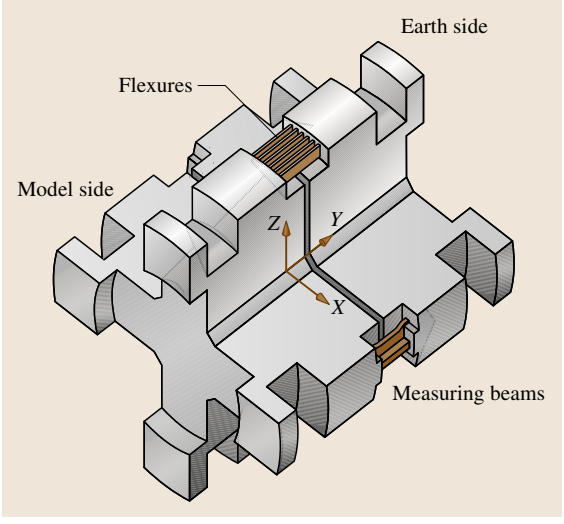

Fig. 8.42 Working of a semi-span balance

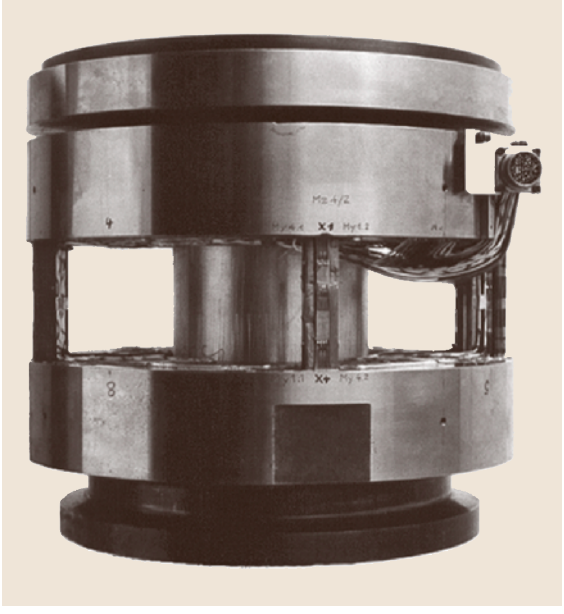

Fig. 8.43 Simple half-model balance

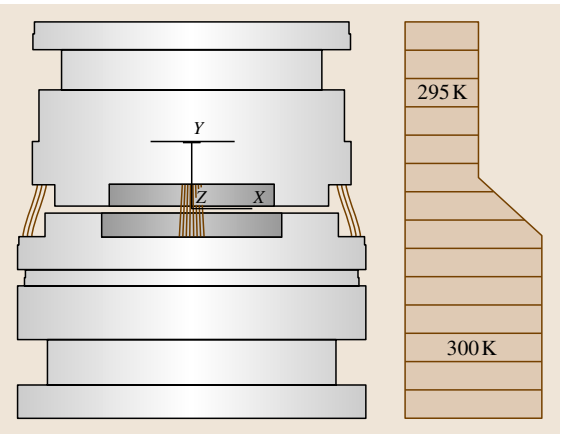

Fig. 8.44 Deformation of semi-span balance due to heat flux

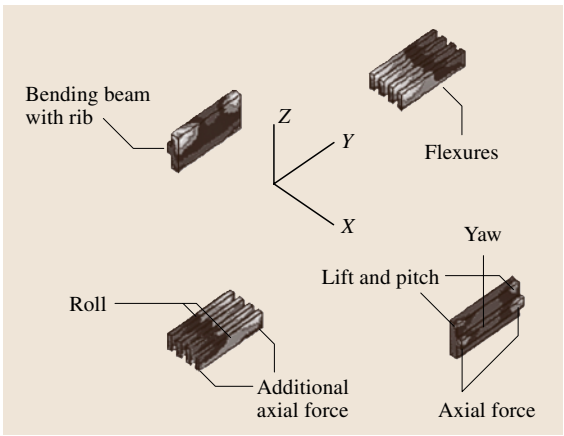

Fig. 8.45 Flexure design for half-model balance

and the form of the main body. Most have simpler flexure systems than that shown in Fig. 8.42, with only one flexure in every corner and circular cross section for the main body as shown in Fig. 8.43.

A common problem with all designs is the enormous temperature sensitivity;, which is even a problem with very slight temperature changes. Such changes occur in most tunnels, which often become progressively warmer with time. The model, with its large surface, is exposed to the tunnel air temperature and reacts very quickly whereas the balance on the outside stays at room temperature. Thus a heat flow is generated through the balance, in which the model and the flexure system are the paths of highest resistance for the heat flow. The result of this heat flow is a temperature gradient inside the balance causing a deformation of the flexures.

In Fig. 8.44 the top of the balance is cooler than the bottom, such that the upper region shrinks relative to the lower part. The stiffness of the main parts is much higher than the stiffness of the measuring flexures such that the shrinking is compensated by deformation of the flexures. This deformation in turn is measured by the strain gauges. As can be seen in Fig. 8.44, the flexures on opposite sides bend in opposite directions. If the sensitivity of both flexures is equal, then the sum of the signals is zero and the temperature gradient effect is canceled out. Therefore the aim in such a case is to build a symmetric balance with flexures of equal sensitivity but on opposite sides. The best compensation for all temperature-related effects is obtained by applying strain gauges bridges on every flexure, measuring each one separately as is typical for moment-type balances [8.13].

Design of Side-Wall Balances

As described previously, a side-wall balance consists of two massive parts plus flexures. Therefore most attention must be concentrated on the flexures and the distance between them. The simplest arrangement consists of four flexures with exactly the same shape, all of which are placed symmetrically around the center of the balance. To adjust the distribution for a force and a moment acting in one plane the same basic results (8.25, 26, 27, 28, 29, 30, 31) can be used to determine the appropriate distance between the flexures.

To adjust the sensitivity of the single component to the specified-load range a more-sophisticated flexure arrangement, as shown in Fig. 8.45, can be used. To calculate the flexure cross sections the formulas for the cage design of an internal balance are nearly identical.

Large External Balances

In contrast to semi-span balances, all large external balances are constructed from discrete parts. Outside of the wind-tunnel test section there is usually much more space available. This makes it possible to build up a large structure, enabling a better decoupling of the various components. Moreover, for such a design precision load cells can be ordered from several suppliers. The load cells define the main characteristics of the external balance such as repeatability, resolution and stability. If the load cell range is well matched to the balance load requirement the maximum resolution of the balance will exactly match the resolution of the load cell. This is usually on the order of 300 000 parts if precision electronic equipment is used. The repeatability of the balance is determined by the load cell. Furthermore, the rigidity of the balance will be at least as good as the resolution of

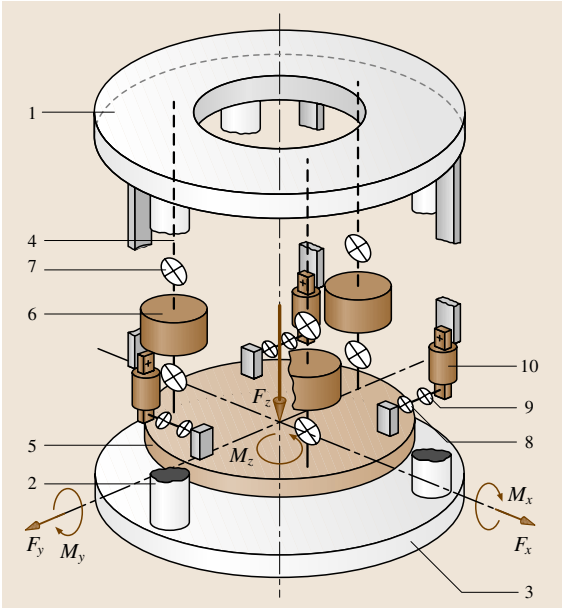

Fig. 8.46 Typical configuration of an external balance (for explanation of numbers, see text)

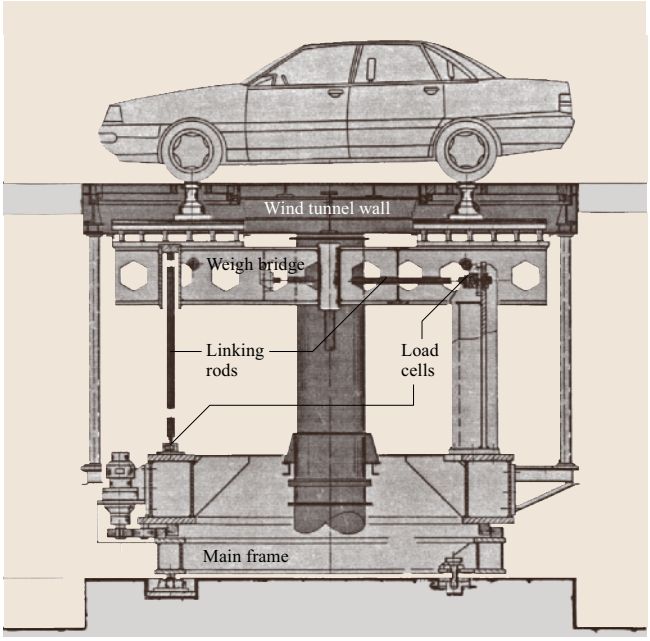

Fig. 8.47 External balance for an automotive wind tunnel (courtesy of Schenck)

the load cell. The large dimensions of the structure make the balance sensitive to temperature changes. Short-term changes in temperature must be prevented such that the whole balance is kept at a stable temperature level. For the case of a conventional wind tunnel this can be easily achieved.

There exist many different types of external balances since they are most often designed for individual wind tunnels with specific requirements. Examples of such designs are platform-, yoke- and pyramidal-type balances [8.14]. The differences between these types of balances are characterized by the design of the structure and the arrangement of the load cells. This arrangement in turn determines the signal combination for the different load components.

The design principle for external balances is nearly always the same (Fig. 8.46). The metric part of the balance is the so-called weighbridge (5). This weighbridge is connected via rods (4, 8) to the load cells (6, 10). To protect the load cells from unwanted moments, flexible knuckles (7, 9) are used on both ends of the connecting rod. These knuckles should be always elastic elements with no ball bearings. Such bearings must be avoided since any friction inside causes hysteresis. The load cells themselves are connected to the main frame (1, 2, and 3), which is itself the nonmetric side of the balance.

For a six-component balance, six load cells are needed. The vertical ones (6) measure the lift force, pitching moment and rolling moment. The horizontal load cells measure side force, drag and yawing moment.

An example in which the weighbridge is located directly under the tunnel wall is that of an automotive wind tunnel (Fig. 8.47). The cars are fixed on pads that are linked through the tunnel wall to the weighbridge of the balance without any contact with the tunnel floor.

This configuration allows for the installation of a moving belt inside the wind-tunnel floor, eliminating the floor boundary layer thus producing more-realistic boundary conditions.

Normally the entire balance is mounted on a turntable such that the balance moves together with the model, as shown in Fig. 8.48. In the case of aircraft half models and automotive testing the model axis system and the balance axis system are always identical and the wind forces and moments must be calculated by transforming the balance loads into the wind axis system.

For full model aircraft testing, the angle-of-attack setting mechanism is integrated into the balance weighbridge such that the balance stays in the wind axis system while the model alone changes its angle of attack. The measured loads in this case are the aero-

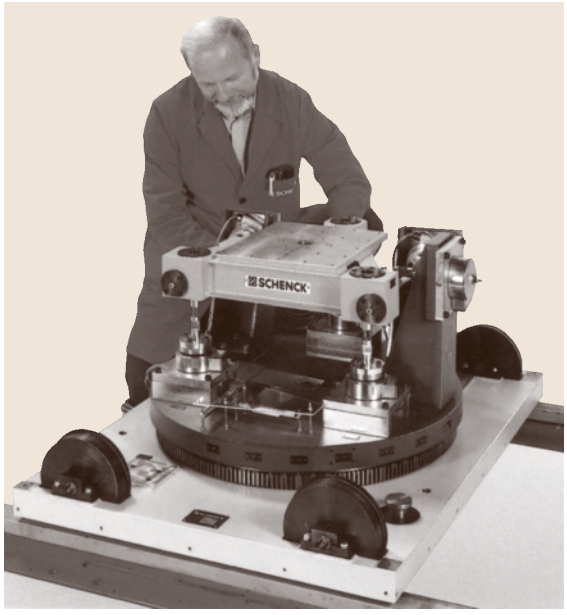

Fig. 8.48 An example of a small external balance (courtesy of Schenck)

dynamic loads in the wind axis system. For a change of yaw angle, however, the balance is moved together with the model such that the side loads must again be transformed into the wind axis system. This has to be taken into account in the balance data-reduction software. Sometimes clients need to have the side load data in the model axis system, although all the loads for the longitudinal direction should be given in the wind axis system. In some external-balance constructions the mechanism for change in angle of attack and yaw angle are integrated into the weighbridge, allowing the balance to be fixed to the earth and to the wind axis system.

8.1.15 Calibration

The primary task of the calibration is to measure the relationship between the balance signal and the measured load. In order to obtain this relationship or sensitivity, the balance must be loaded with precise single calibration loads. Such loads are often referred to as true loads. These loads can either be applied exactly in the direction of the model axis system, or alternatively if this cannot be achieved, then the exact direction of the load must be precisely measured. One of main requirements of true loads is that they are traceable to an international standard.

Another requirement is that the direction of the load during calibration is always the direction of the reference axis system. This requirement can be achieved by either realigning the loading axis system to the model axis system or by measuring the relative movements (translation and rotation) between the axis systems, thus transforming the loads into the model axis system. In the former case, a certain orientation procedure must be repeated after every change in load, whereas in the latter case, as well as the load measurement, the rotation and translation must be measured.

Since several measurements must be performed the uncertainty of the true load increases. These errors cannot be avoided thus the uncertainty of the true load application must be one order of magnitude lower than the required absolute uncertainty of the balance.

The signals of a wind-tunnel balance are more or less influenced by many systematic errors (see Sect. 8.1.2). One of the major systematic errors is the interaction of all loads on a strain gauge bridge. This means that, if a certain load combination is applied to the balance, each bridge will react to every load. This is a very undesirable situation since the original intention of the design is that each bridge should react only to one load. The elimination of the interaction is the other major task of calibration. To do so the balance must be loaded with load combinations, mainly with combinations typical of the desired wind-tunnel tests.

From all this data are the relation between signals and loads must be extracted. As mentioned in Sect. 8.1.12, the fundamental relationship between the loads and the signals of the balance is

$$\boldsymbol{F} = \bar{E} \times \boldsymbol{S} \,, \tag{8.33}$$

where $\boldsymbol{F}$ is the unknown load vector and $\boldsymbol{S}$ the signal vector. The task of the calibration data reduction is to determine the elements of matrix $\bar{E}$, known as the evaluation matrix. This matrix is used in the tunnel software to determine the aerodynamic loads from the measured balance data.

During calibration the load vector is known and the signals are measured, so in this situation the dependent variable is the signal and the corresponding equation is:

$$\boldsymbol{S} = \bar{K} \times \boldsymbol{F} \,. \tag{8.34}$$

Herein the matrix $\bar{K}$ is called the calibration matrix. The usual way to obtain the evaluation matrix from the calibration matrix is to invert the calibration matrix:

$$\bar{E} = \bar{K}^{-1} \,. \tag{8.35}$$

As long as the calibration matrix is a 6×6 matrix it is called a linear matrix and the inversion of this linear matrix is trivial. The matrix is referred to as linear since there is only a linear relation between the interactions and the load. If the requirements on the accuracy of a multicomponent force transducer are not very high and the mechanical decoupling of the load measurement sections is adequate, such a linear matrix is suitable to describe the interactions between the components. This means that for lower accuracy requirements in some external balances a linear matrix is adequate to eliminate the interaction effects.

In reality the characteristics of the interactions are more complicated and nonlinear. This nonlinearity may cause a few-percent difference in the linear characteristic. However, the requirement of an internal wind-tunnel balance is an overall accuracy better than 0.1%, therefore nonlinear effects on direct sensitivity and interactions must be taken into account. Thus matrices on the order of 6×21 to 6×33 are used. Unfortunately, a complex 6×33 calibration matrix cannot be inverted easily to obtain the evaluation matrix. For such a calculation a numerical algorithm must be used.

Description of Interactions

Mathematically the interactions can be understood as the elements of the matrices that are not placed on the diagonal. The matrix (8.33) can be written as a sum of the terms:

$$F_i = \sum_{j=1}^{6} A_{ij} S_j + \sum_{j=1}^{6} \sum_{k=j}^{6} B_{ijk} S_j S_k + \sum_{i=1}^{6} C_{ij} S_j^3 \,. \tag{8.36}$$

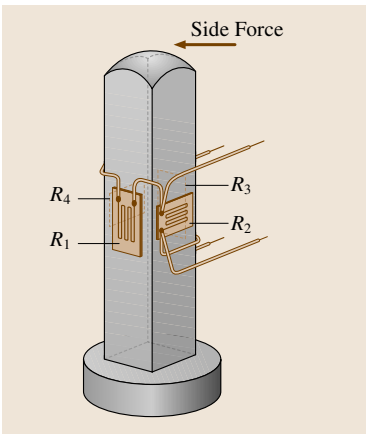

Fig. 8.49 Side-force interaction

This equation takes all elements of the 6×33 matrix into account. A_{ij} represents 36, B_{ijk} 126 and C_{ij} 36 coefficients. The six elements A_{ij} with $i = j$ are the direct sensitivities for the six loads.

Linear Interaction. In (8.36) the elements A_{ij} for $i \neq j$ are the coefficients of the linear interaction. As already described a linear interaction is the influence of a load component that is not to be measured with the transducer. For example, the side force generates a signal in a transducer that is used to measure tension and compression.

The bending stress caused by the side force will also affect the strain gauges since they are strained by the bending too. Another cause for the sensitivity of the side force is misalignment of the strain gauge itself. If they are not perfectly aligned in the vertical and horizontal directions they become increasingly sensitive to the strain in the other directions.

Second-Order or Product Interactions. In (8.36) the elements B_{ijk} are the coefficients of the nonlinear interaction. In the case of $j \neq k$ the interactions are called product interactions. In the case of $j = k$ they are called second-order interactions and describe the second-order nonlinearity of the sensitivity.

Product interactions are described as the sensitivity of a transducer related to the product of the load not to be measured. Take the example of an axial force acting on the parallelogram section of a balance producing a deformation dx (Fig. 8.50). If an additional normal force is loaded an additional deformation dx will be measured by the stain gauges on the flexure. The additional signal is proportional to the product of F_z and F_x.

Third-Order Interactions. In (8.36) the elements C_{ij} are the coefficients of the third-order nonlinearity. Third-order nonlinearity is taken into account only for the

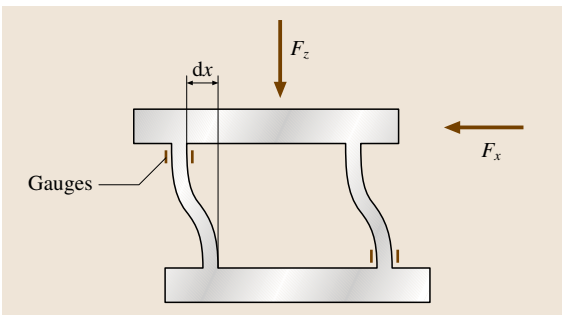

Fig. 8.50 Product interaction of F_x and F_z

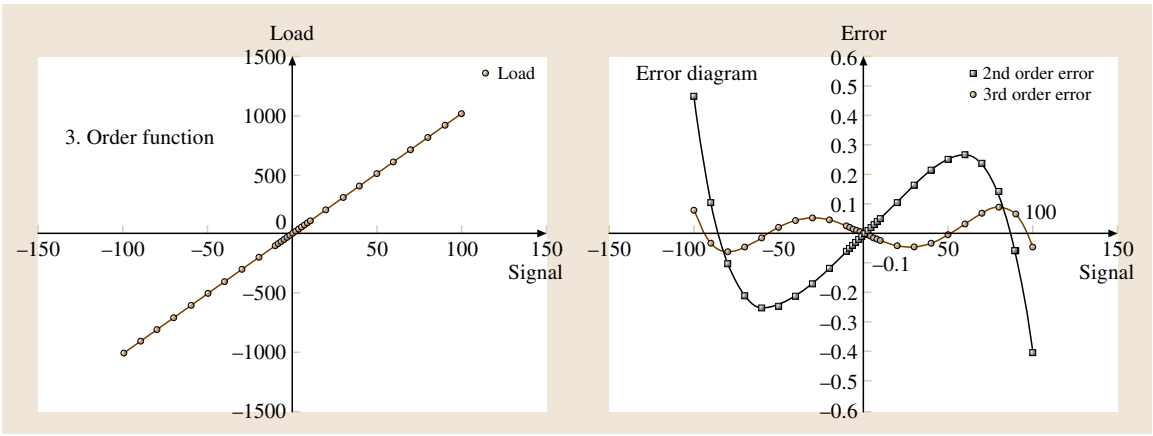

Fig. 8.51 Calibration curve and error diagram

third-order term of the loads and not for any other load combination. The main justification for taking a third-order interaction into account is the nonlinearity about zero when the load changes from positive to negative and vice versa.

The above function is a typical calibration curve of a single load cell. Though the plotted data seems to show a linear behavior, the error diagram indicates that, for a second-order fit, the error increases to up to five times higher than for a third-order fit. The error in this case is defined as the difference between the measured data and the value of the fit function used.

Verification and Accuracy

Since there are so many possible sources, a challenging task is the determination of the uncertainties or the accuracy of a balance. Primary sources include the balance itself, the measurement equipment, the calibration procedure and the loads applied. Error sources can be divided into two groups. The first group consists of the uncertainties that are generated by the calibration procedure itself. Take the example of a dead weight which at first seems to be the best true calibration load. Even a precisely measured weight has some small uncertainties associated with it. When this load is applied to the calibration sleeve of the balance it has to be aligned to the geodetic axis system. This alignment must be controlled by another measurement device, which also has uncertainties. For a moment the distance to the reference center must be measured and so we produce yet another uncertainty of the true load. The second group of errors contains all the uncertainties that are caused by the balance and the measurement equipment.

To calculate the uncertainty from every source would be a rather challenging task, so usually the back-calculated data are used to determine the uncertainty of a balance. The back-calculated data are described as the data obtained from the calculated loads using the balance evaluation matrix and the signal measured during calibration. The difference between the calibration load and the back-calculated load is assumed as the uncertainty of the balance. This data includes all uncertainties of the balance and the calibration process. Normally for a precise calibration the uncertainties caused by the true loads, as well as the uncertainties in the calibration process, are one order of magnitude lower than the uncertainties of the balance itself.

The difference between loading points is also called the residual load. These residuals contain both random errors and systematic errors (bias). Applying a statistical analysis to this data may neither be a physical nor a mathematical solution to describe the quality of the balance. Nonetheless the balance user may find such information useful in order to predict the balance accuracy.

For a proper calibration, between 100–1000 calibration points should be performed, producing one residual load for every calibration loading. This residual load data includes a lot of information but does not provide a good overview of the balance quality. Using a statistical analysis of all the residual loads will however provide some significant quality factors. Widely accepted quality factors include:

1. Minimum and maximum residual loads,
2. Mean value of the residual loads,

3. Experimental standard deviation of the residual loads.

These values can either be provided in engineering units or in a percentage related to the full-scale value of the component. The mean value of the residual loads (ΔF_{rm}) is given as:

$$\Delta F_{\mathrm{rm}} = \sum_{i=1}^{n} \frac{\Delta F_{\mathrm{r}i}}{n} \,. \tag{8.37}$$

Subsequently the experimental standard deviation can be calculated from the following equation:

$$S = \sqrt{\frac{\sum_{i=1}^{n} (\Delta F_{\mathrm{r}i})^2}{n-1}} \,. \tag{8.38}$$

The analysis of the residual loads gives the balance user information about the accuracy class of the instrumentation under certain environmental conditions. All the conditions that were kept constant during calibration, such as temperature and humidity, may have another influence on the accuracy of the measurement in the tunnel itself. Thus the effects of temperature must be corrected or calibrated separately. Another source of error not often taken into account is creep. Creep effects in the balance must be tested separately as well.

All these tests provide information about the accuracy of the balance. However, a few problems remain. Firstly, how to formulate the requirements for the accuracy in a specification? Secondly, how to compare these requirements with the calibration data? One suggestion to solve these problems was made by *Ewald* and *Graewe* in the early 1980s and is briefly described in [8.14]. An equation was formulated that would take into account the error influenced by the number and the magnitude of the interactions:

$$\delta_i = A F_{i\,\max} \left(a_i + b_i \sum_{n=1;n\neq i}^{6} \left| \frac{F_i}{F_{i\,\max}} \right| \right) \,, \tag{8.39}$$

where δ_i is the allowed residual load, $F_{i\,\max}$ is the maximum combined load of component i, and F_i are the loads applied during calibration. The factor A is the general accuracy factor and the accuracy factor a_i is for the individual component i; b_i is a weighting of the interaction. The customer can specify the factors A, a_i and b_i and after calibration the balance manufacturer has to verify if all the residual loads are below these specifications. A more global verification is to calculate the factors A, a_i and b_i from the calibration data and to compare them with the specifications.

All other influences on the accuracy of a balance can be integrated by using the error propagation law. For the influence of the temperature the (8.39) is rewritten as

$$\delta_i = A F_{i\,\max} \left[\left(a_i + b_i \sum_{n=1;n\neq i}^{6} \left| \frac{F_i}{F_{i\,\max}} \right| \right)^2 c_i^2 + (d_i + \Delta T_1)^2 + (e_i + \Delta T_2)^2 \right]^{\frac{1}{2}} \,. \tag{8.40}$$

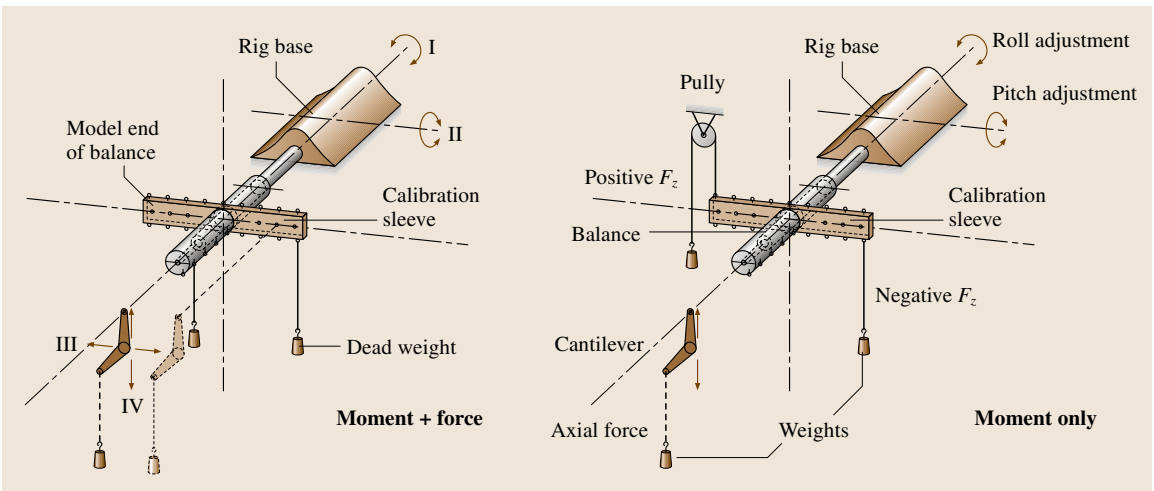

Fig. 8.52 Manual calibration with weights producing: a moment and force (*left*) and a simple moment only (*right*)

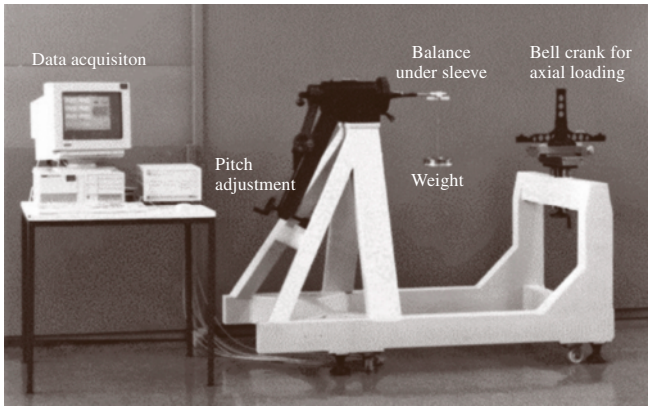

Fig. 8.53 Manual calibration rig

Calibration Principles

To obtain the aforementioned data several principles are used during calibration. The first one, most often used in manual calibration, is shown in Fig. 8.52. Here the balance is fixed with the nonmetric end to the rig base. On the balance metric or model end a calibration sleeve is mounted. This sleeve represents the model, on which the reference axis system is fixed. The calibration loads are hung on sleeves in different directions. To generate pure forces the loads must be applied directly in the axis of the reference system. To generate pure moments a positive and a negative load, as shown in the right-hand side of Fig. 8.52, must be applied to the sleeve, otherwise the loading will generate a force plus a moment as in the left-hand side of Fig. 8.52.

To generate the respective positive and negative forces, hanging weights via pulleys or bell cranks is necessary. Bell cranks are preferred, especially if they are supported with an elastic bearing. The use of pulleys is less desirable as they rely on ball bearings that have relatively high levels of friction. Such high friction causes hysteresis effects. All such mechanical devices are a source of error.

For some calibration data-reduction processes it is not necessary to apply pure moments during calibration. For these cases it is sufficient to load the balance only with a simple combination of moments and forces. On the other hand, during wind-tunnel tests pure loads normally do not occur and therefore it is much better to apply load combinations. Such complex combinations always occur during wind-tunnel testing and provide the best match between the calibration data and the actual wind-tunnel usage. Some data-reduction software is not capable of handling combined loading data and in this case some pure force and moment loadings must be performed to obtain the main sensitivity of each component separately.

In order to generate side forces, produced using positive normal forces without a pulley, the balance inside the calibration sleeve must be rotated by 90°, 180° and 270° relative to the normal position. With this measure normally most of the loads and load combinations can be generated, except for the case of axial force, which must be applied using a bell crank.

For the case of a geodetic axis system, the weight acts in exactly the vertical direction so it is very important to

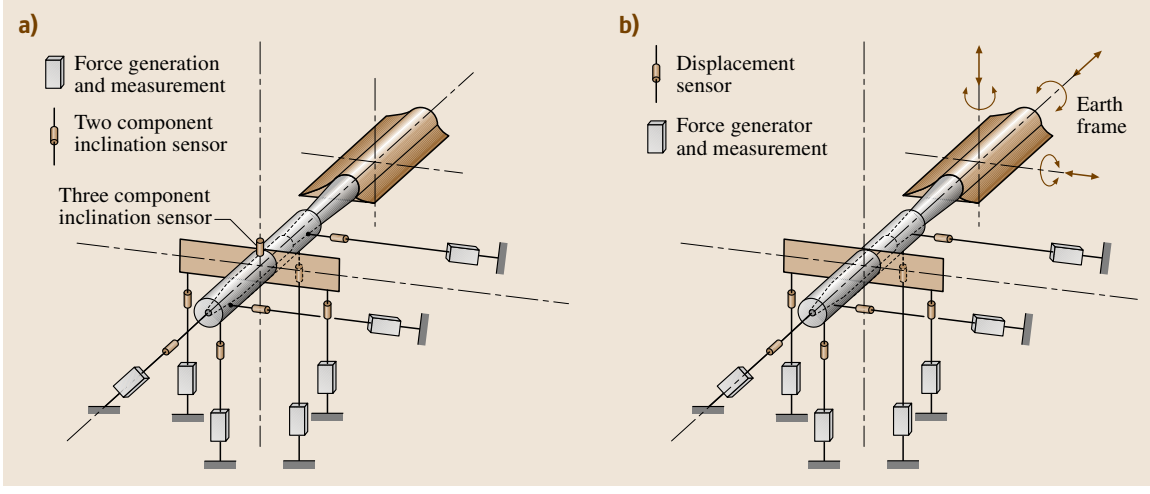

Fig. 8.54a,b Calibration machine using force generators as opposed to weights

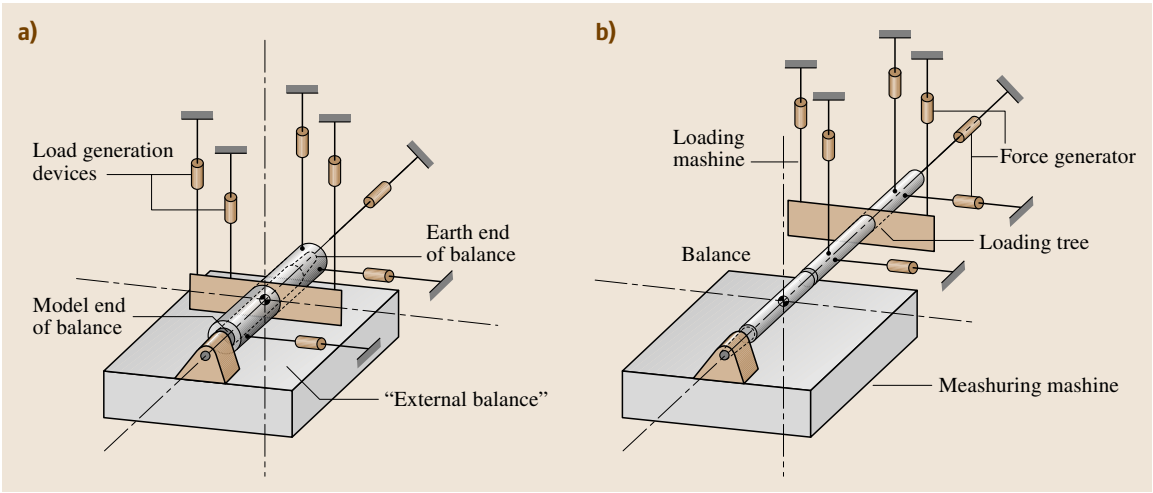

Fig. 8.55a,b Calibration machine with model end fixed to the reference system

realign the calibration sleeve to the geodetic axis system after every change of loading. This is performed to keep the reference axis system exactly in the direction of the load. For this realignment a pitch and roll adjustment in the rig base is necessary.

In the above Fig. 8.53, a manual calibration rig for small balances up to 1500 N of normal force is shown.

Calibration Methods. For automatic calibration there are several possible methods. The first method is similar to the manual one in that the metric end of the balance is fixed to a calibration sleeve and loads are applied to this sleeve. The weights and however and are replaced by force generators. Each generator has to measure the force that it is generating with a very precise load cell. Under a certain load or combination of loads the calibration sleeve will move in some direction and from the force vector related to the reference axis system only the value of the force will be known. To get the correct relative direction of the force vector and the orientation of the calibration sleeve and the orientation of the force-generator axis must be measured with the same accuracy as the force itself (Fig. 8.54a).

The accuracy of the true loads therefore is determined by two different measurement systems and both the force and the displacement measurement systems. This makes it very difficult to get a high precision for the true or calibration loads. Nearly the same principle as above mentioned can be achieved without a realignment system and which replaces the need for an orientation measuring system for the sleeve (Fig. 8.54b). However and in this case the precision of the realignment system must be also very high and the disadvantage of a second measuring system will still exist.

A second method for automatic calibration fixes the metric end of the balance to the reference system of the measuring machine and the sting end is then con-

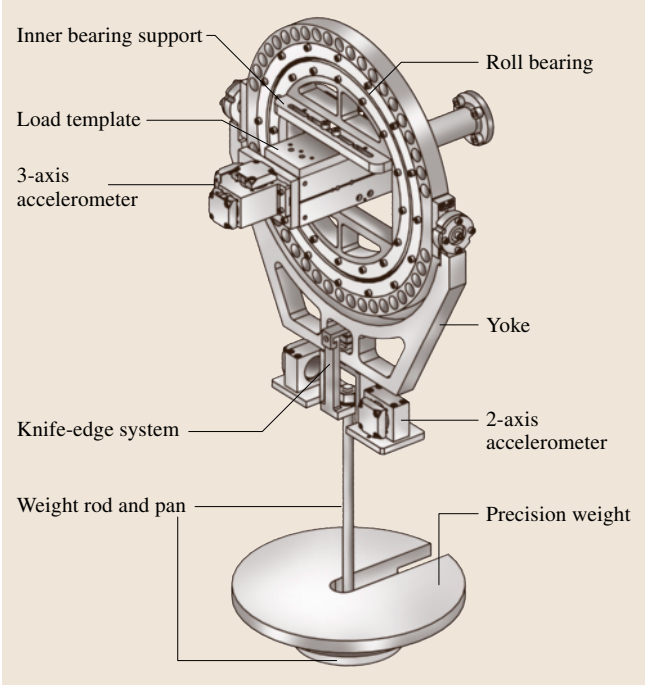

Fig. 8.56 Single vector method as used by NASA Langley

nected to a loading sleeve (Fig. 8.55a) on a loading tree (Fig. 8.55b). The mounting of the metric end of the internal balance onto the metric end of the reference measuring system and labeled as the external balance in Fig. 8.55 and has the great advantage that the reference system of both systems are always the same even when the balance is loaded.

For this method no displacement measuring system is needed and therefore the precision of the true loads is determined by the precision of the load measurement of the reference balance. In this manner the additional uncertainty of the displacement measuring system is avoided.

A final calibration method and namely the single load method and eliminates the uncertainty of the force measurement system by using a single weight as the true load and which is applied over a cardanic suspension to a sleeve which is fixed on the metric end of the balance. This single load remains always vertical. The earth end is fixed to a moving system and which moves the balance to different positions. By changing the orientation of the sleeve and balance and different load vectors are generated with only one load applied.

Additionally the orientation of the sleeve is measured very precisely by a 3-axis accelerometer system and so the orientation of the sleeve-axis system is well known relative to the single load vector. This method eliminates the force-measurement system and uses only a displacement-measurement system to determine the different load vectors. It is also possible to fix the metric end to the moving system. In that way the orientation of the moving system must be measured precisely to obtain the load vector relative to the single vertical load.

8.2 Force and Moment Measurements in Aerodynamics and Aeroelasticity Using Piezoelectric Transducers

Measurement of steady and fluctuating forces acting on bodies in a flowing fluid is the main objective in wind-tunnel experiments. In aerodynamic testing strain gauge balances will usually be applied for this task as, particularly in the past, the main focus was directed on the measurement of steady forces in attached flow, i. e., time-averaged forces acting on wind-tunnel models at rest. Moreover, in most cases the elastic compliance of the balance was neglected and the wind-tunnel models themselves were seen as rigid. With increased interest in understanding and investigating unsteady phenomena, caused for example by flow separation or oscillating models and increased importance of aeroelastic effects, the need for alternative solutions arose. In addition increasing size and lightweight construction principles applied to structures such as aircraft or bridges are coupled with a corresponding larger influence of elasticity. Thus wind-tunnel experiments must also take this into account. The entire force measuring system should be furthermore as rigid as possible, combined with the ability to resolve the unsteadiness of the occurring phenomena. Owing to their inherent stiffness, piezoelectric measuring systems fulfill these requirements very well, although there are restrictions concerning long-time measurement of small, steady forces.

In general, for multicomponent force measurements, one attempts to design the balance as stiff as possible. High rigidity leads to low interferences between the individual force/moment components and to a high natural frequency of the entire force-measuring system. Thus, all balances described in the following are based on three-component piezoelectric force transducers. Usually wind-tunnel balances are based on an arrangement of more or less elastic elements by which strain gauges are applied such that a passive measuring system is formed. In this case, the force measurement is referred to as a strain measurement, where the strain is a consequence of a force measured by a sensor – the strain gauge. A piezo balance, however, works as an active measuring system, where the force is measured directly as a consequence of the deformation of the quartz itself. That means the elastic element and the sensor are identical – the quartz. Consequently, the necessary measuring deflections of a strain gauge balance are one to two orders of magnitude larger than in the case of a piezo balance. This is due to the fact that the relatively low rigidity is a principal property of strain gauge balances.

Two examples will explain the importance of the rigidity of a balance. First, not only for static aeroelastic investigations but also in general, the air loads and the associated deformations of a wind-tunnel model under test are of major interest. Obviously, a relatively elastic balance at the root of a wind-tunnel model would change the model deformations significantly, namely depending on flow parameters. In Sect. 8.2.3 an example

will be presented, where an elastic half-span model of a swept wing is compared with its rigid equivalent. The comparison concerns the behavior of the slope of the force coefficients depending on the Mach number, which is quite different. Again such measurements postulate a stiff balance at the root.

The other examples concern measurements of unsteady forces in general. In this case, the lowest natural frequency of the force-measuring system should be much higher than the frequency range of interest, i. e., vortex shedding – or buffet frequencies. Keeping in mind that, in principle, the balance/model system is an accelerometer comprising the model as a seismic mass and the more or less stiff sensor as the spring, one can imagine that the requirement of a very high natural frequency is much easier to meet using transducers, which are inherently stiff.

In particular, time-series analysis, i. e., the determination of RMS values, spectra, Strouhal numbers, correlation functions etc., needs force/moment data that are nearly free of interference (cross talk) or resonance effects caused by the measuring system itself. To demonstrate that piezo balances are able to cope with these challenges, several examples will be presented in Sect. 8.2.3, involving flow around bluff bodies or wing models, which were at rest or oscillating.

For investigation of small force fluctuations with a large steady preload, a fundamental advantage of piezoelectric measurement systems is that the charge generated by the steady preload can be short-circuited. Thus, for the detection of extremely small fluctuations, the possibility exists to exploit the full resolution of the measuring system independently of the preload.

On the other hand they have the disadvantage that only quasistatic measurements are possible, which is probably the main reason behind the scepticism towards the piezo measuring technique. The decay of the charge and fault currents in the charge amplifier cause a zero-point drift. However this is only essential when measuring small forces over long time periods. Nevertheless, the problem is not as critical as generally believed, since the drift is nearly linearly in time. This problem has been investigated and is discussed in detail.

An early application of piezoelectric force transducers in a large wind tunnel was performed by *Bridel* [8.15]. The mechanical design of his half model balance for the low-speed wind tunnel at Eidgenössische Technische Hochschule (ETH) Zürich was similar to a corresponding strain gauge balance, but he replaced the force-measuring elements by one-component piezoelectric transducers. The first balance applied by the author was for measurements of steady and unsteady forces on two-dimensional bluff bodies in the high-pressure wind tunnel in Göttingen, which was based on multicomponent force transducers and is described in [8.16–18]. *Cook* [8.19] reported unsteady measurements in building aerodynamics using a piezoelectric platform balance.

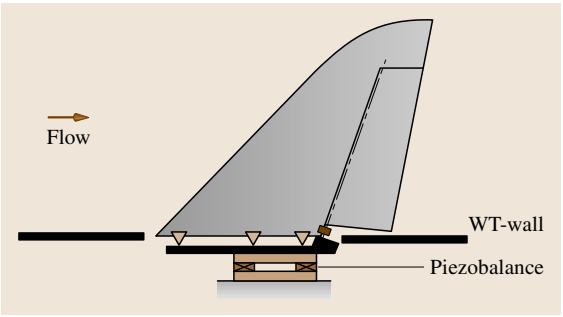

Fig. 8.57 Typical arrangement for force measurement on wall-mounted models using an external platform balance. The model is a fin including a rudder, attached to a massive plate, which is fixed to the balance

In the last 25 years, piezo balances have been applied in many projects performed in close cooperation with colleagues from research and industry, i. e., the Office National d'Etudes et de Recherches Aérospatiales (ONERA), European Aeronautic Defence and Space (EADS), Airbus etc. [8.20, 21]. The largest wind tunnel where piezo balances were applied several times for half model testing was the French transonic wind tunnel, S2, in Modane.

The objective of this section is to give an impression of the possibilities, advantages and limitations offered by the use of piezoelectric balances. Several types of external balances are discussed for wall-mounted models, which can be suspended one-sided or twin-sided.

Figure 8.57 should give an impression of a typical test setup for an external balance measurement at the wall of a wind tunnel. A model, a half wing (here a fin), a car or a building is then attached to a measuring platform such that the cutting forces and moments between the root of the model and a reference base of the wind tunnel can be measured.

Additionally an internal balance is described, which is usually located inside the model under test and was developed by *Psolla-Bress* et al. [8.22].

Reports are given on selected measurements performed in very different wind tunnels ranging from low-speed to transonic flow, from cryogenic to high-pressure principles and from short time to continuous

running. The projects span a wing/engine combination in a low-speed wind tunnel via flutter tests with a swept wing performed in a transonic wind tunnel to bluff bodies in a high-pressure and cryogenic wind tunnel, respectively. These tests serve as examples for the discussion of the fundamental aspects that are essential in developing and applying piezo balances. The principle differences between strain gauge and piezo balances will be discussed.

8.2.1 Basic Aspects of the Piezoelectric Force-Measuring Technique

The piezoelectric effect can be shortly explained as follows. If a crystal without a center of symmetry is composed of ions, then a mechanical deformation of the crystal results in an electric charge on its surface and vice versa (the inverse piezoelectric effect). The reason is that the individual negative grid points (ions) and the positive ones are shifted against each other, resulting in a polarization of the entire crystal (Fig. 8.58). This behavior is typically of quartz (SiO_2) or special ceramics, materials that are usually used for the design of transducers. For high-accuracy measurements, quartz is preferred because it is superior compared to ceramics in terms of long-term stability, linearity, temperature behavior and lack of hysteresis and pyroelectric effects. Depending on how the crystal is cut in reference to its crystallographic axis, distinguishing for example, between a longitudinal and shear effect, it will exhibit different piezoelectric coefficients and consequently different sensitivities. Depending on the measurement problem, one effect may be more appropriate then the other, which will become obvious in the description of multicomponent transducers.

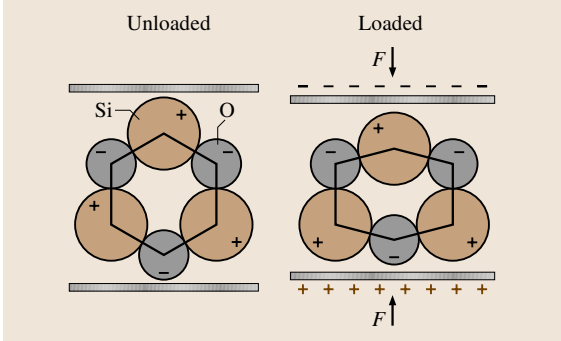

Fig. 8.58 Simplified sketch of a crystal to illustrate the shift of the negative and positive charges against each other due to mechanical deformation (the piezoelectric effect)

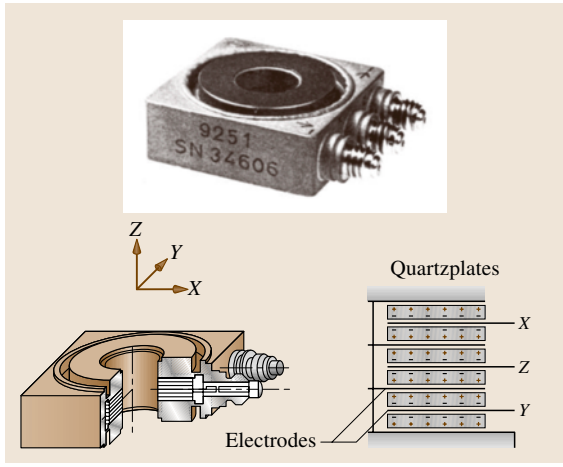

Fig. 8.59 Design of a three-component force transducer (after Kistler). In detail, for every component there is a pair of quartz plates, which are arranged in such a way that the sensitivity is doubled [8.23]

Force Transducer

Typical piezoelectric force transducers have the form of a washer, in which a quartz ring is mounted between two steel plates in the transducer case. If the quartz exhibits the longitudinal piezoelectric effect, then we have a one-component force transducer for axial direction. In the following balance applications we will use three-component transducers; in this case a washer consists of three stacked quartz rings, mechanically operating in series under prestress (Fig. 8.59). Two rings are shear sensitive and are aligned to the measurements of both orthogonal components of a shear force in an arbitrary direction. The third ring is pressure sensitive and measures the compression force on the transducer. As mentioned the quartz packets are prestressed and protected by the rust-proof, tightly welded transducer case. Typical technical data of such transducers, which were applied with the herein described balances, are listed below (Kistler type 9067(9252)). The size is about 56 mm (24 mm) squared. The values in the brackets belong to the smaller transducer (9252).

Shear forces:	F_x, F_y: ±20 kN (2.5)
Axial force*:	F_z: ±20 kN (5)
Rigidity:	C_x, C_y: 3500 N/µm (300)
	C_z: 8000 N/µm (1000)
Sensitivity:	E_x, E_y: 8 pC/N (shear effect)
	E_z: −4 pC/N (longitudinal effect)

*standard prestress = 160 kN (25)

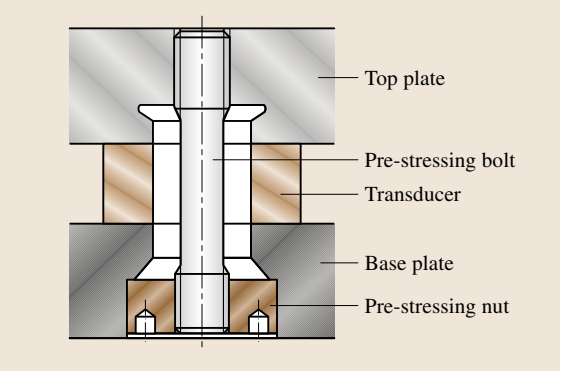

Fig. 8.60 Assembly of a three-component force transducer (after [8.24]). The mechanical rigidity of the prestressing bolt (force shunt) is small (10%) compared with the rigidity of the transducer

The possible range for the axial force F_z depends on the prestress with which the transducer is assembled, a point which will be discussed in the next chapter. The sensitivity is a property of the quartz itself and not of the transducer design, and thus is nearly independent of the size of the transducer and the orientation of the quartz disks when considering shear effects. The criterion for the selection of the transducer is the available space, the required range, the desired rigidity and weight.

Special versions of the force transducers were manufactured by Kistler for applications down to cryogenic temperatures ($T = -150°$) or pressures up to 100 bar, described in Sects. 8.2.2, 2.3. It should be noted that such force transducers were applied both in water and down to helium temperatures (4 K).

Integration and Arrangement for Multicomponent Force and Moment Measurements

Figure 8.60 shows the typical assembly of such an individual load washer. The force transducer is prestressed by an elastic bolt between a base plate and a top plate so that the shear forces can be transmitted by friction. As mentioned, the prestress can have values up to 160 kN, which is required in order that shear forces up to ±10% of the prestress can be transmitted by friction. In order to measure all six components of a force and a moment, a spatial arrangement of at least three multicomponent force transducers is necessary. Experience showed that a platform with four transducers are superior because of its higher stiffness. Figure 8.61 illustrates the principal scheme, which is the same in most platform balances.

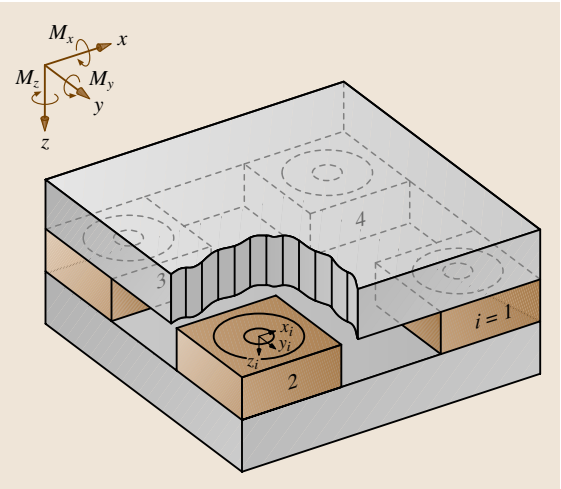

Fig. 8.61 Scheme of a multicomponent platform balance based on four three-component force transducers

The lowest eigenfrequency of such a platform is usually given by the bending of the top plate or the base plate.

It is obvious that, for applications in wind tunnels, such a platform can be installed out of the flow behind the wind tunnel wall, as shown in Fig. 8.57.

In Fig. 8.62 we see a platform balance in more detail, attached to a wing/engine combination. This example shall serve as a paradigm to explain the essential points concerning the design and construction of external piezoelectric balances, typically mounted outside the wind-tunnel walls on a turntable or solid base. The bal-

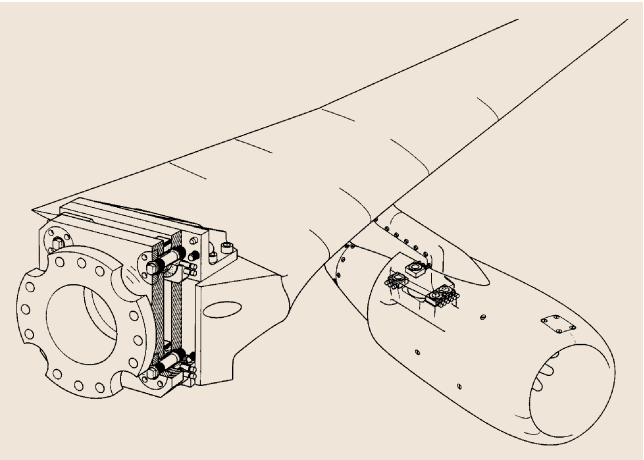

Fig. 8.62 Half-span model including ejector engine, equipped with two piezo balances: one at the root of the wing and the second integrated in the engine

ance integrated in the engine, also shown in Fig. 8.61, is described in *Schewe* [8.25] and *Triebstein* et al. [8.26]. In this case as well four multicomponent transducers are sandwiched between the pylon and the core element of the engine model.

Observing the platform balance at the root of the wing, it is obvious that it corresponds with the scheme of four multicomponent transducers (Fig. 8.62) that are prestressed by elastic bolts between two solid plates. When designing and applying piezoelectric force measuring platforms it is important to consider the force transmission in the balance. This is the junction between the balance and the model, and the attachment of the balance at a device of the wind tunnel (a turntable, for example). When designing the test setup and the balance, one must consider deformations of the solid plates within the balance. Keeping in mind that the measuring deformations are only of the order of microns, one can imagine that even the smallest deformations can produce interference effects between the individual components. Concerning the unavoidable deformations, the balance should be designed in such a way that the deformations that occur are antisymmetric. Such deformations of opposite sign can compensate for each other since the resultant force or moment components are composed (i. e., are the sum) of several (individual) signals. In other words, deformations that fulfill certain symmetry conditions can be seen as internal forces of the balance, which are not present in the resultant values, i. e., composed signals. Thus, in order to achieve a high degree of symmetry, the arrangement of the four load washers should be quadratic, if possible. Further, the base plate of the balance is not directly attached to the more or less plane surface of the test setup. A special flange between the two provides decoupling between the deformations caused by the attachment and the base plate of the balance. On the other side, the wing is screwed to the balance in such a way that the attachment screws are arranged symmetrically and as close as possible to the prestressing bolts of the balance.

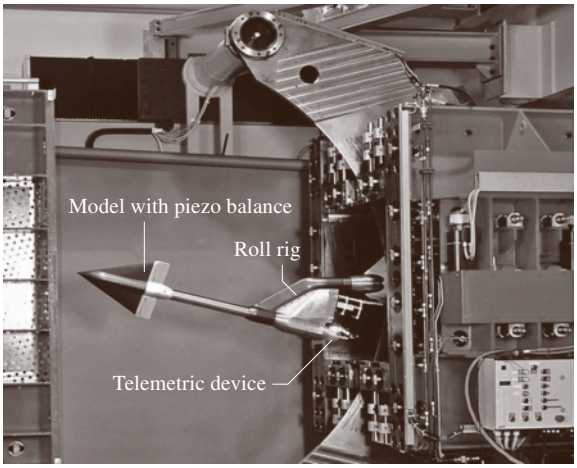

Fig. 8.63 Opened test section of the transonic wind tunnel. The rear sting support of a delta wing model is visible. The internal piezo balance is mounted inside the model [8.22]

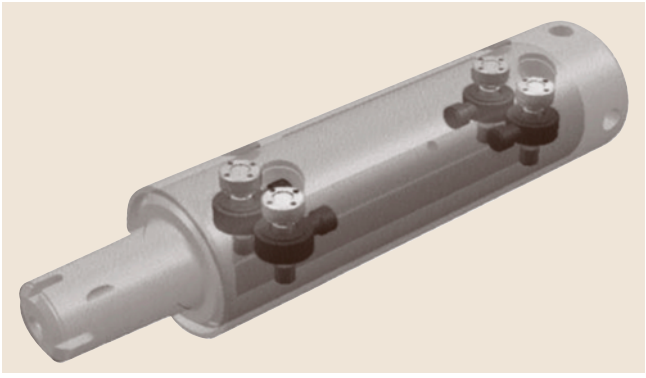

Fig. 8.64 Internal six-component piezo balance developed in cooperation by DLR and Kistler (after [8.22])

In general, a multicomponent piezo balance must be as accurately designed and constructed as high-fidelity optic equipment.

This type of balance has been applied in several variations, mainly differentiated by size. A special application is described later in Sect. 8.2.3, where two such balances, attached at each end of a two-dimensional (2D) airfoil model in a bilateral suspension, were used. In this case, both balances could be connected in parallel, such that they acted electrically as one balance.

A further special version of this type of platform balance was designed for application in cryogenic conditions. This balance, called a *cryo-balance* in the following is also based on four modified transducers (type 9252) as described in Sect. 8.2.2. The parts of the balance are made of special steel for cryogenic applications called *austenitic chrome nickel steel*.

If three-dimensional bodies are to be investigated, for example complete models of aircrafts or delta wings, then a rear sting support for the model is necessary, usually attached at a turning device to vary the angle of attack (Fig. 8.63). In this case, the force measurement is performed by a balance located at the end of the sting and inside the model. This type of balance, called an internal balance, usually has the form of a long circular

pipe segment and is difficult to design due to the small available space.

Psolla-Bress et al. [8.22] developed in cooperation with Kistler such a six-component sting balance also based on four piezoelectric force transducers manufactured by Kistler (type 9017B). These load washers have a circular case with a diameter of 16 mm. The schematic illustration of the balance in Fig. 8.64 shows that the arrangement of the transducers and the principle of operation corresponds to the platform balances described below. The outer annulus of the circular balance at which the model is fixed corresponds to the force conducting top plate and the counterpart acts as the base plate, which is attached at the support of the test section.

Details can be found in [8.22].

Comparison Between Piezoelectric and Strain Gauge Balance for a High-Pressure Wind Tunnel

Given the force measurements in the previously mentioned high-pressure wind tunnel, we have a good opportunity to compare both principles, since there are two external balances for performing three-component measurements on two-dimensional airfoils or bluff bodies.

The principal difference between the active piezoelectric measuring system and the passive strain gauge system was already discussed in the introduction.

Figures 8.65 and 8.66 further illustrate the fundamental differences between these two measurement systems. Figure 8.65 depicts the principle of a strain gauge balance for three-component measurements on a two-dimensional airfoil model. The model is fixed at both ends by a force conducting plate supported by three elastic ring elements. The ring elements, on which

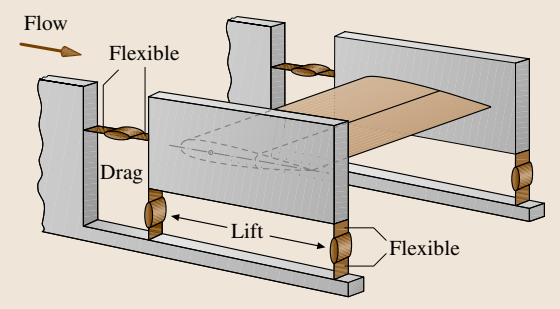

Fig. 8.65 Simplified sketch of a strain gauge balance for airfoil measurements. The strain gauges are fixed onto the individual rings (sketch by K.E. Möller)

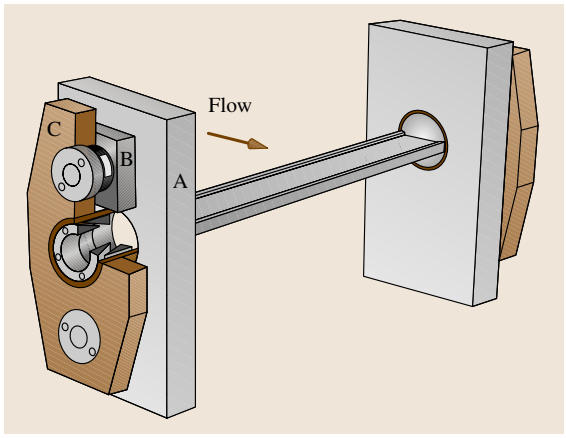

Fig. 8.66 Schematic drawing of the piezo balance for a high-pressure wind tunnel; (A) wall of the test section, (B) three-component load washer (Kistler 9067), (C) force-conduction top plate, the four load washers are prestressed by elastic bolts between A and C such that the shear forces can be transmitted by friction

the strain gauge sensors are applied, represent the force transducers. When considering the drag direction (x), it is obvious that a sufficient measuring deflection in the ring element for drag also requires a corresponding flexibility of the lift measuring elements in the x-direction and vice versa. In other words, the necessary measuring deflections for every component require a mechanical decoupling of the components that are perpendicular to the desired one. This requirement consequently reduces the desired rigidity of the entire system. In reality, the setup is highly sophisticated using six high-end force transducers manufactured by Hottinger, but the mechanical decoupling remains necessary in any case. This balance is described by *Schaake* [8.27].

For comparison we consider the piezo balance in Fig. 8.66 which was the first balance developed, and has been applied by *Schewe* [8.16] since 1980. At first glance, there are no elastic elements, but two rather stiff multicomponent load washers (B) at each side. With the help of elastic bolts and the two common top plates (C), two pairs of load washers are pressed to each vertical wall (A) of the test section. A modification of the force transducer for use up to 100 bar will be described in Sect. 8.2.3. The circular ends of the freely suspended model are passed through the wind-tunnel walls (A) and the ends are clamped in the holes of the force conducting top plate by a ring locking assembly. This detail is noteworthy as it provides rotational symmetry of the strain distribution in the force conducting top plate. The

test section is the basis for the force measurements as the force is introduced over both force conducting top plates (C). This means that the force components, drag (F_x) and lift (F_z), which act as shear forces on the load washers, are transmitted by friction.

It is obvious that mechanical decoupling is not necessary since each of the four load washers is able to measure three components, where here the axial component is not relevant. The possibility to forego the mechanical decoupling further enhances the rigidity of the balance, leading to the favorable property that, applying for example a circular cylinder, the natural frequency is determined by the rather high bending frequency of the model. In the case of the strain gauge balance, the elastic elements act as springs; consequently the balance in combination with the model and attachment mass determine the natural frequency, which is typically rather low.

An important difference between both principles concerns the ability to measure force components of very different magnitude simultaneously. For example, this may be the case when investigating airfoils in attached flow, where the lift is roughly two orders of magnitude larger than the drag force. For this reason the drag force elements of strain gauge balances are typically more sensitive than the lift force elements. In other words, there is the possibility to adapt the individual force ranges by varying the corresponding sensitivities, whereas in the case of multicomponent piezoelectric transducers this possibility does not exist, as the sensitivities in one element are fixed. This small disadvantage can be partly balanced by selecting a range of higher sensitivity in the charge amplifier.

Processing of Signals

Referring to the platform balance (Fig. 8.61) and the balance for the high-pressure wind tunnel it is obvious that the four load washers deliver 12 signals. The proper combination of these signals allows, in principle, all six components of the resultant force and moment to be determined with respect to the geometric center of the four transducers.

Considering first the simpler, two-dimensional case of measurements in the high-pressure wind tunnel, where only a three-component measurement of drag, lift and pitch moment is required. In this case, only shear forces on the load washers are relevant. Since the sensitivity of all elements to the shear forces is equal, related components can be wired electrically parallel and routed to a charge amplifier. Parallel wiring of the four components in the lift direction yields the resultant lift, while the pitch moment is obtained from the difference between the two lower drag components and the two upper drag components. Total drag corresponds to the sum of the lower and the upper drag force. Finally three electric signals are produced for a three-component measurement.

Considering a three-dimensional problem, for example a half model attached to a platform balance or an internal sting balance, in which all six components of the resultant force and moment are desired. In this case the number of charge output signals is reduced to eight, when the corresponding individual components with a common line of action have been paralleled directly.

The charge amplifier converts electrical charge into a proportional electric voltage. It is, in principle, an inverting direct-current (DC) amplifier and integrates the input current $i = \mathrm{d}Q/\mathrm{d}t$, which is created by the changes of charge at the quartz sensor. This is made possible by an amplifier with capacitive feedback, which has the highest possible internal gain and insulation resistance at the input [8.23]. In particular for quasistatic measurements, a high resistance R at the input is a prerequisite for low drift effects. Thus, all cables and plugs between the transducer and the charge amplifier must have an insulation resistance of higher than $R \approx 10^{13}\ \Omega$. This value is more than three orders of magnitude higher than that of ordinary bayonet Neill–Concelman (BNC) cables.

For quasi-steady measurements, the outputs of the three or eight charge amplifiers (for example, Kistler 5007) are evaluated by a personal computer equipped with an analogue/digital (A/D) conversion system. Apart from the calculation of the resultant forces and moment, a simple drift correction procedure, which will be discussed in Sect. 8.2.2, is used.

8.2.2 Typical Properties

Calibration Tests (Interference Effects)

As an example of calibration behavior and interference effects, we use the external balance of the high-pressure wind tunnel, which is referred to as a HDG balance in the following. In the quasistatic mode of the charge amplifiers the static calibration of the balance was performed with weights for the drag force F_x, lift force F_z and pitch moment M_y. Figure 8.67 shows an example of a calibration curve for the lift F_z, including interference on the drag F_x.

The charge Q_z [nC] is plotted against the calibration weight, which was applied in the direction of the F_z component. The weight was varied over two orders of magnitude and it is evident that the linearity of $Q_z(F_z)$ is

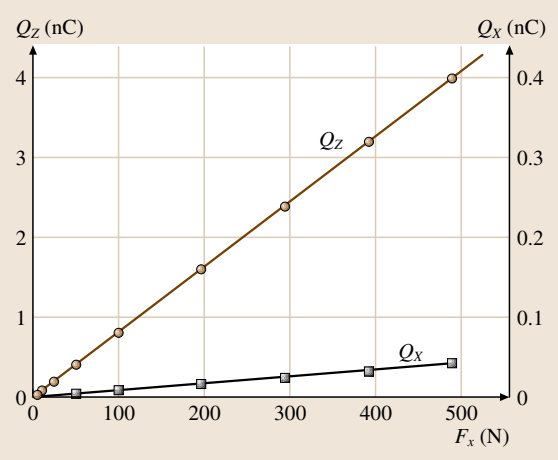

Fig. 8.67 Example of a calibration curve for the lift force F_z and the interference from the z- to the x-component. $Q_x(F_z)$ is enlarged by a factor of 10. The interference $Q_x(F_z)$ is approximately linear ($\mathrm{d}Q_x/\mathrm{d}Q_z = 1\%$)

quite good. The scale of the right-hand ordinate, indicating interference on the x-component $Q_x(F_z)$, is enlarged by a factor of 10. Nevertheless, we see that the interference effects on the x-component are small and nearly linear. A quantitative measurement of the interference is the ratio of the two slopes (i. e., the sensitivities for both components) $Q_z(F_z)$ and $Q_x(F_z)$, which amounts to $\mathrm{d}Q_x/\mathrm{d}Q_z = 1\%$. All calibration results for a multicomponent force-measuring device can be collected in the calibration matrix E_{ij}, which gives a summary of the static properties of the system. The following relation holds:

$$Q_i = E_{ij} F_j \quad E_{ij} = \frac{\partial Q_i}{\partial F_j}$$

with $i, j = 1, 2, 3$ for a three-component calibration. Q_i are the measured charges and F_j are the desired components of the force or pitch moment. The matrix elements $E_{ij} = \mathrm{d}Q_i/\mathrm{d}F_j$ are the sensitivities, determined by calibration using weights for the individual components.

In Fig. 8.67, for example, we determined $E_{22} = \mathrm{d}Q_z/\mathrm{d}F_z = 8.117\,\mathrm{pC/N}$ and $E_{12} = \mathrm{d}Q_x/\mathrm{d}F_z = 0.085\,\mathrm{pC/N}$. With a circular cylinder as a test model, we obtained the following calibration matrix:

$$\begin{pmatrix} Q_x \\ Q_z \\ Q_m \end{pmatrix} = \begin{pmatrix} 8.127 & 0.085 & -0.065 \\ 0.025 & 8.117 & 0.071 \\ -0.036 & 0.066 & 8.187 \end{pmatrix} \begin{pmatrix} F_x \\ F_z \\ M'_y \end{pmatrix} \tag{8.41}$$

The matrix elements of the last column (E_{i3}), belonging to the calibration of pitch moment, are normalized with the length $l = 0.2\,\mathrm{m}$ ($M'_y = M_y/l$). Thus, all matrix elements have the same dimension pC/N. The length l corresponds to the lever arm used in the calibration of the pitch moment. Under ideal conditions, all elements E_{ij}, $i \neq j$ that represent the interferences must be zero, while the diagonal elements ($i = j$) represent the sensitivities for the individual components $E_{11} = \mathrm{d}Q_x/\mathrm{d}F_x$, $E_{22} = \mathrm{d}Q_z/\mathrm{d}F_z$ and $E_{33} = \mathrm{d}Q_m/\mathrm{d}M'_y$.

Nevertheless, it is evident that interference elements with $i \neq j$ are at least two orders of magnitude smaller than the diagonal elements. Furthermore, the sensitivities (i. e., the slopes) for both force components F_x and F_z are identical within the accuracy possible in the drawings ($E_{11}/E_{22} = 1.0012$).

Dynamic Behavior and Resolution

The dynamic behavior can also be demonstrated by means of the high-pressure wind tunnel balance for the following reasons: first, it can be shown that, despite the extensive arrangement of the transducers, there are no eigenfrequencies below the rather high natural bending frequency of a circular cylinder model; second, we have the possibility to compare with a strain gauge balance.

The eigenfrequencies were obtained by the Fourier transform (Fig. 8.68) of the impulse response from the balance signals $F_x(t)$ and $F_z(t)$. Because of the high rigidity of the quartz elements themselves, the lowest eigenfrequency is determined by the bending of the

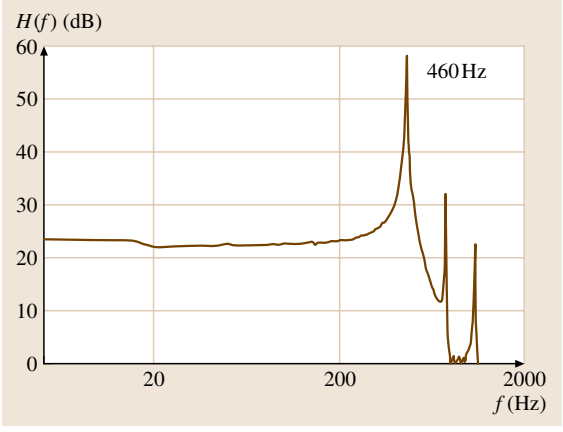

Fig. 8.68 Transfer function for the x-component obtained by Fourier transform of the impulse response, taken using the circular cylinder in the external balance of the HDG

model that connects the two parts of the balance. In this special case of the circular cylinder, the lowest eigenfrequency is $f = 460$ Hz for the x-component. Due to the different clamp conditions, the eigenfrequency is higher for the z-component with a value of $f = 535$ Hz. Finally, Fig. 8.68 shows that there are no significant resonance frequencies lower than $f = 460$ Hz. This value is high enough, considering that in our case typical vortex shedding frequencies of bluff bodies are lower than 200 Hz.

Schaake [8.27] applied in the high-pressure wind tunnel the external strain gauge balance for investigating two-dimensional bluff bodies and found resonance effects around 100 Hz caused by the balance itself. The resonance amplitudes were so high that the balance had to be blocked at high Reynolds numbers, which are coupled with high loads.

Here the undesired situation that the resonances of the force measuring system lie in the frequency range of interest occurs, in this case in the frequency regime of the vortex shedding caused by the bluff bodies.

The next example concerns the cryo-balance, which was mounted at the calibration setup. In addition a large body with rectangular cross-section, a simplified model of a building, was attached to the balance with a minimum bending frequency of 16.4 Hz. The low bending frequency was achieved by a compliant junction between the balance and the model.

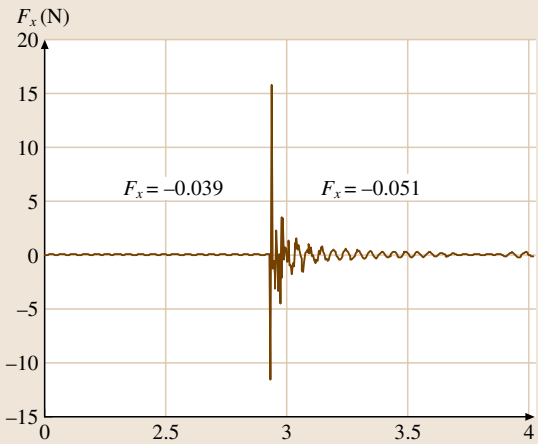

Fig. 8.69 Zoom of the time history for a situation where a weight of 1 g was dropped on the model, which was attached at the balance (height 0.02 m). The excitation of the natural frequency is obvious. Also the jump in the mean values of F_x before and after the impact is measured

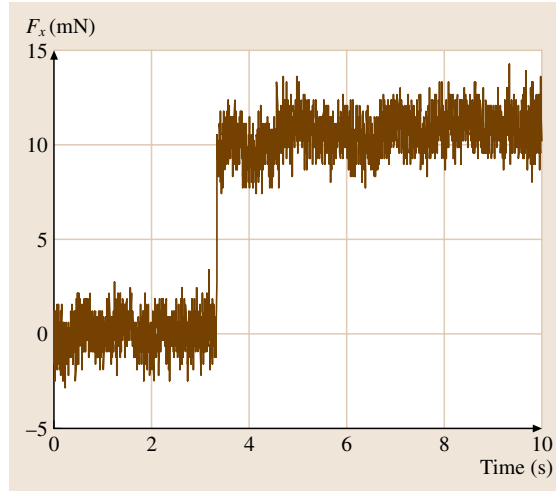

Fig. 8.70 Demonstration of the high resolution of the piezo balance in its range of highest sensitivity. A 1 g weight was hung from the balance, and the significant jump was caused by unloading the weight

A very simple experiment shall demonstrate the static and dynamic behavior using a small weight.

In Fig. 8.69, we see a zoom of the time history $F_x(t)$ for a situation where a 1 g metal weight was dropped on the model; the height of fall was approximately 0.02 m. After a high-frequency response due to the impact of the weight, the excitation of the natural frequency of the cylinder is obvious. Additionally the rather small change in the mean value could be resolved. For the calculation of the mean values of F_x before and after the impact, the entire measuring time of 10 s was used.

In order to demonstrate the limit of resolution at optimal conditions, the 1 g (≈ 10 mN) weight was hung from the balance without a model, and a jump was then caused by unloading the weight. Figure 8.70 shows the corresponding jump in the time function of the balance signal F_x, demonstrating that the resolution is even better than 0.01 N. The peak-to-peak value of the noise of the entire system is roughly 3–4 mN. For this measurement the range of the charge amplifier was switched to highest sensitivity. Finally it should be noted again that these experiments can be performed independent of the static preload and that the results are also typical of balances based on the larger force transducer (type 9067), as the sensitivities are equal.

In order to provide an example illustrating the attainable measuring range, we consider the HDG balance or a platform balance, which are based on four of the larger transducers (9067). The typical maximum load

for each component is at least $F_i \approx 10\,\text{kN}$. Thus, the measuring range extends over six orders of magnitude, since the threshold for dynamic measurements is as low as 0.01 N. Experience shows, as does the later result in Fig. 8.71, that quasistatic measurements are possible down to below $F \approx 1\,\text{N}$. Consequently, in quasistatic mode a measuring range of four orders of magnitude is attainable.

Reproducibility

In order to get a measure for the reproducibility, a calibration cycle was repeated 10 times over a time period of a few hours under normal laboratory conditions. For this test, a platform balance for half-span models, based on the larger transducer (type 9067), was used. One calibration cycle was performed with calibration weights of 5, 10, 20, 35 and 50 kg, lasting roughly 15 min. Table 8.5 shows the results of the measurements. The second column displays the sensitivity of the x-component E_x in [pC/N], determined from the slope of the calibration curves. The third column singles out one measuring point of the calibration cycle, the voltage U_x corresponding to a load of 50 kg.

Calculating the mean and the standard deviation we find for the sensitivity of the x-component:

$$E_x = (7.8634 \pm 0.0005)\,\text{pC/N}\,. \tag{8.42}$$

The ratio between the difference of the peak values and the full-scale range can be seen as a measure of the reproducibility. These values can be derived from the second column: largest deviation $U' = U_{x\max} - U_{x\min} = 0.5\,\text{mV}$, full-scale range $(x_{12} + x_{34})$ each 10 V $\Rightarrow U_{\text{FS}} = 20\,\text{V}$.

Thus the reproducibility has a value of:

$$\frac{U'}{U_{\text{FS}}} = 0.025‰\,. \tag{8.43}$$

These results are also, at least, representative of other external balances and demonstrate that it is possible to attain good accuracy if one is able to hold the ambient conditions constant.

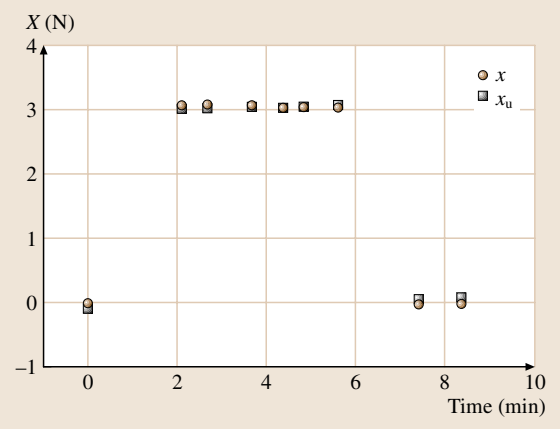

Fig. 8.71 Measurement of a relatively small drag force X on a building model, taken in the boundary layer wind tunnel of the University of Florence using the cryo-balance ($u = \text{const} = 4.3\,\text{m/s}$. Wind off at $t = 0$ and $t > 7\,\text{m}$). X_u: uncorrected values, i. e., without drift correction

Table 8.5 Results of 10 calibration cycles repeated under normal laboratory conditions

Cycle No	E_x (pC/N)	U_x (V/50 kg)
1.	7.8637	1.9287
2.	7.8638	1.9287
3.	7.8625	1.9283 min.
4.	7.8634	1.9285
5.	7.8630	1.9285
6.	7.8633	1.9284
7.	7.8632	1.9285
8.	7.8631	1.9285
9.	7.8644	1.9288 max.
10.	7.8636	1.9285
Mean	7.8634	1.9285
Stand. dev.	0.0005	0.0002

Behavior Under Cryogenic Conditions

As mentioned in the introduction, a piezoelectric balance was built for the cryogenic Ludwieg tube in Göttingen (KRG) in such a way that the balance itself is totally in the cryogenic environment. This fact is not self-evident as such a balance has to withstand a large amount of thermal stresses when the temperature is changed over the entire range of the cryogenic facility.

One motivation for this activity was to clarify the question of to what extent force measurements could be made with piezoelectric transducers under cryogenic conditions.

At our request, a special version of transducer type 9252 was manufactured by Kistler for applications at cryogenic temperatures. The modification concerns the insulators in the plugs, by default made from silicone, which were replaced by ceramic ones such that application down to cryogenic temperatures ($T = -150°$) and pressures up to 10 bar was more feasible. The modification mainly ensures that no humidity diffuses into the transducer case during the unavoidable large temperature changes.

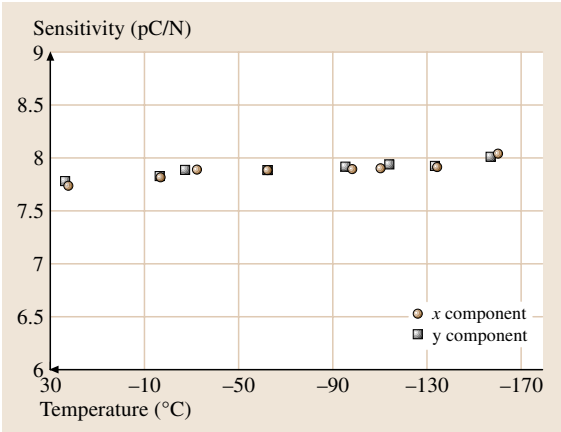

Fig. 8.72 Determination of the sensitivity of the shear components F_x and F_y of the cryo-balance depending on temperature

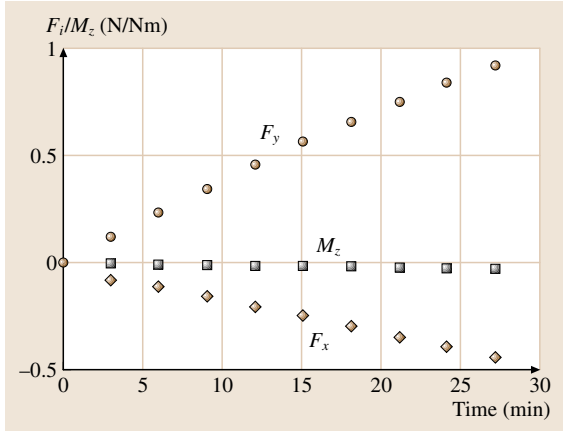

Fig. 8.73 Demonstration of the drift behavior in the range of highest sensitivity of the entire force measuring system under ideal environmental conditions

Before application in the wind tunnel, the balance with the modified multicomponent transducers (Sect. 8.2.1) was tested and calibrated in a cryostat down to a temperature of $T = -160°$. The low temperature was produced by injection of vaporized nitrogen. For the connection between the force transducer in the cryostat and the charge amplifier outside, the usual cables for piezoelectric sensors could be used.

In the pre-tests we found no significant deviation in the behavior of the balance concerning drift or electrical noise of the signals compared with normal conditions.

The calibration was conducted using weights, which were appended outside of the cryostat via cables. Concerning the axial component F_z, it was found that the cool-down from 24° to −169° led to a contraction of the prestressing bolts, resulting in a 1.5 kN increase of the prestressing force, which is one order of magnitude smaller than the standard prestress. This effect was caused by the different thermal expansion coefficients of the transducer and the prestressing bolt.

Both shear components F_x and F_y showed good linearity compared to that at normal conditions, and the slopes, i. e., the sensitivities, as a function of temperature are displayed in Fig. 8.72. It is obvious that the sensitivity changes slightly with temperature. This sensitivity shift is caused by the fact that the corresponding piezoelectric coefficient (d_{11}), which is responsible for the shear effect, increases slightly with decreasing temperature [8.23].

In this context, it should be mentioned that, at normal conditions, arrangements of force transducer are also sensitive to temperature changes during a measurement cycle. This problem concerns, in particular, the direction of the prestressing bolts. Thus, in any case the balances must be protected against changes in thermal distribution, at least while running a measurement.

Measuring Time for Quasistatic Measurements

As mentioned, the piezoelectric measuring system is an active one and generates an electrical quantity. Herein lies a fundamental disadvantage, namely that only quasistatic measurements are possible. A time constant $T = R_g C_g$, characteristic of the exponential decline of the charge signal, results from the entire input capacity C_g and the finite insulation resistance R_g, posed by the transducer, cord, plugs and amplifier input etc. Further fault currents in the charge amplifier, which are fortunately independent of the load, cause the zero point to drift. Thus the combined error is smaller for larger charges on the quartz, meaning that the effective measuring time increases as the loading and the sensitivity increase. Fortunately, the drift is dominated by the fault currents in the input devices of the charge amplifier, which are nearly constant, leading to a linear drift depending on time at the output. The sign of the drift can be positive or negative. A simple linear correction for every test point in time can be computed as follows. For each measurement, the raw data, integrated over time, and the corresponding time are stored. Knowing the zero point before the measurement (flow speed $U = 0$) and after the measurement (where the flow speed is zero again), a correction can be computed by linear interpolation.

In order to give an impression of the drift behavior under extreme conditions, the time function of the

three components of the cryo-balance were recorded, while the balance was attached to the calibration setup, i. e., without load and under good environmental laboratory conditions. In addition, the cables and plugs were verified as having an overall resistance of at least $R \approx 10^{13}\,\Omega$. In another (unfavorable) condition, the system was switched in the range of highest sensitivity, where the drift effect was maximal. Figure 8.73 shows, firstly, that the drift was rather linear for all three components, and secondly, that at least under good environmental conditions the drift effects are not as extensive as generally believed. In other words, the results show the probable lower reachable limit when components such as plugs and cables are selected and the test conditions are nearly optimal.

In order to provide an impression of the drift error at small loads, an example is presented in Fig. 8.71, taken in the boundary-layer wind tunnel of the University of Florence. A simplified building model was mounted on the cryo-balance as shown in the sketch in Fig. 8.57. This figure shows a measurement of a relatively small drag force of $X = 3.1$ N at a low flow speed $u = \text{const} = 4.3$ m/s over time t. The airflow was started at $t = 0$ min and switched off for $t > 7$ min. The index u (X_u) denotes values without drift correction. Looking at the square symbols (uncorrected) at $t = 0$ min, we see a small deviation in the negative direction, caused by switching to the operate mode. At the end of the measurement run at $t = 8.5$ min, there is also a small deviation but in the positive direction. The small difference in the outputs between the start and end is caused by a drift in the positive direction. After correction, the corresponding points (○) lie on the zero line.

Although the wind-tunnel speed is not exactly constant, we can state that the effect of the drift of the zero point is not as extensive as generally believed.

8.2.3 Examples of Application

Bluff Bodies in a High-Pressure Wind Tunnel

The flow around a circular cylinder is a classic problem of fluid dynamics, which exhibits strong Reynolds-number effects, mirrored in drastic variation of the drag coefficient and Strouhal number. A second classic bluff-body case is the sharp-edged square-section cylinder, which has a high drag coefficient that is nearly independent of the Reynolds number.

Thus, both sections were selected as examples concerning force measurements performed in the high-pressure wind tunnel (HDG). The flow speed ranged from 2 m/s to 38 m/s; the pressure could be increased up to 100 bar and the test section measures $0.6 \times 0.6\,\text{m}^2$. Since even steady loads in this low-speed wind tunnel can vary over four orders of magnitude merely by changing the flow parameters, the results give an impression of the large dynamic range of a piezo balance. Indeed, this property of the wind tunnel and the deduced requirement of a large dynamic range motivated the author to design and built his first piezo balance [8.16].

The principle setup of the balance was described in Sect. 8.2.1 (Fig. 8.66). We selected the larger three-component force-measuring elements (Kistler, type 9067), because of their large load range. A special difficulty when measuring in the high-pressure wind tunnel is the fact that the model, the sensors and the balance are located in the high-pressure section, while it is desirable to have the electronic equipment outside at atmospheric pressure. Since one of the primary prerequisites for quasistatic measurements is that an insulation resistance of $R \approx 10^{13}\,\Omega$ is reached for all connections between the force element and charge amplifier, a special solution was necessary for the crossover from the high- to the atmospheric-pressure sections. Because this requirement is difficult to satisfy with hermetic connectors, the necessary cables were inserted into flexible pressure-resistant hoses, which were pressure-seal connected at the transducer and then laid through the wind tunnel

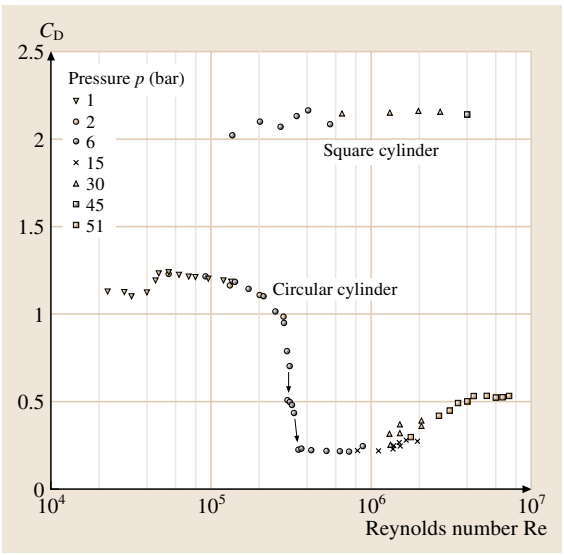

Fig. 8.74 Measurement of drag coefficients of a circular and a square cylinder in a high-pressure wind tunnel. Due to the large dynamic range of the balance the individual Re number ranges could be overlapped by merely changing the flow parameters

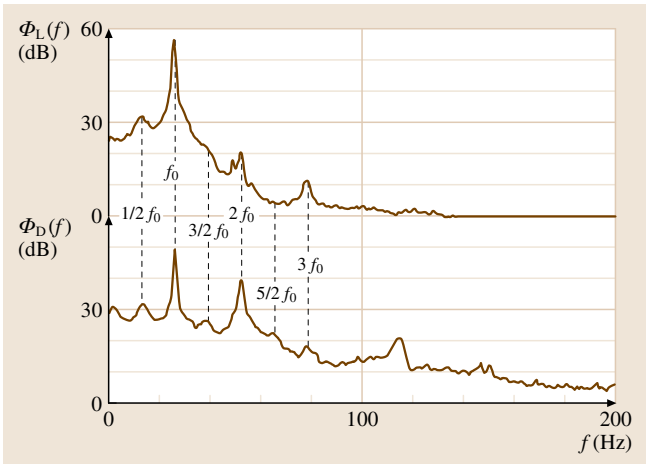

Fig. 8.75 Power spectra of the lift and drag fluctuations on a square cylinder at an angle of incidence of $\alpha = 10°$. Even the very low intense sub- and superharmonics can be resolved. The distance of the peak height is up to 50 dB

wall and connected to the charge amplifier outside of the high-pressure section. In this way, atmospheric pressure was maintained within the element, as well as in the corrugated hoses, so that an increase of static pressure in the wind tunnel acts as a preload on the element. Since the zero point in the sensor/charge-amplifier system can be chosen arbitrarily by short-circuiting the charge, the preload in the axial direction has no significant influence on the accuracy of the measurement.

This modification of the force transducer for application at high pressure up to 100 bar was also manufactured by Kistler.

Such modified transducers were also applied in several water tanks in Hamburg to measure the forces on ship models and marine structures [HSVA Jochmann]. A detailed description of the balance and many results concerning flow around more or less bluff bodies can be found in [8.17, 18, 28–30].

As an example of a quasisteady measurement, Fig. 8.74 shows drag coefficients of a circular cylinder and a square cylinder as a function of the Reynolds number. The flow speed was increased to 40 m/s and the pressure up to 51 bar. In the case of the circular cylinder, the smallest drag force was 0.8 N at the lowest Reynolds number. The largest drag force was about 2000 N for the square cylinder at $\mathrm{Re} \approx 5 \times 10^6$. Since only about 20% of the range of the balance was used, it was demonstrated that, in principal, steady measurement over four orders of magnitude was possible. As for fluctuating forces, the dynamic range is extended to six orders of magnitude because the resolution is about 0.01 N.

Figure 8.75 depicts a typical dynamic measurement, which is representative of the ability to resolve and detect even very weak nonlinear effects in a global force measurement. The figure shows the power spectra of the lift – and drag fluctuations on a square cylinder at an angle of incidence of $\alpha = 10°$. In this state, the free separated shear layer is probably more or less regularly attaching to the side wall of the square cylinder, producing sub- and superharmonic peaks. It is surprising that this localized effect can be found and resolved in a global, i. e., integrated measurement. In addition, apart from the fundamental Strouhal peak and the sub- and superharmonics, there are significant peaks at 3/2 and 5/2 of the vortex shedding frequency [8.31]. The dynamic is reflected in the distance between the spectral densities, which is up to 50 dB.

Further applications concerning force measurement on a bridge section and an airfoil at a high angle of attack can be found in *Schewe* [8.29].

Typical Half-Span Model in a Conventional Low-Speed Wind Tunnel

The wing/engine combination described in Sect. 8.2.1 was tested in the low-speed wind tunnel ($3 \times 3\,\mathrm{m}^2$) in Göttingen. The project comprised force and pressure distribution measurements. The influence of the thrust of the ejector engine on the aeroelastic and aerodynamic behavior of the wing/engine combination was of particular interest. For this reason, in the engine model four multicomponent force transducer were installed to measure separately the global forces on the engine. More about the motivation for the project, a detailed description of the test setup, and the results of the pressure measurements can be found in *Triebstein* et al. [8.26].

Figure 8.76 shows as an example of the steady normal force and its RMS value for angles from −4° up to 14°, taken at a flow speed of 60 m/s. In this case the balance was not fixed to the wind tunnel, but rotated with the model, thus the normal force on the wing and not the lift was measured. The results demonstrate that the measurement of steady forces is possible with sufficient accuracy. The angle $\alpha = 0$ was measured twice – at the beginning and at the end of the test run. Within drawing accuracy, both measuring points overlap.

Referring to the span of the measurement range, it should be mentioned that, at the maximum normal force of more than 1000 N, only about 6% of the range of the balance is used, meaning that this balance can also

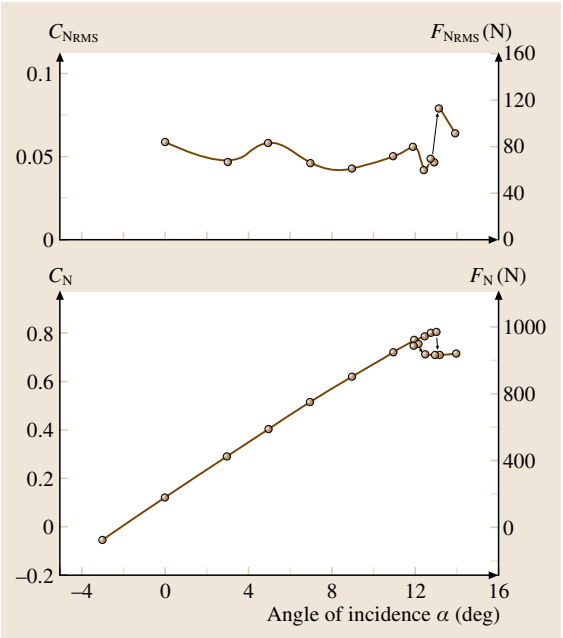

Fig. 8.76 Normal-force coefficient and corresponding root-mean-square (RMS) value depending on the angle of incidence of a wing/engine combination in a low-speed wind tunnel. $C_N(\alpha)$ is not a straight line since the balance is rotated with the wing. After the discontinuous drop of the steady normal force at 13°, the RMS jumps to nearly double its previous value

be applied at much higher loads (i. e., in the transonic range) without any changes being necessary.

As an example of an unsteady measurement, in the upper part of Fig. 8.76 the RMS value of the normal force is presented, being nearly constant below the onset of flow separation. After the discontinuous drop of the steady normal force at 13°, the RMS jumps to nearly double its previous value. One has to bear in mind that inertia forces are included.

The RMS of the bending moment was also measured, and showed similar behavior. All RMS values were obtained by integrating the corresponding power spectra. Figure 8.77 shows two examples of normal force spectra immediately before and at the onset of the flow separation. The dotted line represents the spectrum taken at $\alpha = 13.2°$, while the solid line represents the spectrum taken at 13°. The spectra are dominated by a rather narrow peak at the bending frequency of the wing. The bending frequency is excited by the noise-like random contributions that are inherent to the flow. Particularly after the onset of flow separation, the intensity

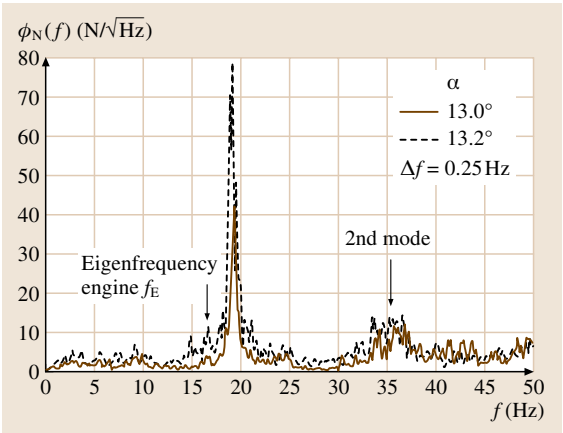

Fig. 8.77 Power spectra of the normal force immediately before ($\alpha = 13°$) and at the onset ($\alpha = 13.2°$) of flow separation. Concerning the balance, there are no resonance peaks caused by the force-measuring system itself

of the fluctuating aerodynamic loads, and consequently the bending vibration of the wing, increase drastically. Hence, the RMS jumps to nearly double its previous value in the normal force and bending moment. When considering these unsteady force measurements, it is important to remember that the signals contain several components. In addition to the aerodynamic loadings, contributions from elastic and inertia forces due to the vibration are also present.

Finally, it can be stated that the changes of the flow field at the onset of separation lead to a small frequency shift of the bending frequency. This frequency change, Δf, represents a small contribution to the stiffness, caused by aerodynamic effects.

As for the balance, the spectrum shows that there are no significant peaks that could be produced by the balance itself.

Aeroelastic Experiments: Oscillating Models in a Transonic Wind Tunnel

Aeroelasticity studies the interplay between elastic structures in an air stream and aerodynamic forces and moments. The interaction between aerodynamic and structural forces may lead to complicated nonlinear, static and dynamic effects, for example the feared flutter oscillations. Thus knowledge of the steady and unsteady forces and moments is essential. Therefore three different setups for aeroelastic experiments at airspeeds up to the transonic regime have been developed. These setups are usually applied in the 1 m × 1 m adaptive test section of the transonic wind tunnel in Göttingen.

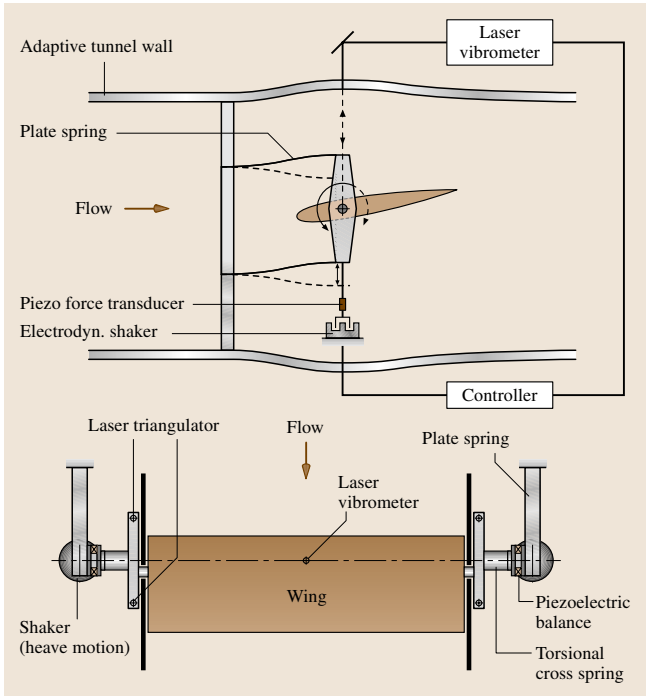

Fig. 8.78 Sketches of the setup for self-excited oscillations of an airfoil with two degrees of freedom. A piezoelectric balance is installed on each side between the bending and the torsion spring. A laser vibrometer, the electrodynamic exciter and the controller form the flutter control system. The exciter force is also measured using piezoelectric force transducers

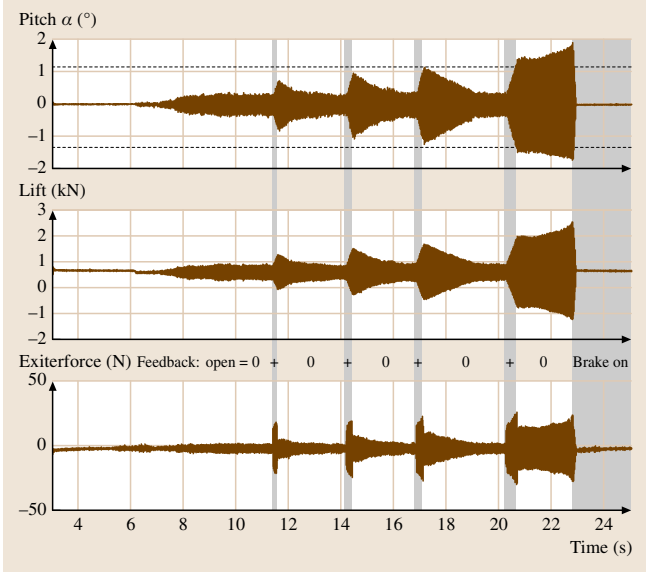

The first setup sketched in Fig. 8.78 is designed for investigating flutter phenomena of airfoil models. It is symmetrically built from blade- and cross-springs for bilateral elastic suspension. To measure the steady and unsteady forces, a piezoelectric balance is installed on each side between the bending and the torsion spring. Each balance corresponds to the platform balances, consisting of four multicomponent elements (type 9252) as described for half models in Sect. 8.2.1. In the case of flutter or forced motion the balance oscillates in the heaving direction. Therefore the smaller transducers were selected due to their lower weight and the advantage gained by reducing the moving masses.

Figure 8.78 also shows a schematic representation of the flutter control system used to dampen or excite oscillations of the model. A laser vibrometer was used to measure heaving motion of the airfoil oscillations. The heave-speed signals were fed into an operational amplifier and then into one electrodynamic exciter at each side. The excitation acts directly on the bending springs in the heave direction, whose connecting box forms the basis for the piezoelectric balance. Thus the excitation forces do not act directly on the piezoelectric balance, but rather appear only indirectly in the balance signals since the heave motion of the airfoil induces inertial forces. Forced heave oscillations can be driven by replacing the electrodynamic exciters by stronger hydraulic linear actuators. The exciter force F_{ex} itself can be measured directly with the one-component piezoelectric force sensor (Kistler 9301A), built into the heave rod.

Figure 8.79 shows an instructive example of a flutter measurement using a symmetrical National Advisory Committee for Aeronautics (NACA) 0012 airfoil taken at the flutter boundary. The state of the system is critical, i. e., in the transition range between stability and instability. We will see that it is a hysteretic-encumbered transition (subcritical bifurcation), which was recorded at a mean angle of attack of $\alpha = 1.1°$. The curves plotted in the Fig. 8.79 are: (a) the angle of attack $\alpha(t) - \alpha_{mean}$, (b) the lift force $L(t)$, and (c) the heave-rod force F_{ex} of the excitation, measured with the piezoelectric transducer. First we see in the offset that the mean lift is 0.7 kN. Second the time functions demonstrate how the

Fig. 8.79 Artificial initiation of self-excited flutter oscillations in a hysterisis regime (subcritical bifurcation). The initial amplitudes are set for different temporal lengths via positive feedback. The limit amplitude of $\alpha = 1.2°$ acts as a repeller. Depending on whether or not the initial amplitudes lie below or above this threshold value, the oscillations will be damped or excited

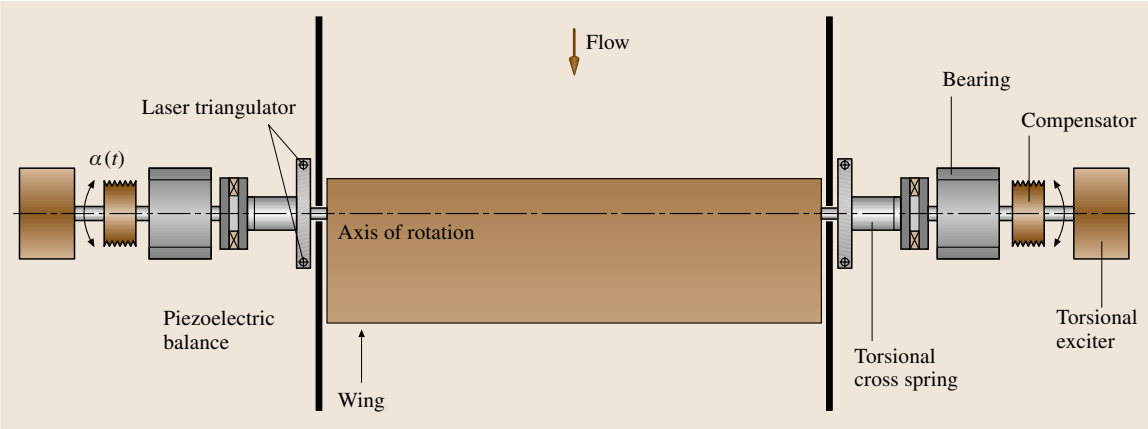

Fig. 8.80 Pitch test setup for forced torsion oscillations. The installation of both optional torsion springs (cross springs) gives the wing a torsional degree of freedom for investigating torsional flutter. The piezoelectric balances are between the hydraulic actuators and cross springs

system reacts to disturbances of different strengths or durations. Such a disturbance occurred when the control device was switched to positive feedback for a short time. The period of excitation of the system can be clearly seen in the curve for $F_{ex}(t)$, where the amplitudes shoot up at the indicated time points at $t \cong 11.3$, 14.2, 16.5, and 20.0 s. It is also obvious that the time span of the disturbances increases with increasing time. Whereas the flutter oscillations decay after the first three short bursts of excitation, they diverge after the fourth, the longest of the excitations. This behavior indicates that we must be in the hysteresis range of a subcritical bifurcation, i. e., the last disturbance was sufficient to lift the system above an unstable limit cycle, which then acted as a repeller to cause the increase in the amplitudes. At this point, we should note that the forces needed to influence the system are about two orders of magnitude smaller than the lift forces that occur, even though $F_z(c)$ still contains inertial forces.

Finally the example shows that it is possible to perform measurement of steady and unsteady forces under very difficult conditions, i. e., while the balance is oscillating.

By use of the second test setup (Fig. 8.80), the aerodynamic effect of forced pitching motions of a model may be investigated. In this case, two torsional hydraulic actuators work with a 180° phase shift and force the pitching motion of a two-side suspended model in the air stream. It is successfully used for example in testing airfoil models equipped with piezoelectrically driven flaps for dynamic stall control. The piezoelectric actuators use the inverse piezoelectric effect and are described by *Schimke* et al. [8.32]. This test setup can be upgraded with a torsional degree of freedom to investigate free pitch oscillations of the model. To measure the steady and unsteady forces, the same piezoelectric balances described above can be installed on each side between the hydraulic actuators, the model, and the optional cross-springs, respectively.

The ability to investigate unsteady phenomena such as buffet oscillations in transonic flow is demonstrated

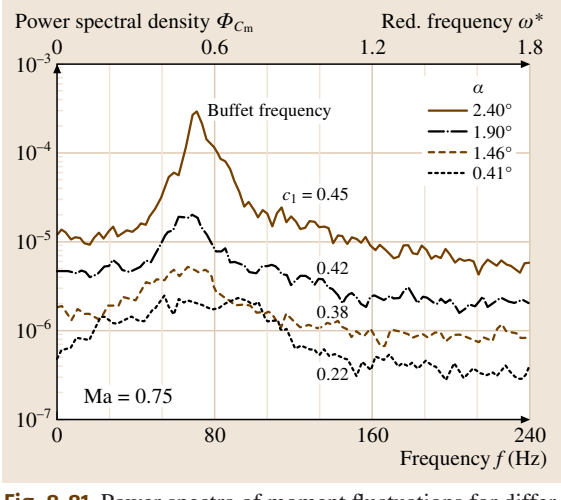

Fig. 8.81 Power spectra of moment fluctuations for different angles of attack for a fixed supercritical airfoil. With increasing α a peak at the buffet frequency of $\omega^* = 0.56$ appears. The corresponding steady lift coefficients c_l are also included

in Fig. 8.81, where spectra of the moment fluctuations are presented. In this case, the cross-springs were not installed, the model with supercritical section (NLR 7301) was at rest, and the angle of incidence α was varied using the hydraulic actuators.

These spectra show what happens when α is increased while the Mach number is held constant at Ma = 0.75. Above an angle of attack of $\alpha = 1.5°$, peaks appear in the spectra that can be traced back to self-excited shock oscillations (buffet) and, therefore, because of the absence of the necessary degrees of freedom for oscillations, have purely fluid-dynamical origins. The nondimensional buffet frequency has a value of $\omega^* = 0.55$, which corresponds to a frequency of $f = 72.7$ Hz. Simultaneously, the mean lift was measured and the values are included in the figure. For this type of measurement, the high stiffness of the twin-sided piezo balance is a significant prerequisite. The test setups and the experiments are described in more detail by *Schewe* et al. [8.33].

The third test setup, sketched in Fig. 8.82, shows a wing model mounted on a turntable device such that the wing meets the sidewall with a negligible gap. The turntable device allows the model's angle of attack around an axis perpendicular to the sidewall of the test section to be adjusted. Furthermore, the model can be forced by means of a hydraulic rotation actuator to perform pitch oscillations around the spar axis plotted in Fig. 8.82. Laser triangulators are used to measure the pitch according to the spar axis. Also here, a piezoelectric platform balance is used to measure the root loads outside of the test section. The time-averaged signal of the balance allows the global aerodynamic loads to be determined, while the unsteady part of the balance signal represents the sum of unsteady air loads and inertia forces.

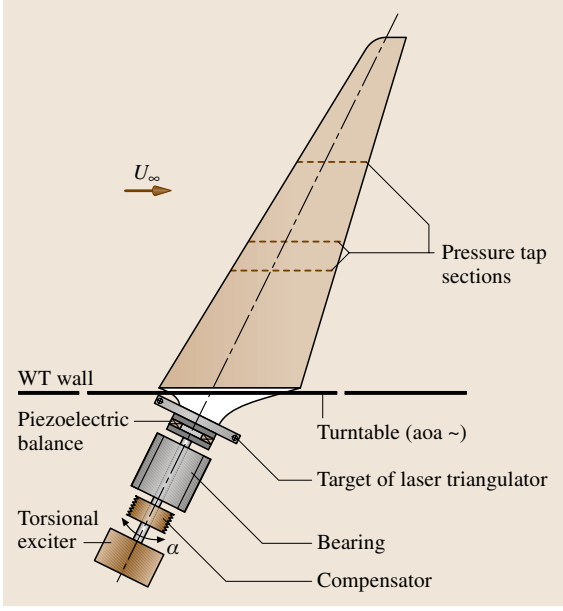

Fig. 8.82 Test setup for oscillating half models in a transonic wind tunnel. The piezo balance is located at the root of the wing

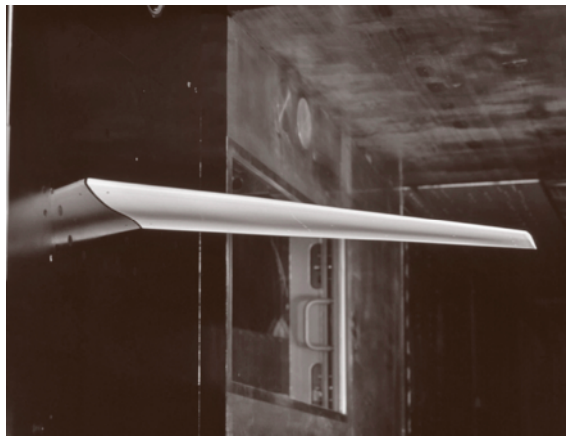

Fig. 8.83 Elastic wing models in the adaptive test section of a transonic wind tunnel

Figure 8.83 shows the half-span model of the *Aerostabil* project [8.34] mounted in the adaptive test section of the transonic wind tunnel in Göttingen (TWG). There are two models with the same outer geometry, representing the outer part of a transport aircraft wing with a supercritical airfoil section. The first model was designed conventionally, i. e., as rigid as possible, while the second was elastically scaled corresponding to the prototype. The aim was to study static aeroelastic effects, which have often been ignored in the past. Figure 8.84 shows the influence of the elasticity of the swept wing on the dependence of the lift curve slope $\partial C_L/\partial\alpha$ and the pitching-moment slope curve on the Mach number at a constant angle of incidence at the model root and constant Reynolds number. Significant differences due to elastic deformation can be seen as the lift curve slope is reduced up to 16% at Ma = 0.83. For the highest Mach numbers, the regions on the wing with flow separation are probably larger in the case of the rigid model, resulting in smaller values of the lift curve slope.

If the elasticity of a half-span model is designed in an appropriate way, flutter tests can be performed in this test setup, as can be seen in Fig. 8.85. We see a snapshot of the half wing twisted and bent by the steady air loads; in

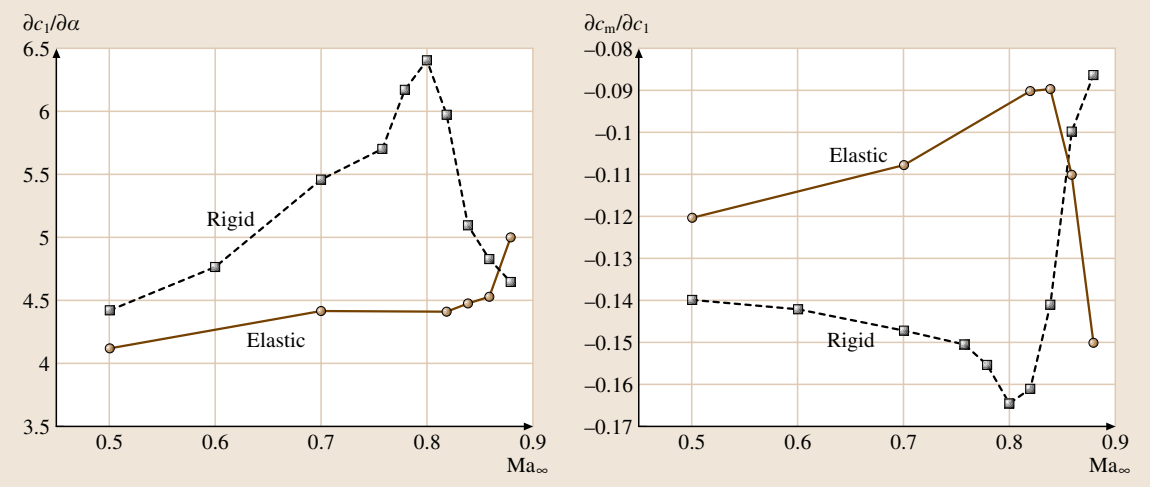

Fig. 8.84 Comparison of the lift-curve slope $\partial 2c_l/\partial\alpha$ and $\partial 2c_m/\partial c_l$ for the rigid and the elastic model as a function of Mach number

addition the wing is undergoing flutter, i. e., a limit-cycle oscillation (LCO) at a Mach number of Ma = 0.865.

Circular Cylinder in a Cryogenic Ludwieg Tube

The flow around a circular cylinder and its dependence on the Reynolds number is one of the most important problems and favorite test cases in fluid dynamics. Thus, this simple geometry was selected for the first application of the piezoelectric balance under cryogenic conditions [8.35].

The measurements were performed in the cryogenic Ludwieg tube in Göttingen (KRG), which is a blow-down wind tunnel for high-Reynolds-number research in transonic flow and is described by *Rosemann* [8.36]. The Mach number range is $0.28 < \mathrm{Ma} < 0.95$ and high Reynolds numbers up to more than 10^7 are achieved by cooling down the fluid medium to nitrogen temperature and by pressurizing up to 10 bar. The test section measures $0.4 \times 0.35\,\mathrm{m}^2$ and the effective measuring time is roughly 0.5 s.

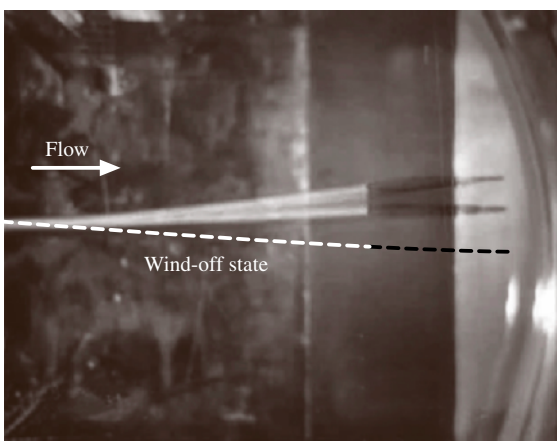

Fig. 8.85 Half-span model twisted and bent by air loads in the state of a limit cycle oscillation (LCO). Such measurements postulate a rigid balance

The test setup is similar to others using two-dimensional models such as airfoils or cylinders. Behind each wall of the rectangular test section there is a cryo platform balance, attached to a solid base at the test section. Similar to the high-pressure wind tunnel, the circular ends of the freely suspended circular cylinder are passed through the wind tunnel walls and the ends are clamped in the holes of the force conducting top plate of each balance by a ring locking assembly. In this case, both balances can also be connected in parallel, thus electrically they act as one balance, yielding three signals for drag, lift and moment.

Figure 8.86 shows a typical result for the drag force as a function of time, measured on a smooth circular cylinder (aspect ratio 11.4) at extreme values of the operating range of the facility. The intention was to get the highest possible Reynolds number in nearly incompressible flow. Thus the measurement was taken at the lowest temperature of $T = -150\,^\circ\mathrm{C}$, the highest pressure possible $p_0 = 10\,\mathrm{bar}$ and the lowest attainable Mach number of Ma = 0.28, resulting in a Reynolds number of $\mathrm{Re} = 5.8 \times 10^6$. The curve clearly shows that, with the onset of flow, the drag in-

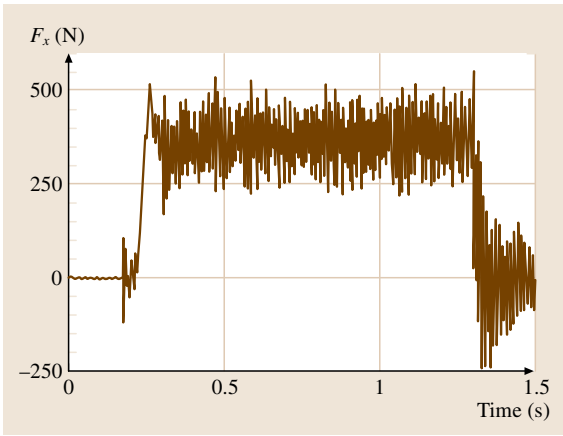

Fig. 8.86 Drag as a function of time for a circular cylinder, measured with a piezo balance in the cryogenic Ludwieg tube at extreme conditions ($\mathrm{Re} = 5.8 \times 10^6$, $\mathrm{Ma} = 0.28$, $T = -150\,^{\circ}\mathrm{C}$, $p_0 = 10\,\mathrm{bar}$). The drag coefficient is $c_\mathrm{d} = 0.53$, taken in the time window Δt between 0.8 and 0.9 s

creases rapidly up to a certain level, remains there as long as flow continues, then decreases quickly to zero when flow ceases. The drag coefficient is $c_\mathrm{d} = 0.53$, and a narrow peak in the spectrum of the lift fluctuations (Fig. 8.87) generated by the Karman vortex street, leads to a Strouhal number of $\mathrm{St} = 0.25$. In order to substantiate the force measurements, pressure measurements at the shoulder of the cylinder ($\varphi = 90°$) were performed with a pressure sensor (Kulite). The lower spectrum in Fig. 8.87 displays the behavior of the fluctuating pressure and thus confirms that the corresponding peak in the force spectrum is indeed due to the Karman vortex street at the same Strouhal number.

The RMS value of the lift fluctuations for this case amounts to $c_1' = 0.20$, which is more than double the value in other measurements [8.17]. The reason is that, at the lowest Mach number and with this low flow velocity, the low vortex shedding frequency ($f_\mathrm{V} = 465\,\mathrm{Hz}$) was quite near the natural frequency of the cylinder ($f_\mathrm{n} = 435\,\mathrm{Hz}$), leading to superelevation due to resonance effects.

The measured drag coefficient and the Strouhal number are in good agreement with the result in the high-pressure wind tunnel [8.17].

The strong oscillations in the drag signal, in particular after the flow has ceased ($t > 1.3\,\mathrm{s}$) may have many causes. One could be the mentioned proximity to the vortex resonance range. Although the vortex-induced drag fluctuations have double the value of f_Vortex, a higher-

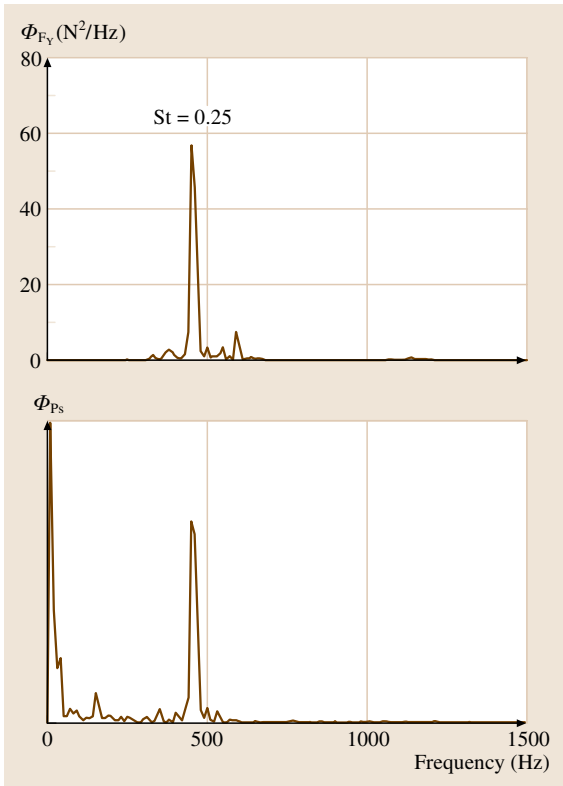

Fig. 8.87 *Upper*: power spectrum of the lift fluctuations corresponding to above measurement. *Lower*: power spectrum of the pressure fluctuations at the shoulder of the circular cylinder ($\varphi = 90°$)

order resonance due to nonlinear interaction may be responsible for the significant oscillations in the drag signal. In any case the rapid decrease of the flow velocity acts as a transient or jump excitation on the cylinder. This effect was not observed when both frequencies were well separated.

Nevertheless, it is interesting to note that, in spite of the pulse operating mode of the tunnel, the steady and unsteady processes can be measured very well.

8.2.4 Conclusions

Based on the applications described before, the typical positive properties of a piezo balance can be summarized as follows:

- High rigidity, which leads to small static deformations and to high natural frequencies
- Low interferences, typically lower than 1%

- High resolution (< 0.01 N), which is independent of the preload
- A large dynamic range; dynamic: six orders of magnitude, quasistatic: up to four orders of magnitude possible
- Applications in difficult ambient conditions such as cryogenic conditions, very high pressures and water, are possible.

The properties of piezoelectric measuring systems that can be disadvantageous when the generated charges are small are:

- Restriction to quasistatic measurements imposed by drift of the zero point, although this is not as extensive as generally believed and drift corrections are possible
- Sensitivity to temperature changes during the measurement, in particular in the direction of the prestressing bolts

Finally, in the field of aircraft aerodynamics, where the flow is attached and interest is focused on drag measurements with a resolution of drag counts ($\Delta C_d = 0.0001$), the application of strain gauge balances is suggested, since so far piezoelectric measuring systems cannot guarantee accuracy for very small steady values.

In all problems where the flow is more or less separated, for example in bluff body flows or situations around stall or when the model is oscillating, a high-end drag measurement has less significance and the disadvantages of piezo balances are more than outweighed by its inherent rigidity, which leads to well-known positive consequences.

References

8.1 ISO: *Guide to the Expression of Uncertainties in Measurements* (International Organization for Standardization, Geneva 1995)

8.2 AIAA: *Assessment of Experimental Uncertainty with Application to Wind Tunnel Testing, AIAA S-071A-1999* (AIAA, Reston 1999)

8.3 AIAA: *Calibration and Use of Internal Strain Gauge Balances with Application to Wind Tunnel Testing, AIAA R-091-2003* (AIAA, Reston 2003)

8.4 B. Ewald, G. Krenz: *The accuracy problem of airplane development force testing in cryogenic wind tunnels, AIAA Paper 86-0776, Aerodynamic Testing Conference Palm Beach* (AIAA, 1986)

8.5 B. Ewald: *Balance Accuracy and Repeatability as a Limiting Parameter in Aircraft Development Force Measurements in Conventional and Cryogenic Wind Tunnels, AGARD FDP Symposium, Neapel, September 1987* (AGARD, 1987)

8.6 B.C. Carter: *Interference Effects of Model Support Systems, AGARD Rep. R 601* (AGARD, 1973)

8.7 F.G. Tatnall: *Tatnall on Testing* (American Society of Metals, Metals Park 1966)

8.8 K. Hoffmann: *An Introduction to Measurement using Strain Gages* (Hottinger Baldwin, Darmstadt 1989), Company Print

8.9 Measurement Group: *Strain Gage Based Transducers* (Measurement Group, Raleigh 1988), Company Print

8.10 B. Ewald: Multi-component force balances for conventional and cryogenic wind tunnels, Meas. Sci. Technol. **11**, 81–94 (2000)

8.11 K. Hufnagel, B. Ewald: Force testing with internal strain gage balances, AGARD FDP Special Course, AGARD R-812. In: *Advances in Cryogenic Wind Tunnel Technology* (AGARD, 1996)

8.12 M. Dubois: *Feasability Study on Strain Gage Balances for Cryogenic Wind Tunnels at ONERA, Cryogenic Technology Review Meeting, NLR Amsterdam* (1982)

8.13 K. Hufnagel: *A new Half-Model-Balance for the Cologne-Cryogenic-Wind-Tunnel (KKK), The Second International Symposium on Strain Gauge Balances, Mai 1999, Bedford* (TU Darmstadt, Darmstadt 1999)

8.14 A. Pope, K.L. Goin: *High-Speed Wind Tunnel Testing* (Krieger, New York 1978)

8.15 G. Bridel: *Untersuchung der Kraftschwankungen bei einem querangeströmten Kreiszylinder, Dissertation, Nr. 6108* (ETH Zürich, Zürich 1978), in German

8.16 G. Schewe: A multicomponent balance consisting of piezoelectric force transducers for a high-pressure windtunnel, Techn. Messen **12**, 447–452 (1982), in German

8.17 G. Schewe: On the force fluctuations acting on a circular cylinder in crossflow from subcritical to transcritical Reynolds numbers, J. Fluid Mech. **133**, 265 (1983)

8.18 G. Schewe: *Force measurements in aerodynamics using piezo-electric multicomponent force transducers. Proc. 11th ICIASF '85 Record, Stanford Univ* (IEEE, New York 1985) p. 263

8.19 N.J. Cook: A sensitive 6-component high-frequency-range balance for building Aerodynamics, J. Phys. E **16**, 390–393 (1983)

8.20 H. Hönlinger, J. Schweiger, G. Schewe: *The use of aeroelastic windtunnel models to prove structural design methods, Proc. No. 403 of the 63rd SMP Meeting of AGARD, Athens, Greece* (AGARD, Neuilly-sur-Seine 1986) pp. 9-1–9-15

8.21 H. Zingel: *Measurement of steady and unsteady airloads on a stiffness scaled model of a modern transport aircraft wing. Proc. Int. Forum on Aeroelasticity and Structural Dynamics, Aachen, DGLR-Bericht 91-06* (DGLR, Bonn 1991) p. 120

8.22 H. Psolla-Bress, H. Haselmeyer, A. Hedergott, G. Höhler, H. Holst: *High roll experiments on a delta wing in transonic flow, Proc. 19th ICIASF 2001 Record, Cleveland, Ohio, Aug. 27-30 2001* (IEEE, New York 2001) p. 369

8.23 G. Gautschi: *Piezoelectric Sensorics* (Springer, Berlin, Heidelberg 2002)

8.24 J. Tichy, G. Gautschi: *Piezoelektrische Meßtechnik* (Springer, Berlin, Heidelberg 1980), in German

8.25 G. Schewe: Beispiele für Kraftmessungen im Windkanal mit piezoelektrischen Mehrkomponentenmeßelementen, Z. Flugwiss. Weltraumforsch. **14**, 32–37 (1990), in German

8.26 H. Triebstein, G. Schewe, H. Zingel, S. Vogel: Measurements of unsteady airloads on an oscillating engine and a wing/engine combination, J. Aircr. **31**(1), 97 (1994)

8.27 N. Schaake: *Querangeströmte und schiebende Zylinder bei hohen Reynoldszahlen, Dissertation* (Univ. Göttingen, Göttingen 1995), DLR-Report No FB 95-37 (DLR, Götzingen 1995)

8.28 G. Schewe: Sensitivity of transition phenomena to small perturbations in flow round a circular cylinder, J. Fluid Mech. **172**, 33 (1986)

8.29 G. Schewe: Reynolds-number effects in flow around more-or-less bluff bodies, J. Wind Eng. Ind. Aerodyn. **89**, 1267 (2001)

8.30 G. Schewe: *Reynolds-number-effects and their influence on flow induced vibrations, Proc. Structural Dynamics Eurodyn 2005* (Millpress, Paris 2005) p. 337

8.31 G. Schewe: Nonlinear flow-induced resonances of an H-shaped section, J. Fluid Struct. **3**, 327–348 (1989)

8.32 D. Schimke, P. Jänker, V. Wendt, B. Junker: *Wind tunnel evaluation of a full scale piezoelectric flap control unit, Proc. 24th European Rotorcraft Forum, Marseille, 15-17. Sept. 1998* (Organizer, 1998)

8.33 G. Schewe, H. Mai, G. Dietz: Nonlinear effects in transonic flutter with emphasis on manifestations of limit cycle oscillations, J. Fluid Struct. **18**, 3 (2003)

8.34 G. Dietz, G. Schewe, F. Kießling, M. Sinapius: *Limit-Cycle-Oscillation Experiments at a Transport Aircraft Wing Model, Proc. Int. Forum Aeroelasticity and Structural Dynamics 2003, Amsterdam* (Netherlands Association of Aeronautical Engineers, 2003)

8.35 G. Schewe, C. Steinhoff: Force measurements on a circular cylinder in a cryogenic-Ludwieg-tube using piezoelectric transducers, Exp. Fluids **42**(3), 489–494 (2007)

8.36 H. Rosemann: The Cryogenic Ludwieg-Tube-Tunnel at Göttingen, AGARD Special Course. In: *Cryogenic wind tunnel technology* (AGARD, Neuilly-sur-Seine 1997)